
Engineering of Bioactive Papers: Site-specific, Covalent Immobilization of Peptides and Proteins



TECHNISCHE
UNIVERSITÄT
DARMSTADT

**Vom Fachbereich Chemie
der Technischen Universität Darmstadt**

zur Erlangung des Grades
Doctor rerum naturalium
(Dr. rer. nat.)

**Dissertation
von M.Sc. Valentina Liebich**

Erstgutachter: Prof. Dr. Harald Kolmar

Zweitgutachter: Prof. Dr. Markus Biesalski

Darmstadt 2022

Liebich, Valentina: Engineering of Bioactive Papers: Site-specific, Covalent Immobilization of Peptides and Proteins

Darmstadt, Technische Universität Darmstadt

URN: urn:nbn:de:tuda-tuprints-228539

Jahr der Veröffentlichung der Dissertation auf TUpriints: 2023


Veröffentlicht unter CC BY-SA 4.0 International

<https://creativecommons.org/licenses/>

Tag der Einreichung: 30. August 2022

Tag der mündlichen Prüfung: 31. Oktober 2022

Der experimentelle Teil der vorliegenden Arbeit wurde unter der Leitung von Herrn Prof. Dr. Harald Kolmar am Clemens-Schöpf-Institut für Organische Chemie und Biochemie der Technischen Universität Darmstadt im Zeitraum von Oktober 2017 bis September 2020 angefertigt.



Für meine Familie

Danksagung

Ich möchte an dieser Stelle all denjenigen von Herzen danken, ohne die diese Arbeit niemals zustande gekommen wäre:

Meinem Doktorvater Prof. Dr. Harald Kolmar: Danke, für die Möglichkeit meine Arbeit in deiner Arbeitsgruppe anzufertigen, für die Bereitstellung des interessanten Themas und das stets entgegengebrachte, große Vertrauen.

Prof. Dr. Markus Biesalski, Prof. Dr. Gerd Buntkowsky und PD Dr. Tobias Meckel: Danke, für die Übernahme des Korreferats, sowie für die Übernahme der Rollen als Fachprüfer.

Dr. Olga Avrutina: Danke, für Deine Hilfsbereitschaft und Deinen Rat, für die zahlreichen Stunden im Lektorat meiner Texte und dass Du immer Zeit für mich hattest. Danke auch für die zauberhaften Schneewanderungen im Kleinwalsertal. Unseren „Lawinen-Schock-Moment“ werde ich wohl nie vergessen!

Laura Hillscher: Danke, für die gute Zusammenarbeit bei unserer gemeinsamen Publikation und für Deine Hilfsbereitschaft. Insbesondere für die Bereitstellung der TEMPO-oxidierten Fasern und der Bestimmung des Aldehydgehalts.

Dr. Aileen Ebenig, Dr. Desislava Yanakieva, Jan Habermann, Dr. Lukas Deweid und Sebastian Bitsch: Danke für die Bereitstellung der rekombinant hergestellten Proteine und für die Unterstützung, sodass ich die Herstellung nun teilweise auch selbst hinkriege.

Dr. Bastian Becker, Simon Englert und Peter Bitsch: Danke, für die Synthese und Bereitstellung des TAMRA-NHS.

Dr. Tobias Meckel und Dr. Markus Langhans: Danke für die lehrreichen Stunden am CLSM, die schönen Bilder, die daraus für diese Arbeit und die Publikationen entstanden sind und die interessanten Gespräche.

Dr. Andreas Christmann: Danke, für Deine Hilfsbereitschaft insbesondere bei der Anwendung statistischer Methoden auf meine Ergebnisse.

Dr. Aileen Ebenig: Danke, für die gute Zusammenarbeit, Deine stete Unterstützung, die bereichernden Diskussionen und hilfreichen Ratschläge. Danke auch für alles was nichts mit der Arbeit zu tun hatte, für die gemeinsamen Laufrunden während unserer gemeinsamen Zeit im AK und Deine Verbundenheit und Freundschaft darüber hinaus.

Allen zuvor genannten und auch nicht namentlich genannten ehemaligen und aktuellen Mitgliedern der AG Kolmar möchte ich für die stete Unterstützung und die gute Zeit im Labor danken. Sei es durch einen guten Rat, die musikalische Untermalung des Laboralltags, die gelegentlichen Pausen am Tischkicker, das Mittagessen in der Mensa, laue Abende auf der Dachterrasse, die Fahrradtour nach Nierstein oder die wundervolle Zeit im KWT. Ohne all das, wäre es nicht dasselbe gewesen und ich heute vermutlich nicht an dieser Stelle. Danke!

Mein besonderer Dank gilt meinen Freunden und meiner Familie, allen voran meinen Eltern Eva-Maria und Manfred: Ihr habt diese Doktorarbeit erst möglich gemacht. Danke, dass ihr mich bei all meinen Entscheidungen im Leben unterstützt, für eure Geduld und euren unerschütterlichen Glauben an mich!

Der größte Dank gilt meinem Mann Philipp: Ohne Dich hätte ich das nie geschafft! Du bist meine Stütze und hältst mir den Rücken frei. Danke, dass Du schon so lange an meiner Seite bist und alle Phasen des Lebens mit mir mitmachst, auch wenn ich in der letzten Zeit bestimmt oft nicht einfach war. Ich kann kaum fassen, was für ein Glück ich mit Dir habe!

Publications derived from this work

Parts of this work have been published in:

Liebich, Valentina J.; Avrutina, Olga; Habermann, Jan; Hillscher, Laura M.; Langhans, Markus; Meckel, Tobias; Biesalski, Markus; Kolmar, Harald (2021): Toward Fabrication of Bioactive Papers: Covalent Immobilization of Peptides and Proteins. *Biomacromolecules* 22 (7), S. 2954-2962.

Hillscher, Laura M.*; **Liebich, Valentina J.***; Avrutina, Olga; Biesalski, Markus; Kolmar, Harald (2021): Functional paper-based materials for diagnostics. *Chemtexts* 7 (2), S. 14.

*The authors contributed equally to this work.

Hilberg, Valentina; Avrutina, Olga; Ebenig, Aileen; Yanakieva, Desislava; Meckel, Tobias; Biesalski, Markus; Kolmar, Harald (2019): Light-Controlled Chemoenzymatic Immobilization of Proteins towards Engineering of Bioactive Papers. *Chemistry* 25 (7), S. 1746–1751.

Contribution to conference:

Hilberg, Valentina; Avrutina Olga; Ebenig, Aileen; Yanakieva, Desislava; Meckel, Tobias; Biesalski, Markus and Kolmar, Harald. A chemoenzymatic strategy for the immobilization of functional proteins on paper for bioanalytical applications. Poster presentation at *CPS 2019: 8th Chemical Protein Synthesis Meeting 2019*, Berlin, Germany (16.-19.06.2019)

Abstract

Bioactive papers are of growing interest regarding point-of-care testing devices that do not require extensive analytical equipment and have with Covid-19 made their way to everyone's household. The generation of such papers that comprise - in their simplest form - a bioactive protein presented on a cellulosic material, typically relies on four very different immobilization principles, which can be divided into covalent/non-covalent and site-specific/non-site-specific strategies. Covalent, site-specific approaches are of special demand if a uniform, site-directed distribution of the biomolecule throughout the paper substrate is required along with a stable binding. Modular, chemoenzymatic approaches enable the formation of such bonds.

To the best of our knowledge, we are the first to investigate chemoenzymatic approaches for functional protein immobilization on cotton linters-based materials aimed at a versatile toolbox of strategies for the efficient and reliable generation of bioactive papers. The synthetic peptide immobilization strategies rely on:

- 1) highly efficient, spatially controllable phototriggered cycloaddition,
- 2) near to "green" oxime ligation,
- 3) fast reductive amination with subsequent amidation, or
- 4) straightforward esterification with subsequent amidation.

All approaches are followed by site-specific sortase A- or microbial transglutaminase-catalyzed transamidation. These four different conjugation strategies for peptide immobilization were evaluated with respect to reproducibility and fiber loading efficiency. The two enzymes employed for protein conjugation were able to recognize the same oligoglycine peptide anchor. Both proved suitable for controlled and site-directed conjugation of substrate proteins at physiological conditions. The method was engineered to allow unidirectional and covalent immobilization of several proteins displaying different functional properties, with ramifications for application in paper-based diagnostics.

List of contents

Danksagung	III
Publications derived from this work	V
Abstract	VI
List of contents	VII
1. ... Introduction	1
1.1. Paper and its current use	2
1.2. Fiber morphology	4
1.3. Chemical and supramolecular structure of cellulose	4
1.4. Immobilization of proteins by conventional coupling strategies	6
1.5. Bioorthogonal immobilization	10
1.5.1. Sortase A	11
1.5.2. Microbial transglutaminase	12
2. ... Objective	15
2.1. Part I	15
2.2. Part II	16
2.2.1. Strategy 1: Light-controlled peptide coupling	16
2.2.2. Strategy 2: Peptide coupling by oxime ligation	16
2.2.3. Strategy 3: Reductive amination	16
2.2.4. Strategy 4: Esterification of the first amino acid	17
3. ... Results and discussion	18
3.1. Experimental design	18
3.1.1. Overview	18
3.1.2. Cellulosic material	20
3.1.3. Chemical linkers and peptides	20
3.1.4. Enzymatic ligations and protein design	28
3.2. Part I: Light-controlled peptide immobilization	31
3.2.1. Proof-of-concept studies	31
3.2.2. Quantification of primary amines on paper	36
3.2.3. Protein quantification of immobilized model protein tGFP	37
3.2.4. Sortase A-mediated ligation of proteins with different biologic function	39
3.3. Summary: Part I	43
3.4. Part II: Preliminary experiments for optimization and variations	44
3.4.1. Strategy 1: Optimization of the light-controlled strategy on fibers	44
3.4.2. Strategy 2: Oxime ligation as a strategy for peptide immobilization	48

3.4.3.	Strategy 3: Reductive amination as strategy for peptide immobilization	51
3.4.4.	Strategy 4: Esterification as initial peptide immobilization step	53
3.4.5.	Suitability of mTG as ligating enzyme	56
3.5.	Part II: Comparison of the strategies	57
3.5.1.	TNBS assay: Quantification of amine content	57
3.5.2.	Enzyme-mediated ligation: tGFP fluorescence comparison	59
3.5.3.	BSA blocking towards improved ligation	63
3.5.4.	CLSM of the tGFP-conjugated fiber networks	66
3.6.	Summary: Part II	68
4. ...	Graphical summary	70
5. ...	Conclusion and outlook	72
6. ...	Zusammenfassung	75
7. ...	Experimental section	78
7.1.	General	78
7.1.1.	Solvents	78
7.1.2.	Reagents	78
7.1.3.	Supported materials	78
7.1.4.	Removal of organic solvents	79
7.1.5.	Lyophilization	79
7.1.6.	Storage	79
7.2.	Characterization	79
7.2.1.	NMR spectroscopy	79
7.2.2.	X-ray photoelectron spectroscopy	80
7.2.3.	High performance liquid chromatography (HPLC)	80
7.2.4.	Mass spectrometry	80
7.2.5.	UV-Vis spectroscopy	81
7.2.6.	Fluorescence imaging	81
7.2.7.	Confocal laser scanning microscopy	81
7.3.	Biological materials and methods	81
7.3.1.	Materials	81
7.3.2.	Bacterial strain for tGFP expression	82
7.3.3.	Culture media and buffers	82
7.3.4.	Immobilized metal ion affinity chromatography (IMAC)	83
7.3.5.	Sodium dodecyl sulfate polyacrylamide gel electrophoresis (SDS-PAGE)	84
7.3.6.	Production and purification of tGFP-derivatives 7 or 23	84
7.4.	Solid phase peptide synthesis (SPPS)	85
7.4.1.	General procedure for manual SPPS	85

7.4.2.	Peptide 4: <i>H</i> -GGG- β A-K(4-maleimidobutyric acid)-AWGG-NH ₂	86
7.4.3.	Peptide 4.1: TAMRA- β A-K(4-maleimidobutyric acid)-AWGG-NH ₂	87
7.4.4.	Peptide 14: <i>H</i> -GGG- β A-K(aminooxyacetic acid)-AWGG-NH ₂	87
7.5.	Small-scale papermaking	88
7.6.	TNBS assay: Indirect amine quantification assay	88
7.7.	Part I	89
7.7.1.	Pretreatment of paper discs 1	89
7.7.2.	Synthesis of 4-((2-formyl-3-methylphenoxy)methyl)benzoic acid 2	89
7.7.3.	PE-functionalization of paper 1 resulting in paper 3	91
7.7.4.	Diels-Alder reaction of PE-functionalized paper with maleimido-peptides 4 or 4.1 using a stencil to produce papers 5 or 5.1	91
7.7.5.	Diels-Alder reaction of PE-functionalized paper with GGG-maleimido-peptide 4 for quantification and further ligations of 5	92
7.7.6.	SrtA-mediated ligation of filter papers 5 with stencil and tGFP 7	92
7.7.7.	SrtA-mediated ligation of GGG-photoconjugates 5 with proteins 7, 9 or 11	92
7.7.8.	Quantification of protein load using tGFP fluorescence	92
7.7.9.	Hydroxamate assay: microbial transglutaminase activity test	93
7.7.10.	ZZ-conjugation test: paper-based ELISA	94
7.8.	Part II: Preliminary experiments	94
7.8.1.	Optimization of strategy 1 regarding PE input	94
7.8.2.	Preliminary experiments of strategy 2 regarding oxime ligation	95
7.8.3.	Preliminary experiments on strategy 3	96
7.8.4.	Preliminary experiments on strategy 4 regarding primary functionalization	98
7.9.	Part II: Comparison experiments	99
7.9.1.	Synthesis of fibers 5	99
7.9.2.	Synthesis of fibers 15	99
7.9.3.	Synthesis of fibers 19	99
7.9.4.	Synthesis of fibers 22	100
7.9.5.	Enzyme-mediated ligation of tGFP 7 or 23 onto papers	100
7.9.6.	Co-localization with CBM fusion proteins	101
8. ...	Supporting information	102
8.1.	Spectra of photoenol 2	102
8.1.1.	NMR spectra	102
8.1.2.	UV/Vis spectrum	104
8.2.	Peptide analysis	104
8.2.1.	Peptide 4	104
8.2.2.	Peptide 4.1	105
8.2.3.	Peptide 14	106

8.3.	Data of TNBS assays	106
8.3.1.	Part I	106
8.3.2.	Part II	106
8.4.	SDS-PAGE of tGFP derivatives	107
8.5.	Data of tGFP quantification	108
8.6.	CLSM Part II	108
9. ...	Register	109
9.1.	List of figures	109
9.2.	List of tables	115
9.3.	List of abbreviations and symbols	116
10..	References	119
	Erklärungen	128

1. Introduction

Recently, with the Covid-19 antigen rapid tests, paper-based sensors have - and it is not an overstatement to say - found their way into each household. Being it the simple-handling, very low in cost and giving an easy-to-read answer on everyday questions, paper-based sensors became a fascinating field of research (Figure 1).¹⁻³

The prototypic paper-based devices have been described already in 1883, when the English physician George Oliver reported on glucose and protein analysis in urine using paper and linen.^{4,5} Further enhancements during the 20th century, especially driven by the scientist couple Helen M. and Alfred Free, resulted in the first commercially available dipstick test for urinary glucose which has been marketed in 1956. One year later the test set for urinary proteins followed. Further development of the technology has allowed for the analysis of up to ten biomarkers simultaneously, with a single dipstick.⁶

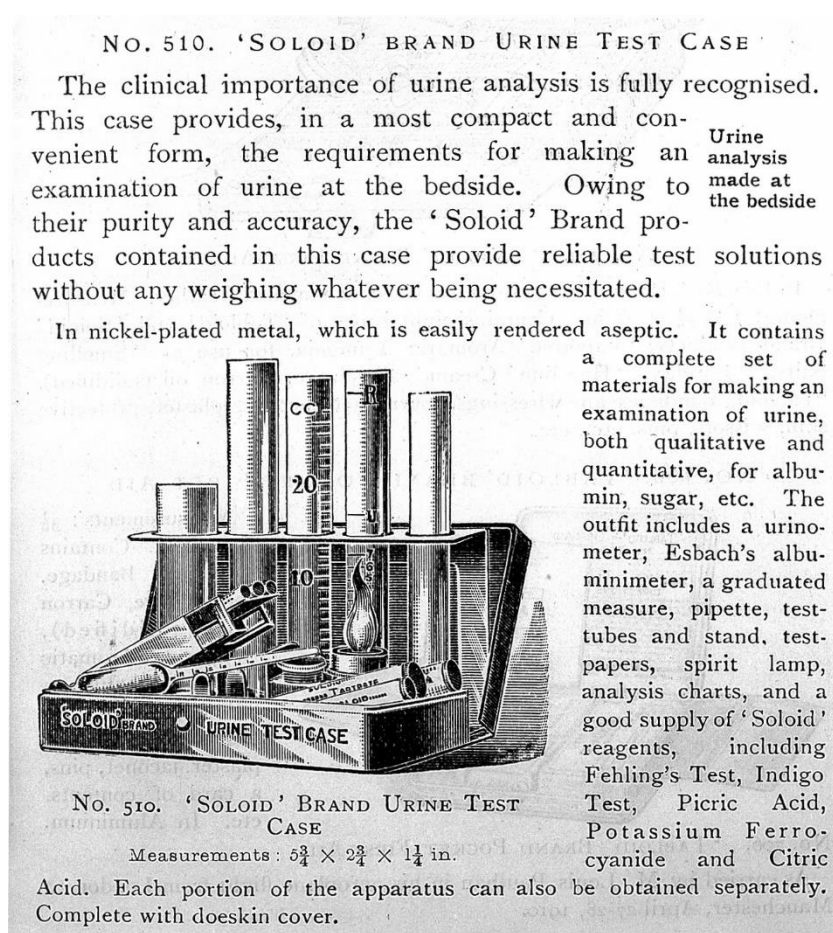


Figure 1: An early bedside urinary test kit comprising several components including test papers showing the complex setup of early urine testing. ©Wellcome Collection. Attribution 4.0 International (CC BY 4.0)⁷

Having started in 1956, the scientific base for lateral flow immunoassays was built. Various types of test systems were developed and throughout the 1980s the lateral flow technique was mature enough for commercialization. Already in the 1980s it revolutionized e.g., pregnancy testing, as the respective assay was developed and marketed for a convenient home application. To date, the interest in this kind of simple and easily adaptable test methods is still rather vivid - indeed, over 500 patents are linked to the development of this technology.⁸

Currently, the usability of functional papers is amplified by microfluidic paper-based analytical devices (μ PADs), the most recent field of development around functional papers. With the adaptability to a broad methodological basis, a vast variety of analytical questions can be addressed using μ PADs.^{2,9}

Affordable, Sensitive, Specific, User Friendly, Rapid and Robust, Equipment Free and Deliverable (ASSURED) are the adjectives that describe the ideal point-of-care testing (POCT) device for resource-limited areas, according to the World Health Organization.¹⁰⁻¹² Noticeably, paper-based applications have great potential to meet the ASSURED requirements. Indeed, cellulose, the main component of paper, is abundantly available. Being produced by nearly every plant, it is an inexpensive raw material.^{1,13} It is biocompatible, easily biodegradable, and thus environmentally sustainable. The biopolymer is insoluble both in common organic solvents and in water. However, water-soluble substances can be stored in or carried through the fibers by capillary action and without the application of an external power source. Furthermore, paper is chemically and thermally resistant, its production, stacking and storage are equally easy. It is portable and once used, safely disposable, even if it may contain bio-hazardous material. In summary, these advantageous properties are probably the reason for the constantly increasing interest in paper-based analytical devices.^{1,14,15}

1.1. Paper and its current use

Paper is defined as a flat, porous, and non-woven material made of layered fibers from predominantly natural sources. It is commonly manufactured through drainage of a fiber suspension on a sieve, followed by desiccation of the resulting fiber fleece under heating and compression. The individual fibers in this fleece are randomly and statistically distributed, making the product highly porous.¹⁶⁻²⁰

Every year, approximately 420 million metric tons of paper are produced worldwide for a big variety of final refined products.²¹ In Germany, the largest share of paper produced annually is packaging materials, followed by graphic, hygiene and special-purpose papers used e.g., for diagnostics, décor, or filter applications (Figure 2). Although holding the smallest share, this

last segment holds 6.5 %, which accounts for 1.4 million metric tons of paper produced, that is usually sold at significantly higher prices than those of the other segments. ²²

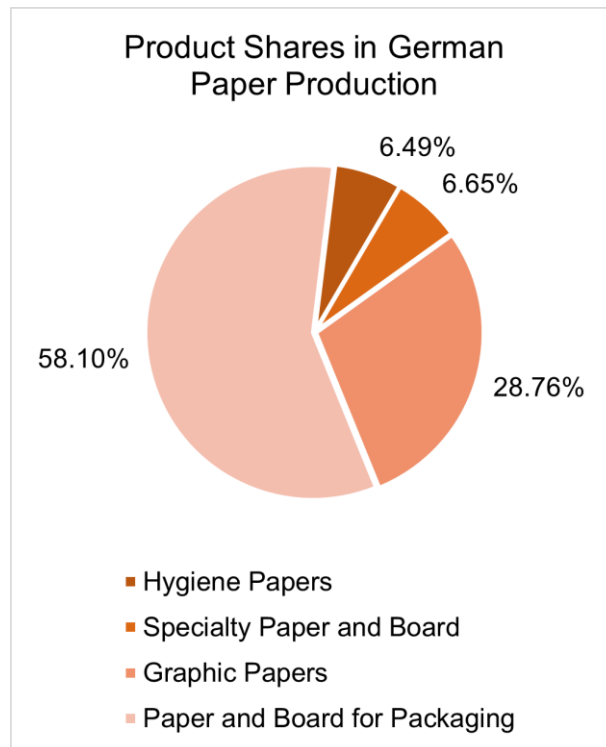


Figure 2: Shares of the individual paper grades in the total annual paper production in Germany in 2021. Total output is 21.0 million metric tons.²²

While for a long time the main research focus in this area was on the processing and properties of paper as print medium or packaging material, the needs of a modern world dictate the trend of renewable resources. Thus, paper and cellulose as biogenic materials lately have experienced increasing research interest and will get even more attention apart from these classic fields of application in the future.^{18,23,24}

Paper properties depend on a variety of factors, differing greatly in terms of the origin, type of fiber and the production process. Additives or fillers, as well as refinement or functionalization allow further tuning of the characteristics. Built of foremost cellulosic polymeric architectures, the world's most abundant raw material, fibers swell and absorb water differently if they contain non-polar lignin or hemi-celluloses, compared to pure cellulose.^{16,18,25} Highly appreciated for their purity, namely, high cellulose content (>95 %), cotton and cotton linters fibers are the preferred raw materials for the production of papers for biomedical applications.^{26,27} The manifold of functionalization possibilities yields a vast range of versatile functional materials for microfluidics or sensor technologies based on paper materials.^{9,23,24,28}

1.2. Fiber morphology

From a chemical point, a fiber consists mainly of three different macromolecules in the morphological hierarchy of the fiber, which fulfill specialized functions. Cellulose builds the skeleton; hemicellulose performs as the embedding compound and lignin strengthens the mechanical resistance of the cell wall. For visualization, a single fiber can be compared to a straw. The solid part represents the fiber wall that encloses a hollow, representing the lumen. Several single strands of macromolecular cellulose form an elementary fibril with a cross-section of 3 to 35 nm (Figure 3). One level up in the hierarchy, multiple elementary fibrils are joined into a microfibril with a cross-section of 10 to 35 nm. In a similar fashion macrofibrils are formed from microfibrils on the next level and are embedded in a matrix of hemicellulose and lignin. Hydrogen bonds stabilize the fiber structure at every level of the morphological hierarchy, including intermolecular bonds between cellulose, hemicellulose, and lignin.^{23,24,29}

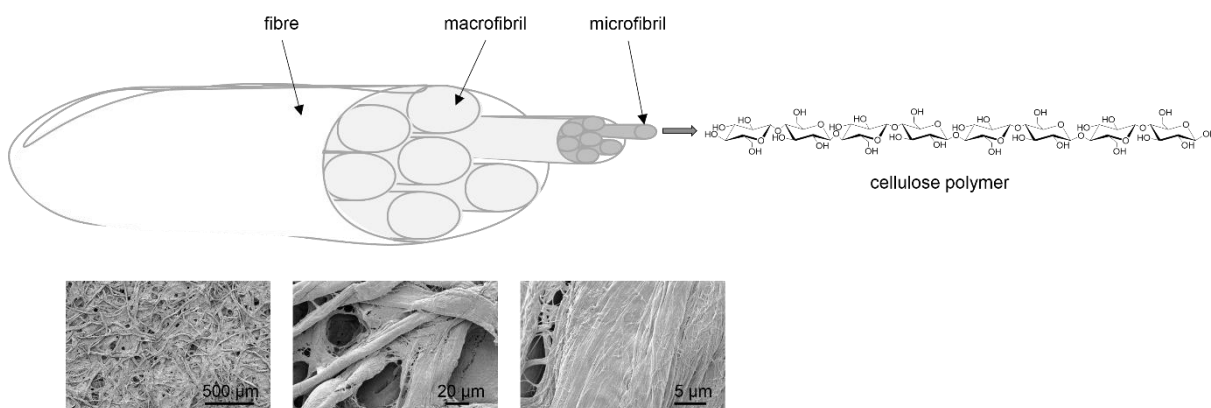


Figure 3: Supramolecular structure of cellulose. Depiction of the morphological hierarchy of a cellulose fiber, divided in macrofibrils, microfibrils, and the cellulose polymer. After Hillscher et al.²³

1.3. Chemical and supramolecular structure of cellulose

Cellulose consists of D-anhydroglucopyranose units (AGU) connected through β -(1,4)-glycosidic bonds with a fully extended, linear secondary structure. The repetition unit of cellulose is cellobiose, the AGU-dimer. Each cellulose chain has two ends. The non-reducing end possesses an anomeric carbon atom involved in the chain formation by a glycosidic bond and a free hydroxyl group at the C4 atom. The reducing end is in equilibrium between the pyranose form and the open ring with an aldehyde function at C1.^{24,30} Figure 4 shows the chemical structures of an AGU, cellobiose and the different end groups.

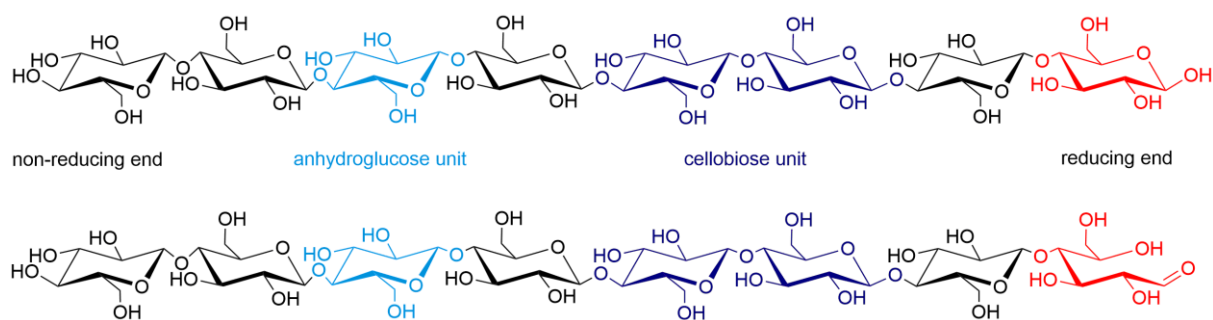


Figure 4: Chemical structures of AGU (light blue)), cellobiose (dark blue), the non-reducing at the left side of the chains, and respectively the reducing end groups (red) of a cellulose polymer chain. After Hillscher et al.²³

Every AGU along the chain contains three reactive hydroxyl groups, the primary hydroxyl at the C6 atom and two secondary ones at the C2 and the C3. Due to linearity of the individual cellulose chains, the high density of hydroxyls facilitates the formation of hydrogen bonds. Thus, a strong connection between the polymer chains is formed, resulting in inelastic fibrils with a high tensile strength.^{15,30,31} Figure 5 shows a scheme depicting the underlying hydrogen bond network stabilizing the supramolecular structure of native cellulose.

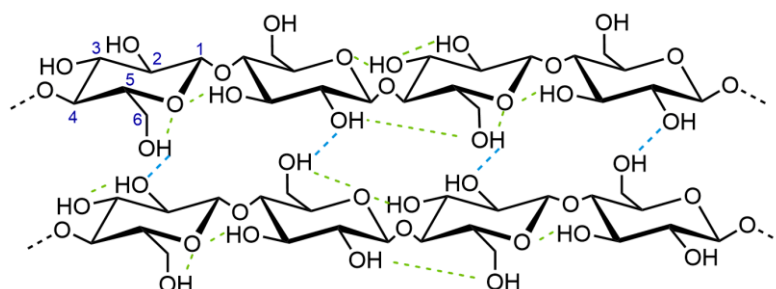


Figure 5: Schematic depiction of the native cellulose supramolecular structure with intermolecular hydrogen bridges in blue and intramolecular ones in green. After Hillscher et al.²³

Cellulose polymer chains with strong parallel arrangement form a hydrogen bond network resulting in highly ordered, crystalline regions on the supramolecular level. Besides, in amorphous regions cellulose chains are less linearly arranged, thus resulting in a rather random alignment.^{32,33} Both structures provide unique mechanical properties to a fiber, which is characterized, on one hand, by high tensile strength and stiffness supported by crystalline regions and, on the other hand, by elasticity and flexibility due to amorphous regions.³⁴

The strong cohesiveness of the semi-crystalline structure makes cellulose a chemically resistant molecular architecture, which is insoluble in common organic solvents and water. However, the hydrophilic character of the macromolecule allows water to penetrate paper fibers. Water only enters amorphous parts of the cellulose, interacting with inter- and intramolecular hydrogen

bonds. Between 8 and 14 wt.-% of water can be taken up by a fiber in equilibrium, thus increasing its volume. The supramolecular structure of a fiber can be altered by concentrated sodium hydroxide solution. The solution penetrates also crystalline cellulose regions, as hydroxyl groups interact strongly with hydroxyls of the solution, resulting in broken hydrogen bonds. Thus, additional amorphous regions can be generated. This treatment is often irreversible. Two organic solvents, making fibers swell even stronger than when surrounded by water, are ethanolamine and DMSO. Thus, the swelling behavior of cellulose depends not only on the strength of the hydrogen bonds, but also on the polarity of the medium.³²

1.4. Immobilization of proteins by conventional coupling strategies

The functionalization of a polymer under conservation of its macromolecular backbone is referred to as a polymer analogue reaction. By this type of reaction, chemical cellulose functionalization is predominantly performed on its hydroxyl groups. Three - theoretically - accessible hydroxyl groups are present on a glucose unit in the cellulose backbone. Their addressability depends, amongst other things, on the involvement in intra- or intermolecular hydrogen bond formation. The reactivity of the hydroxyl groups increases from C3 over C2 to C6, as the inclusion in the hydrogen bond network decreases statistically in the same order. Steric hindrance arising from the molecular structure, or the reagent also influences the addressability. Furthermore, the predominant morphology is a key factor for the accessibility, as chemicals can only enter amorphous regions, thus, hydroxy groups within crystalline regions would remain unmodified. The number of accessible hydroxyls can be increased by chemical and mechanical procedures. Beating of the fibers enhances fibrillation, while the most popular method is the treatment with aqueous sodium hydroxide, as the supramolecular structure can be modified without altering the fibrillar structure. Thereof unaffected is the maximum degree of substitution (DS), which cannot be greater than three, as the DS is defined as the maximum number of substituted hydroxyls per AGU. In the literature, numbers of up to 1.5 have been reported.^{15,24,35}

Regarding biofunctionalization, the orientation and coverage of an immobilized biomolecule on the paper surface is important, as it affects its optimal binding efficiency and specificity. Four different binding techniques are reported in the literature, which are based on either (1) physical or (2) high-affinity interactions, (3) formation of covalent chemical bonds, and (4) bioorthogonal coupling (Figure 6).³⁶⁻³⁸ The latter one will be explained in a separate chapter (1.5) as this strategy will be in the main focus of this work.

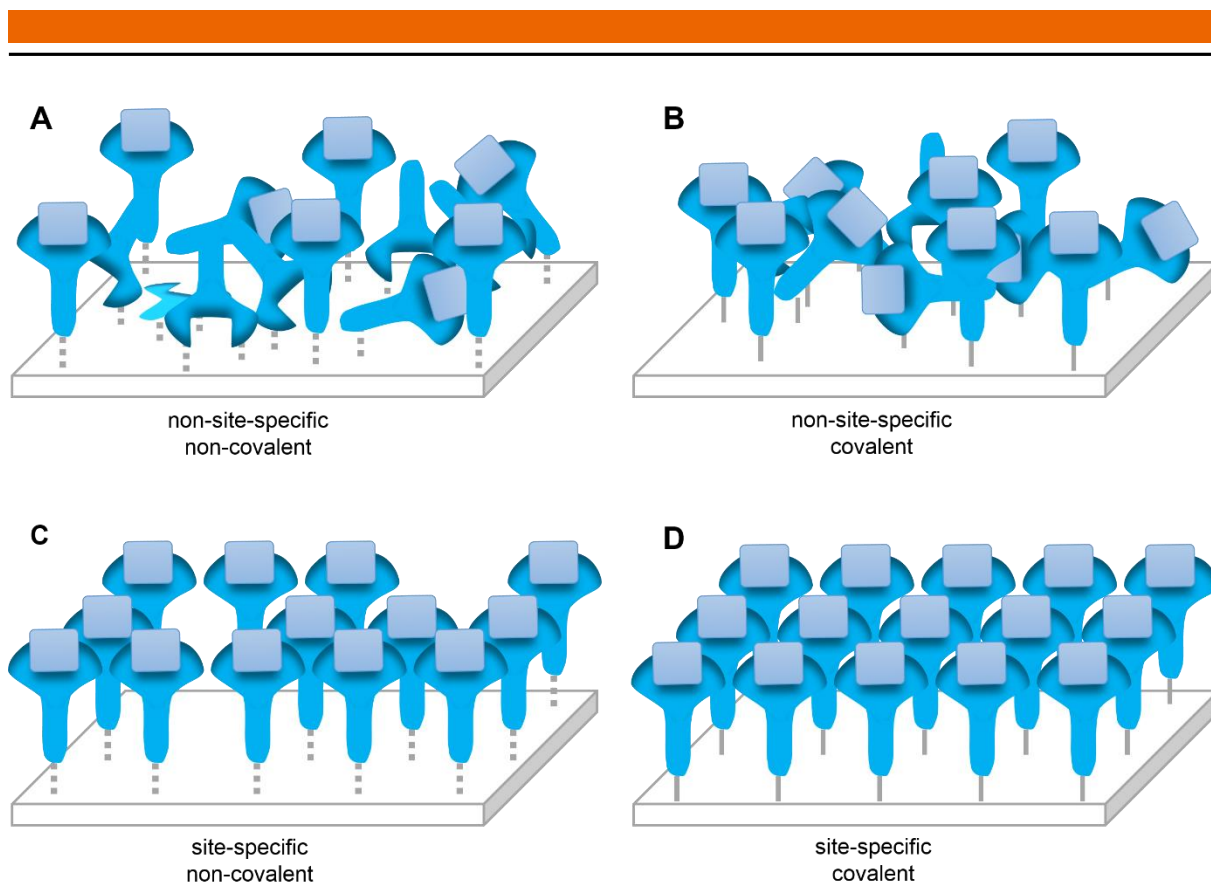


Figure 6: Schematic depiction of the different immobilization methods for biomolecules on surfaces. **A** non-site-specific, non-covalent immobilization e.g., by physical adsorption. **B** non-site-specific, covalent immobilization by covalent binding using intrinsic functional groups of the biomolecule. **C** site-specific, non-covalent immobilization e.g., by bioaffinity coupling. **D** site-specific, covalent binding by bio-orthogonal coupling. The dashed lines between the biomolecule and the surface in **A** and **C** visualize weak physical interactions, whereas the solid lines in **B** and **D** represent covalent bonds respectively. After Steen Redeker et al. ³⁸

Underlying modifications on hydroxyl groups used for the biofunctionalization of cellulose are depicted below (Figure 7).

Immobilization by physical adsorption is achieved by bringing paper in contact with a protein-containing solution, by either dipping, coating, or printing, followed by an optional washing step. In general, no additional pre- or post-treatment is necessary. However, to effectively bind proteins to paper by physical interactions, such as van der Waals forces, hydrophobic interactions, electrostatic and ionic interactions, or hydrogen bonds, often the following two polymer-analogue reactions are applied. Esterification of cellulose with nitric acid in the presence of strong inorganic acids results in nitro groups on the surface. So-called nitrocellulose adsorbs proteins due to strong electrostatic interactions, hydrogen bonds, and hydrophobic effects. The material is the industrially most important cellulose derivative for protein immobilization, being the substrate for most lateral flow immunoassays.^{15,35,39,40}

Another effective protein-adsorbing material is carboxymethylated cellulose (CMC). Carboxylic groups are conjugated to the cellulose hydroxyls applying monochloroacetic acid and sodium hydroxide following a Williamson ether synthesis.¹⁵

Being, due to the simple coupling steps, the most straightforward among the four immobilization methods, protein immobilization by physical adsorption is also the most frequently used technique. It is prevalently used for especially inexpensive proteins or for large-scale production. However, the binding is relatively weak and non-site-specific.^{38,41,42}

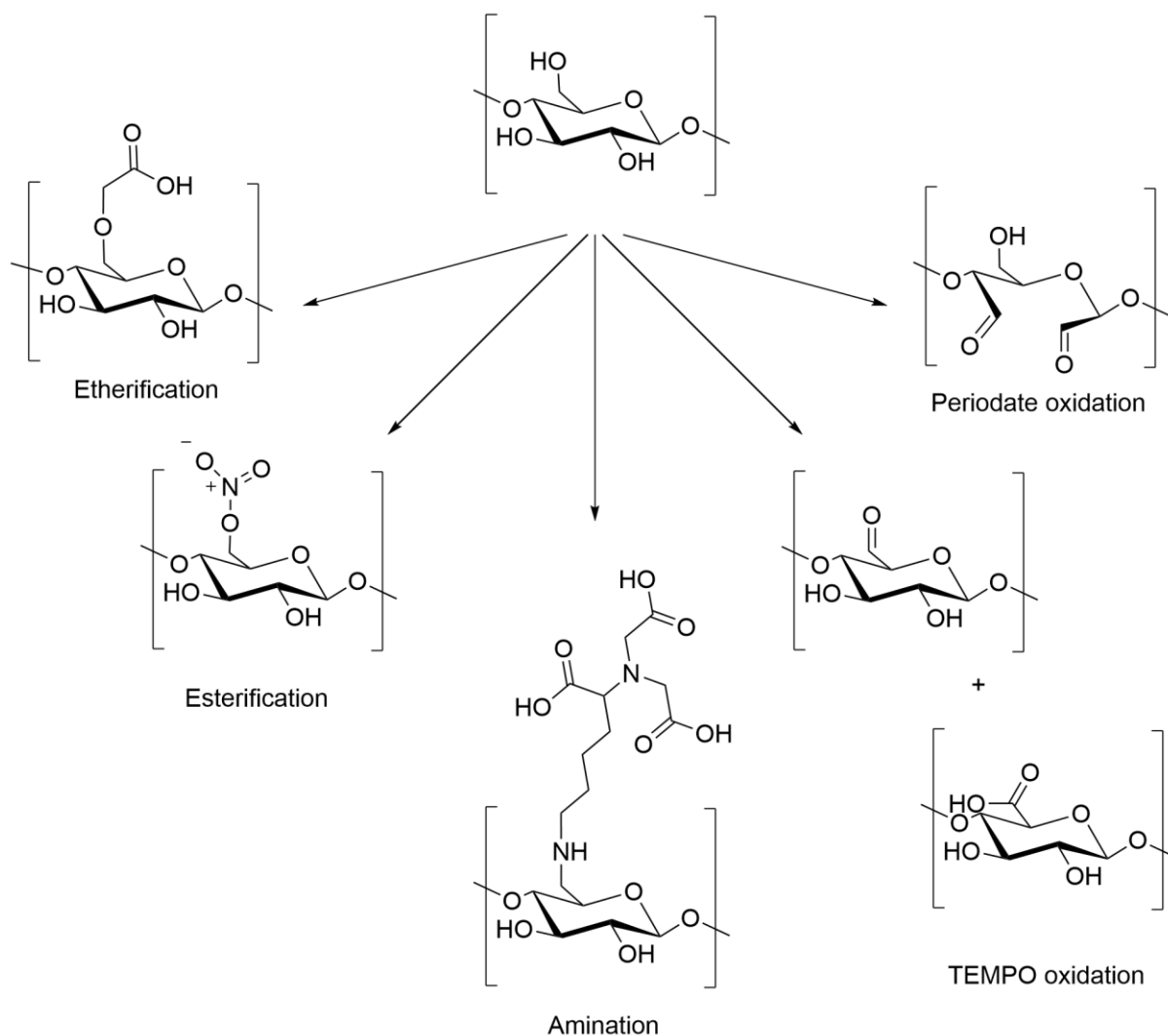


Figure 7: Exemplary functionalization of cellulose hydroxyls.

High-affinity interaction as protein coupling method assures a directed and highly specific immobilization of the biomolecule under preservation of its biologic activity. Molecular pairs to be considered are, e.g. the naturally occurring antibody-antigen and avidin-biotin interactions or different sorts of molecular tags such as the His-tag, which builds a chelating complex with nickel ions.^{15,38,43} The latter strategy is enabled by the amination of cellulose films with *N*-(5-amino-1-carboxypentyl) iminodiacetic acid, a nitrilotriacetic acid (NTA) derivative. Therefore, pre-activation of the coupling components is required. Tosylation of the cellulose hydroxyl group, as well as persylation of NTA with trimethylsilyl chloride are performed prior to the

actual amination. Nickel ions can eventually be loaded on NTA cellulose films, which capture His-tagged proteins. This system is commonly used for purification of different biomolecules.^{15,30,44} However, high affinity immobilization is a rather complex method, as it usually requires the modification of the cellulose substrate and one of the immobilized biomolecular species. On the other hand, the orientation of the protein on the substrate can be adjusted by rational selection of the employed functionality and the anchoring point at the biomolecule. Thus, high affinity-based immobilization of a target biomolecule is a site-specific, non-covalent method, often resulting in a higher biologic activity compared to adsorption or covalent strategies.^{15,38,43}

A robust, thus permanent, bond can be assured by covalent immobilization with chemical functional groups from each counterpart, the paper, and the biomolecule. To keep the biomolecule intact, physiological conditions need to be maintained throughout the chemical reactions.^{15,38} Commonly, proteins are coupled on cellulose by their functional side chains, via reactive amines or thiol groups besides other possibilities. Reactions with lysine side chains possess comparably good reactivity and bond stability and are thus preferred over those with cysteine residues.⁴¹ To this end, ϵ -amines of lysine react with carbonyl or carboxylic groups on the cellulose, resulting in imine or amide bonds, respectively. However, unmodified cellulose does not provide respective functional groups in amounts large enough for efficient immobilization. Therefore, additional functions need to be generated.⁴⁵ Poorly reacting hydroxyl groups can be activated, e.g., aldehydes that are formed by oxidation of vicinal secondary hydroxyl groups (at C2 and C3) with sodium periodate (NaIO_4). This treatment, however, leads to a disruption of the pyranose ring, probably affecting the linearity of the cellulose chain and the hydrogen bond system.¹⁵ A non-disruptive treatment is realized by the oxidation of primary hydroxyl groups with the catalyst 2,2,6,6-tetramethylpiperidinyloxy (TEMPO) under aqueous, alkaline conditions, with the co-catalyst sodium bromide (NaBr) and the oxidant sodium hypochlorite (NaOCl) (Figure 8). This reaction generates carbonyl and in a second step carboxyl groups within cellulose polymer chains at C6. As the C6 is not part of the pyranose ring, the polymer backbone remains intact. In general, covalent bonds provide a more robust immobilization of biomolecules than physical methods.^{15,46–49}

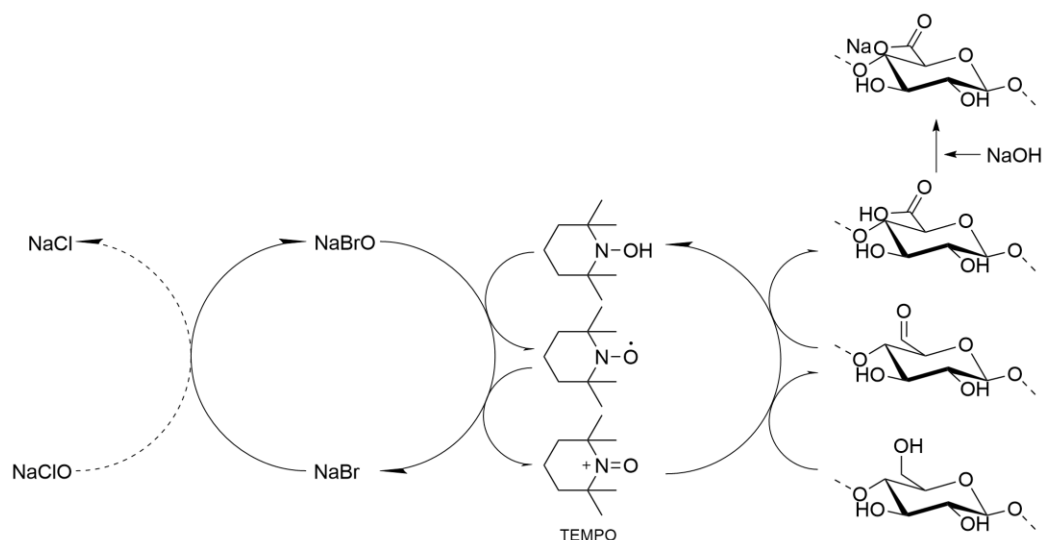


Figure 8: TEMPO-mediated cellulose oxidation. After Saito et al. ⁴⁶

Taking into consideration that proteins carry multiple lysine residues, the possibilities for immobilization through these residues are also numerous. The orientation can hardly be tuned, meaning the linkage is mostly random, thus non-site specific. This can have negative effects on the loading capacity or the functionality, e.g. on the accessibility of the protein active site, or can even cause denaturation, depending on the position of the linkage. ^{38,50–52}

1.5. Bioorthogonal immobilization

Bioorthogonal coupling is a covalent strategy ensuring site-specificity of the immobilized protein. The strategy is comparably complex as the system demands unique requirements for both counterparts. The cellulose substrate and the biomolecule need to carry functional moieties that react exceptionally with each other. Additionally, the functionality at the biomolecule needs to be one single moiety and at a structurally specific site, to ensure stability and the accessibility of the active site. The so-called “click-reactions”,⁵³ such as Cu(I)-catalyzed or strain-promoted azide-alkyne cycloadditions are popular tools in chemical bioorthogonal approaches.^{15,38,54,55}

In view of the ecological goals of green chemistry, several enzymatic approaches for the structural and thus behavioral modification of polysaccharides have been developed in recent years, including those based on laccases or tyrosinases.⁵⁶ However, only few chemical or biocatalytic methods have been described that ensure site-specific but gentle binding of the ligand.^{38,50} Recently, Uth et al.⁴⁹ have reported on a modular approach for bioorthogonal site-directed immobilization of proteins on crystalline nanocellulose (CNC). In this research, native cellulose fibers were modified by TEMPO-mediated oxidation. As described, aldehyde and

carboxylic functionalities are simultaneously introduced. Within a classic approach, conjugation to protein's lysine residues could be performed leading to randomly conjugated biomolecules. Sortase A-mediated ligation was chosen for immobilization to overcome this problem of randomness, as it has been shown to be a reliable tool for connecting two constructs.⁵⁷ The enzyme recognizes two short peptide sequences and links them through a new native amide bond. Thus, a two-step approach for covalent coupling of different biomolecules was developed. The first step is the immobilization of a peptide containing a sortase recognition sequence on cellulose. For this purpose, an aminooxy functionality was introduced on a lysine side chain that can react with aldehydes present on the cellulose surface to form an oxime ether. Various functional proteins genetically engineered to contain the complementary recognition sequence at the C-terminus and recombinantly expressed in *E. coli* were successfully immobilized on the CNC surface.⁴⁹

1.5.1. Sortase A

Staphylococcus aureus sortase A (srtA) is a thiol transpeptidase that in its natural function attaches surface proteins to the bacterial cell wall. This enzyme, extensively studied in the past, is calcium-dependent, which is explained by a stabilizing effect due to complexation of a calcium ion. Thus, substrate binding is facilitated.^{58–61} Due to its sequence specificity, the sortase A wild-type enzyme ligates two specific peptide sequences and follows the so-called “sortagging” mechanism.⁶² Substrates are an N-terminal oligoglycine and a conserved five amino acid motif “LPXTG” near the C-terminus. For “X” any amino acid can be chosen, however very often it is glutamic acid (E) as LPETG is the natural sorting motif.^{57,63} Additionally, the fastest conversion was observed when the sequence contained a supplementary glycine residue in the C-terminal direction.⁶⁴ For the enzyme-mediated exchange of the C-terminal sequence, sortase A cleaves the amino acid fragment after the threonine residue and simultaneously generates a thioester bond between the substrate and the active-site cysteine residue, resulting in an enzyme-acyl intermediate (Figure 9). The intermediate is attacked by the nucleophilic α -amino group at the complementary sequence, resulting in a new bond between LPXT and the oligoglycine.^{57,58,65–67} The major drawback of the wild-type srtA is its low catalytic activity, which requires long ligation times and/or large amounts of the enzyme or LPXTG substrate. To overcome these limitations, improved variants regarding reaction rates or Ca^{2+} dependency were developed. The sortase A pentamutant is still a Ca^{2+} -dependent variant, but ligates the same motifs as the wild-type enzyme, up to 120-times faster.^{57,68,69}

The short recognition motif and the high selectivity of the enzyme along with the mild reaction conditions is beneficial for a manifold of reaction types. Thus, its potential has been exploited in various *in vitro* applications, including peptide circularization, site-specific labeling, and immobilization of proteins on solid supports.^{49,64,70–72}

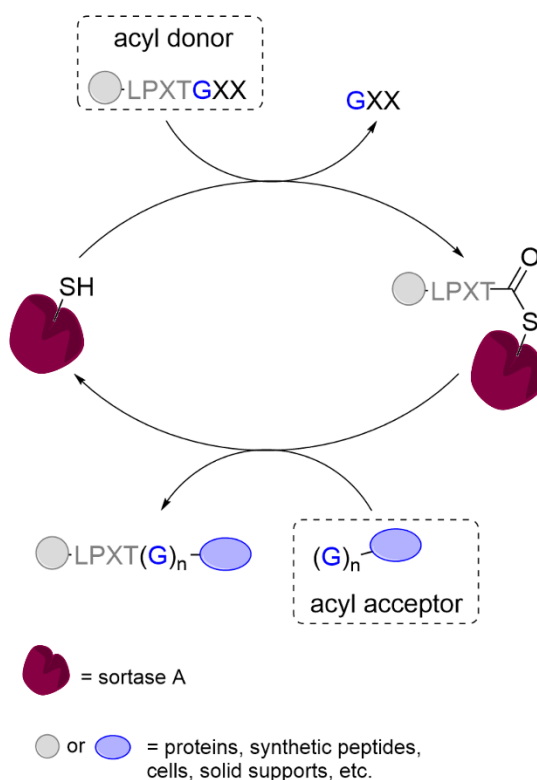


Figure 9: Mechanism of the sortase A-mediated transpeptidation. After Antos et al.⁵⁷

1.5.2. Microbial transglutaminase

Transglutaminases are another class of bond-forming enzymes and catalyze the formation of isopeptide bonds. The donor, a γ -carboxamide residue, and the acceptor, a primary amine, can be linked intra- or intermolecularly. *In vivo*, this posttranslational modification of proteins is deployed to increase resistance to mechanical stress, which is an important function e.g., in the wound-healing process.^{73–75}

Microbial transglutaminase (mTG) from *Streptomyces mobaraensis* was the first non-mammalian one isolated. The mechanism of catalysis is calcium-independent with a cysteine-protease-like active site.^{73,76} The enzyme is produced in *Streptomyces mobaraensis* as inactive zymogen and is activated by proteolytic cleavage after secretion to prevent uncontrolled cross-linking of intra-cellular proteins. The pro-sequence is located at the *N*-terminus, is 41 amino acids long and covers the active site to hinder substrate binding. It is cleaved in two steps. The

first one relies on transglutaminase-activating metalloprotease and results in FRAP-mTG derivative which is subsequently modified by a tripeptidyl aminopeptidase.^{77–79}

The acyl transfer mechanism begins with a nucleophilic attack by the thiolate ion of the active site cysteine against the glutamine residue side chain (Figure 10). An aspartic acid residue donates a proton to the resulting oxyanion intermediate, while ammonium is released. The acyl acceptor performs a nucleophilic attack against the acyl-enzyme intermediate. This step is further supported by the negatively charged aspartic acid accepting a proton from the primary amine substrate. Eventually the new amide bond is built, and the product is released. A histidine residue is passively involved in the reaction as it stabilizes the conformation of the active site.⁷⁶

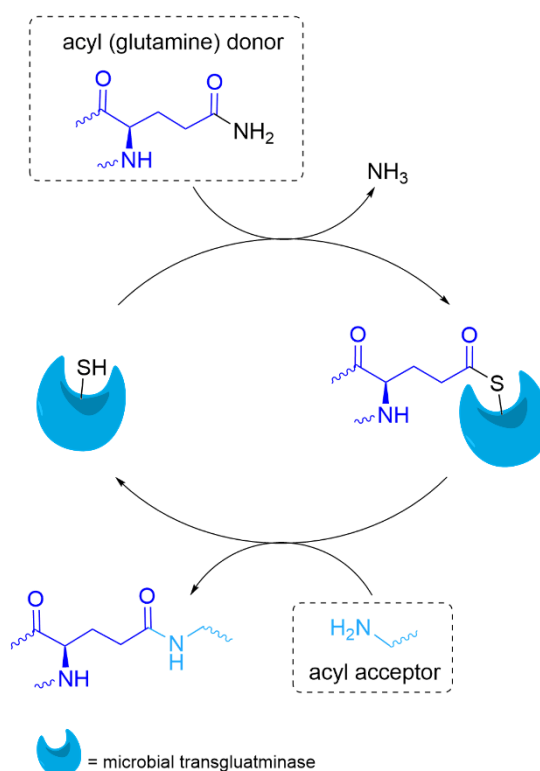


Figure 10: Mechanism of transpeptidation catalyzed by microbial transglutaminase. After Deweid et al.⁸⁰

Several factors influence mTG recognition of a reactive glutamine residue, among them the nature of surrounding amino acids, the secondary structure, and the flexibility of the polypeptide chain. Hence, surface exposure of a glutamine residue alone is not a guarantee for mTG recognition.^{81–87} In case the protein of interest is not an mTG substrate, the mTG-recognition motif can be introduced recombinantly.^{88,89}

In contrast to the acyl donor, the acyl acceptor is promiscuous, but aromatic amino acids or lysine residues in the direct environment of the reactive amine can have a positive effect on the ligation reaction.^{90,91}

mTG has found a broad applicability. Being an important tool in the food industry, it was further used in biotechnological applications, such as production of antibody-drug conjugates or immobilization of proteins on solid supports.^{86,91–93}

2. Objective

The site-specific and covalent immobilization of functional proteins on cellulosic carriers under mild conditions is obviously challenging. With the hydroxy groups of cellulose, paper fibers offer numerous, but chemically poorly differentiable and not directly addressable targets for immobilization of biopolymers. Conventional covalent conjugation methods are not able to directionally immobilize biomolecules on the surface of paper fibers in such a way that a uniform alignment of protein ligands on the matrix results in a dense population. Thus, the aim of this PhD thesis should be to establish a generally applicable system, for the directed conjugation of bioactive proteins to paper with the potential for high protein charge and to expand the toolbox for future applications.

The strategies should match the following terms:

1. Pre-functionalization of paper fibers with thermostable peptides as anchor molecules
2. Formation of a stable covalent bond;
3. Site-specificity;
4. Mild reaction conditions;
5. Preservation of biomolecule's function

The work should be divided into two parts. The first part should cover the development of a novel, synthetically most demanding “light-controlled” strategy and the proof-of-concept study for the modular approach applied to cotton linters-based paper with sortase A as ligating enzyme. The second part should include further optimization of the original strategy for application on cotton linters fibers and expand the modular approach by the development of three alternative strategies. The greater surface of single fibers compared to pre-formed papers should enable a higher peptide immobilization charge. The toolbox should further be complemented by microbial transglutaminase for enzymatic ligation.

2.1. Part I

The enzyme-recognition peptide is attached via a UV-light-enabled Diels-Alder reaction to a photoreactive moiety coupled to cellulosic paper after an adapted strategy published by Barner-Kowollik et al.⁹⁴ The biologic cargo is covalently attached by sortase A-promoted ligation (Figure 11).

To this end, an *o*-methyl benzaldehyde (further called photoenol or PE) is coupled to the paper surface via carbodiimide-mediated esterification. Under UV light, covalent grafting of an

enzyme recognition sequence, synthesized by solid phase peptide synthesis (SPPS), is enabled by a [4+2]-cycloaddition of the photoenol with an electron-poor ene-bearing peptide counterpart, e.g. a maleimide. Proteins with different biologic function are immobilized by sortase A catalysis and tested for functionality (see chapter 3.2)

2.2. Part II

2.2.1. Strategy 1: Light-controlled peptide coupling

The approach from part one should be further optimized for peptide immobilization on cotton linters fibers (Figure 12 A). While in the first part the proof-of-concept study was performed on commercial cotton linters-based filter paper, in the second part, the approach is tested for optimal signal outputs in respect to PE functionalization of cotton linters fibers (Figure 12 F). Therefore, fluorescence signals are recorded at different wavelengths after PE, peptide and *turboGFP*⁹⁵ (tGFP) coupling (see chapter 3.4.1). Based on the optimal setup, comparative studies are performed along with the following other strategies (see chapter 3.5).

2.2.2. Strategy 2: Peptide coupling by oxime ligation

The second strategy based on an adapted strategy reported by Uth et al.,⁴⁹ relies on TEMPO-oxidized cotton linter fibers (Figure 12 B), enriched with aldehyde functionalities, which are modified by oxime ligation. The click-type chemical reaction takes place under mild conditions at pH 4.5. It results in a stable covalent bond as an oxime ether (Figure 12 E).

Thus, aldehyde enriched, TEMPO-oxidized cotton linters are reacted with a recognition peptide sequence carrying an aminooxy residue in the middle of the molecule assembled via SPPS. The approach is tested for optimal peptide inputs for oxime ligation in respect to signal intensity after tGFP coupling (see chapter 3.4.2). Based on the optimal setup, comparative studies were performed along with the other strategies (see chapter 3.5).

2.2.3. Strategy 3: Reductive amination

The third strategy, as the second one, relies on TEMPO-oxidized cotton linters (Figure 12 B). This time the fibers are modified following reductive amination with cadaverine followed by HATU/DIPEA coupling of the recognition sequence, GGG (Figure 12 D). The synthesis is performed in two consecutive steps, with readily available building blocks.

Thus, formerly introduced aldehyde functionalities on the cotton linters are reacted with cadaverine in large excess together with 2-picoline borane complex, a non-toxic alternative to sodium cyanoborohydride, after an adapted strategy published by Ruhaak et al.⁹⁶ The achieved amine linker on cotton linters is further converted with a triglycine building block using a standard HATU/DIPEA reaction. After acidic cleavage of the protecting Boc group, the *N*-terminus is accessible to the enzyme.

The enzyme ligation efficiency is tested with differently functionalized substrates regarding linker length and glycine count (see chapter 3.4.3) before comparative studies were performed along with the other strategies (see chapter 3.5).

2.2.4. Strategy 4: Esterification of the first amino acid

The fourth approach tested relies on paper-own hydroxyl groups (Figure 12 A), to which the enzyme recognition unit is coupled via two subsequent reaction steps, a carbodiimide-mediated esterification followed by HATU/DIPEA coupling of the recognition sequence GGG with readily available building blocks (Figure 12 C).

Thus, Fmoc-6-aminohexanoic acid (Ahx) is coupled to the fibers in an esterification reaction. After removal of the Fmoc protecting group at the *N*-terminus, the triglycine building block is attached with a standard HATU/DIPEA reaction to complete the recognition unit on the fibers. After acidic cleavage of the protecting Boc group, the *N*-terminus is accessible to the enzyme.

The approach is tested for an optimal tGFP signal output in respect to primary functionalization, with the first amino acid. Therefore, fibers were functionalized with different amounts of Ahx and an excess of GGG. Fluorescence signals are recorded after tGFP coupling (see chapter 3.4.4). Based on the optimal setup, comparative studies were performed along with the other strategies (see chapter 3.5).

3. Results and discussion

3.1. Experimental design

3.1.1. Overview

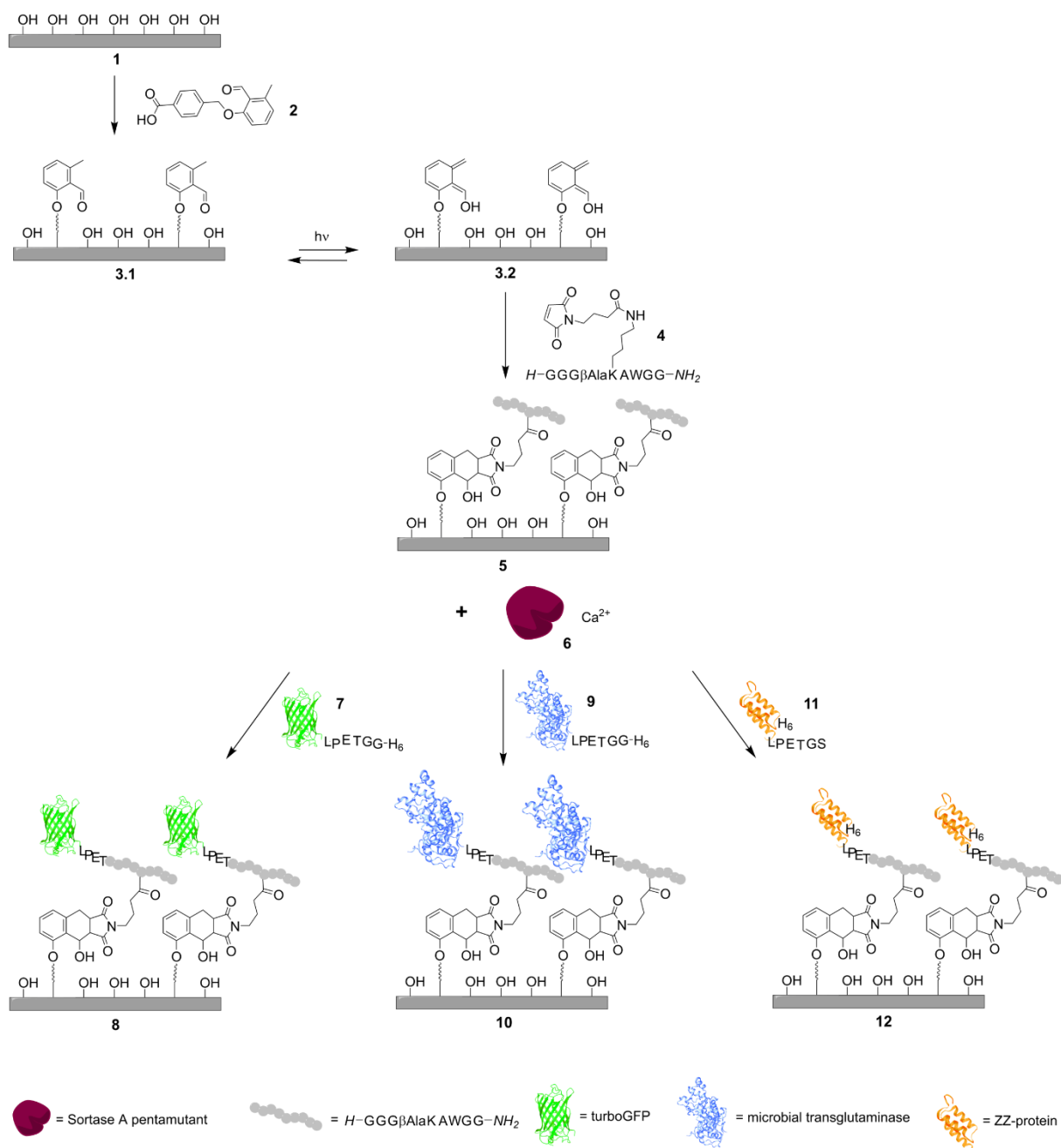


Figure 11: Overview of the first investigated light-controlled peptide immobilization approach. Ready cellulose paper was functionalized with a recognition sequence **4** resulting in peptide-paper hybrid **5**. tGFP **7**, microbial transglutaminase (mTG) **9** and ZZ-protein **11** were coupled by sortase A (**6**) ligation as model proteins with different biologic function. Structures for visualization from PDB for tGFP (GFP; PDB-ID: 1EMA)⁹⁷, mTG (PDB-ID: 1IU4)⁹⁸ and ZZ-protein (Z-domain; PDB-ID: 2spz)⁹⁹. Preliminary experiments are not depicted. Modified after Hilberg et al. ¹⁰⁰

In the first part of this work, the light-controlled peptide immobilization strategy resulting in product **5** (Figure 11), being the chemically most sophisticated of the tested ones, was investigated to a greater extend. Three proteins of different biologic function, tGFP⁹⁵, microbial transglutaminase (mTG) and ZZ-protein, were coupled to the actual peptide recognition sequence on paper **5** with sortase A-mediated ligation. Figure 11 shows the full synthesis routes of part I for the light-controlled approach to protein immobilization on paper.

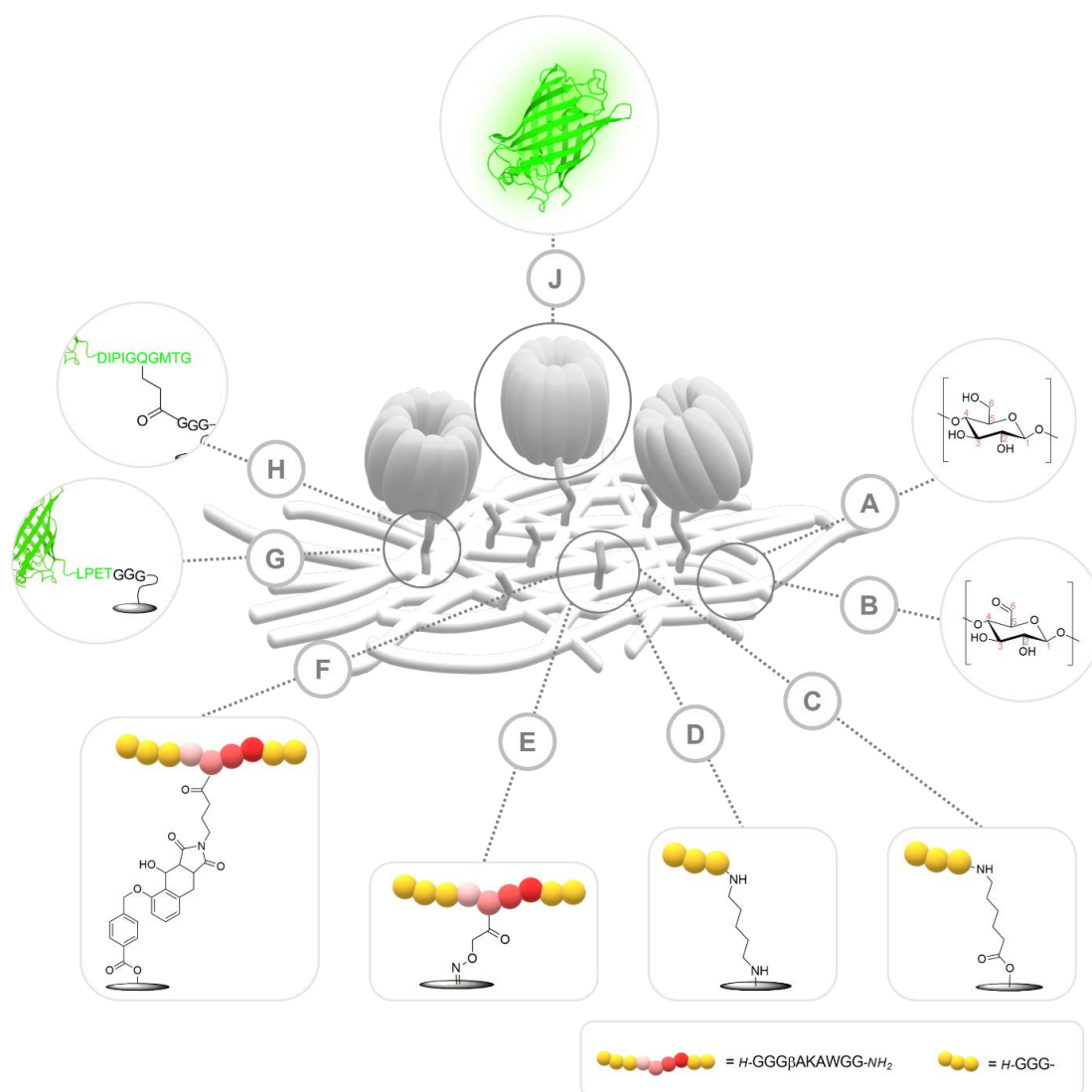


Figure 12: Overview of the tested immobilization strategies. Starting materials are cotton-based substrates **A** treated with NaOH to increase amorphous regions in the fibers and **B** fibers reacted with TEMPO, NaBr and NaClO to generate reactive aldehydes in AGUs. Letters **C** to **F** depict the examined combinations of linkers and recognition sequences. **C** 6-aminoheptanoic acid and the triglycine building block were coupled subsequently on type **A** starting material. **D** Cadaverine and the triglycine building block were coupled subsequently on type **B** starting material. **E** A synthetic recognition peptide bearing an aminoxy linker was reacted with type **B** material. **F** Material of type **A** was first modified with a photoreactive moiety that undergoes a chemical reaction with the maleimide-bearing synthetic recognition peptide. The final connection of functional proteins with peptide/paper hybrid materials is depicted in **G** for srtA ligation and in **H** for mTG ligation. **J** The functional protein to be coupled with the cellulosic support, here tGFP. Protein structure for visualization from PDB for tGFP (GFP; PDB-ID: 1EMA).⁹⁷ Modified after Liebich et al.¹⁰¹

In the second part of this work, the toolbox of modular covalent protein conjugation on paper was extended to four approaches. Each one was finally realized with not only sortase A, but also microbial transglutaminase-mediated ligation. Thus, two derivatives of tGFP served as model proteins in semi-quantitative comparative studies. Figure 12 shows an overview of the peptide immobilization strategies, and products of the enzymatic ligations of part II.

3.1.2. Cellulosic material

For the first part of this work, commercial cotton-based filter papers were used. Medium-fast filtrating papers (Macherey Nagel MN616 or Whatman® Grade 40) were chosen, showing no significant disruption under chemical and low mechanical treatment.

The second part of this work was performed on unmodified cotton linters fibers (Grade 225 HSR-M, Buckeye Technologies) or TEMPO-oxidized ones.

3.1.3. Chemical linkers and peptides

The linker is the key component of the setup in this work, as it has the purpose to furnish a paper with a peptide that comprises an enzyme recognition sequence in a covalent manner. Four chemically different conjugation strategies were employed (Figure 13). The build-up of the peptide linkers on paper are presented in this subchapter. The final peptide load is analyzed with 2,4,6-trinitrobenzenesulfonic acid (TNBS) solution (for part I see chapter 3.2.2 and for part II chapter 3.5.1).

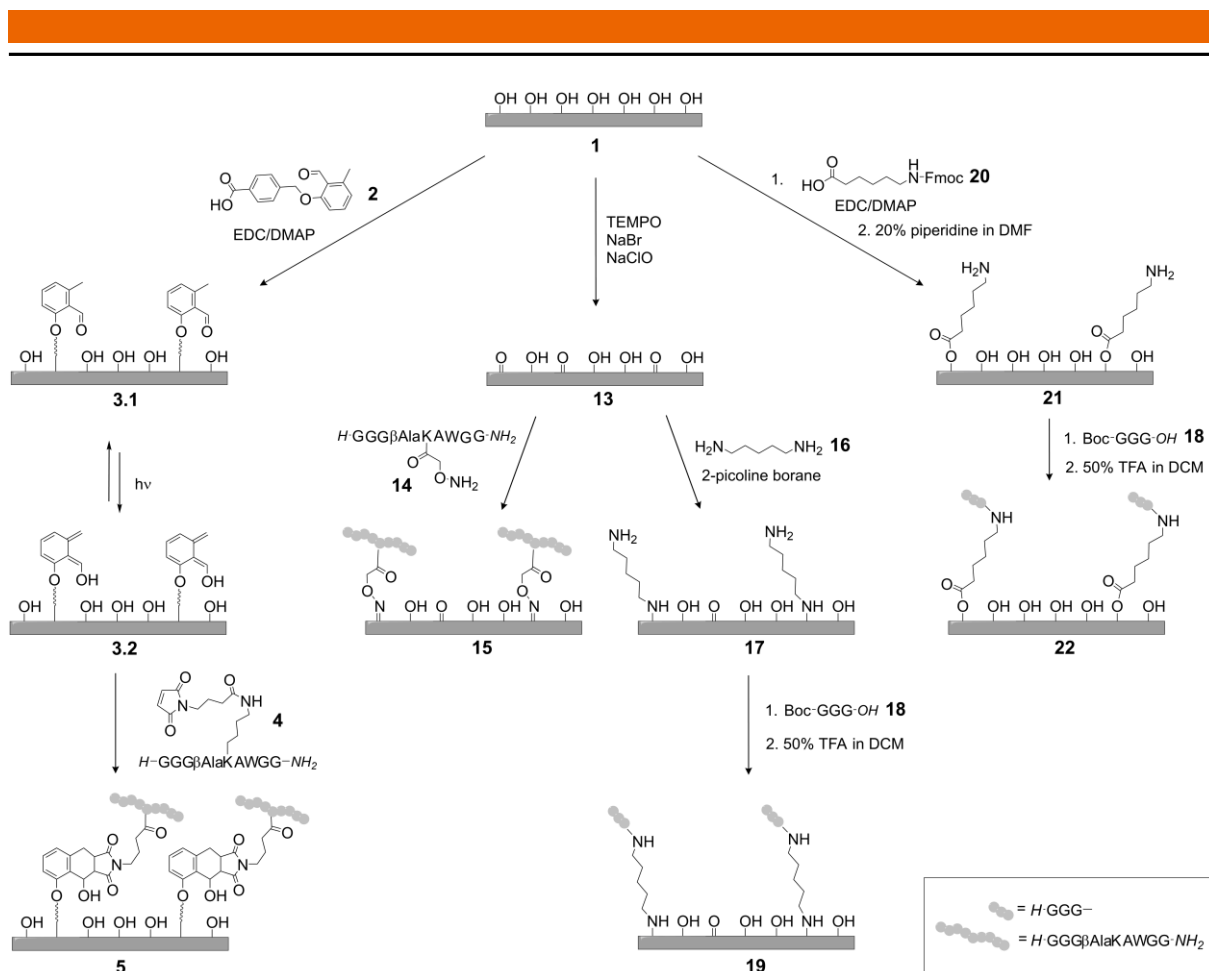


Figure 13: The four tested strategies for peptide immobilization on cellulose paper are depicted. Strategy 1: Light-controlled approach resulting in **5**. Strategy 2: Oxime ligation approach resulting in **15**. Strategy 3: Reductive amination approach resulting in **19**. Strategy 4: Esterification approach resulting in **22**.

Strategy 1: Light-controlled approach

In the first part of this work, a photoreactive moiety was introduced to paper in a first step via a carbodiimide-mediated esterification. This reaction with DMAP as catalyst allows for a direct coupling of a carboxylic acid to cellulose hydroxyl groups.

Under irradiation with intense UV-B light, the linker experiences a tautomeric shift, which generates dienes in the *o*-quinodimethane derivative, able to react in a Diels-Alder reaction. The Diels-Alder reaction is a click-type reaction, commonly appreciated in organic chemistry for regio- and stereo-selectivity. The classic [4+2] cycloaddition yields a new cyclohexane ring between a diene and a dienophile, like a maleimide, by simultaneous bond breakage and formation. Thus, up to four contiguous stereogenic centers can arise in this single reaction step. From two possible stereoselective products that can be generated under mild conditions, the endo-product is the preferred one. The molecule builds two dienes, an endocyclic and an exocyclic one. Both can contribute to a Diels-Alder reaction; however, the exocyclic diene is preferred. Additionally, the formation of the 1,2-disubstituted regioisomer is favored over the

formation of the 1,3-isomer.^{102–104} The scheme for the grafting of the recognition sequence following strategy 1 is given in Figure 14.

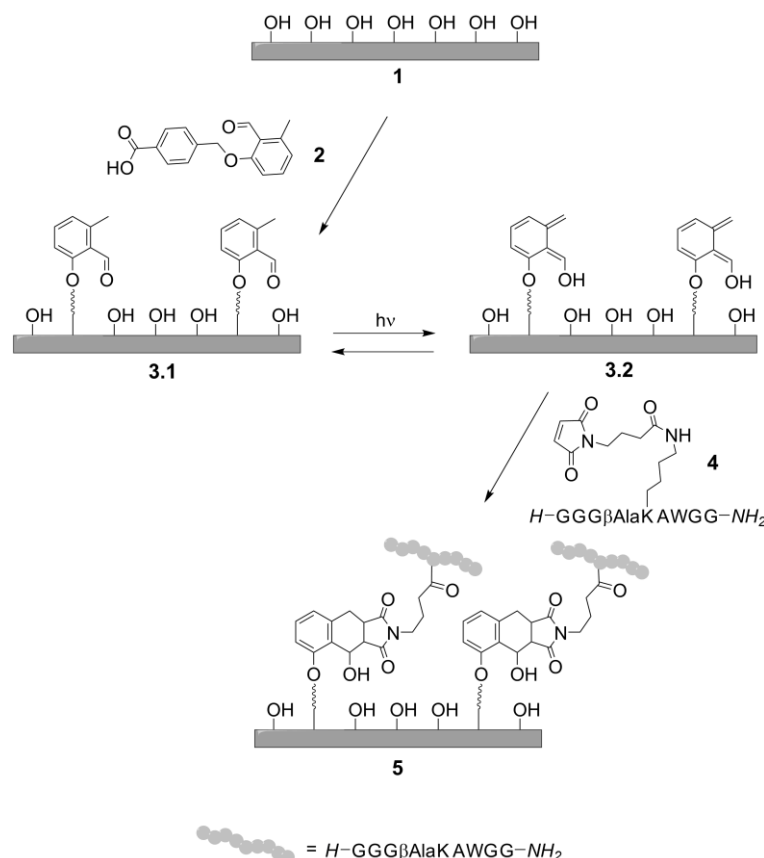


Figure 14: Synthesis of paper 5.

The underlying peptide immobilization strategy was first reported by Barner-Kowollik et al.⁹⁴ on cellulose surfaces. However, the experimental setup of the previous investigation was different. Thus, preliminary studies were performed with this approach.

The photoreactive compound 4-((2-formyl-3-methylphenoxy)methyl)benzoic acid **2** was synthesized in four steps from 2, 3-dimethylanisole, as reported by Oehlenschlaeger et al.¹⁰⁵ and Pauloehrl et al.¹⁰⁶ (Figure 15). A detailed description of the synthesis can be found in chapter 7.7.2.

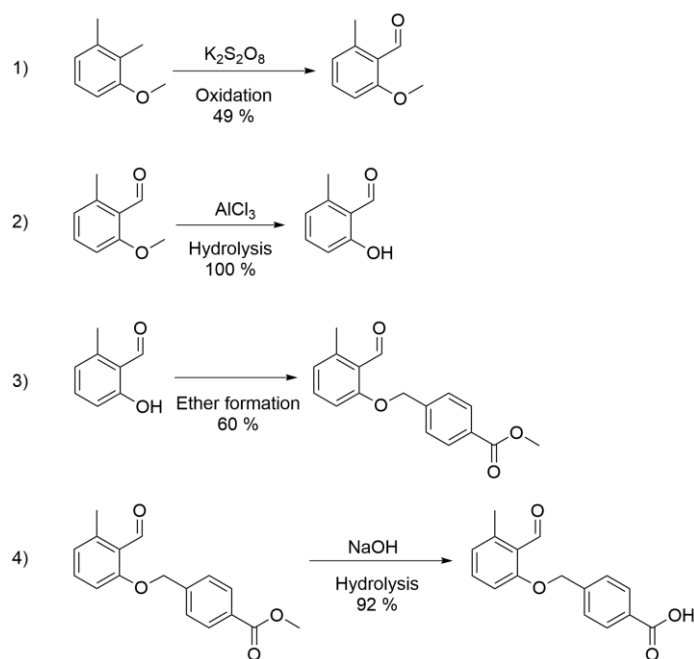


Figure 15: Four-step synthesis of 4-((2-formyl-3-methylphenoxy)methyl)benzoic acid **2** (photoenol **2**) starting from 2, 3-dimethylanisole. After Pauloehr et al.¹⁰⁶

The photoenol **2** was tethered by esterification under carbodiimide activation (Figure 16) to the prepared cellulosic support **1**. The resulting photoenol-paper **3.1/3.2** was analyzed by X-ray photoelectron spectroscopy and confocal laser scanning microscopy (CLSM, 3.2.1).

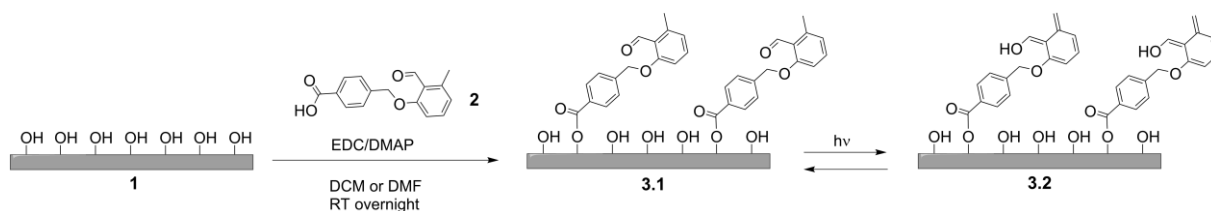


Figure 16: Carbodiimide-mediated attachment of the photoenol moiety **2** to hydroxyl groups on fibers **1** resulting in products **3.1/3.2**.

The enzyme-recognition peptide **4** carried a maleimide for effective conjugation to photoenol **2** and three subsequent glycines at the *N*-terminus for effective enzymatic ligation. A tryptophan residue was introduced for analytical and purification reasons, due to pronounced absorbance of this amino acid's residue at 280 nm. The spacer amino acid β -alanine was introduced, as in preliminary experiments instead of the oligoglycine sequence, a fluorophore was coupled. As degradation occurs for some fluorophores coupled *N*-terminally through SPPS by the Edman pathway, the introduction of a spacer, a non α -amino acid can avoid this phenomenon.¹⁰⁷ Eventually, TAMRA was the chosen fluorophore, which did not show this degradation effect. However, the presence of β -alanine as spacer allowed for the free choice of chromophore. The

required maleimide-functionality was coupled to the lysine side chain after sequence completion. Therefore, Dde-protected Fmoc-lysine was coupled as a standard building block during SPPS. Dde was selectively cleaved by repeated treatment with 2 % hydrazine in dry DMF or in a mixture of hydroxylamine hydrochloride and imidazole in NMP. When the ϵ -amine was completely deprotected, 4-maleimidobutyric acid was coupled under standard HATU/DIPEA activation. The peptides were purified by preparative RP-HPLC and analyzed by analytical RP-HPLC and ESI-MS (chapter 7.4). The designs of peptides **4** and **4.1** are depicted in Figure 17.

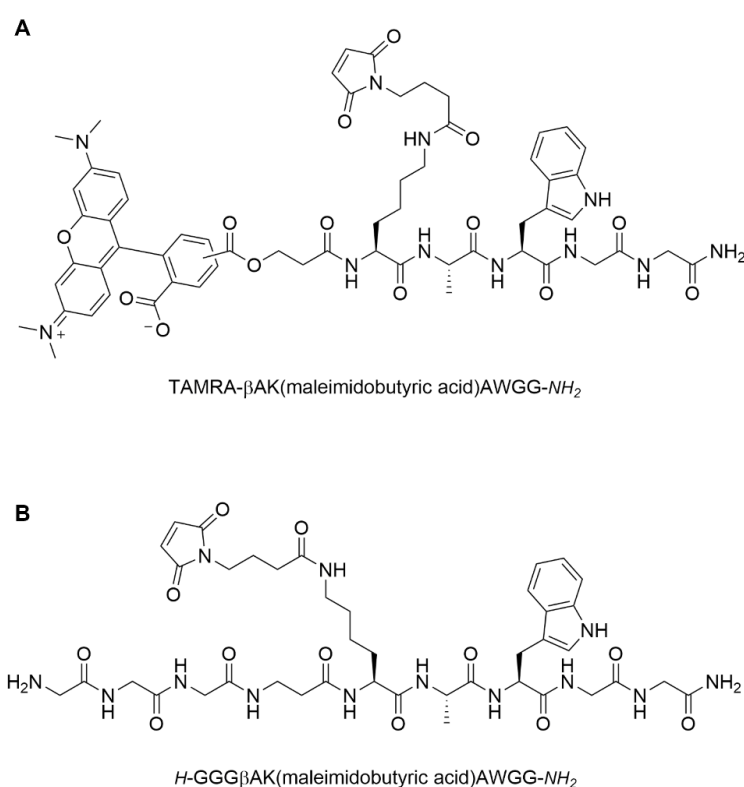


Figure 17: **A** TAMRA-peptide **4.1** for the light-controlled approach. **B** Recognition peptide **4** for the photochemical approach.

For the proof-of-concept studies of this first approach, ready filter papers, standardized by a hole puncher to 1.6 cm in diameter, were furnished first with the photoenol compound. Therefore, the functionalized paper was placed in a self-made photoreactor. The reactor consisted of a shortened 20 mL syringe, closed at the outlet, and equipped with a frit. On top of the paper substrate a copper foil was placed. This was punched with a star shaped cavity to serve as template. It was fixated on the paper by piercing the template / paper / filter-sandwich with two sterile cannulas (Figure 18). Further studies in the first part of this work were

performed on standardized papers with 0.5 cm in diameter, that were fully functionalized, without a photo-pattern.

For light-controlled Diels-Alder coupling peptide **4** or **4.1** was dissolved in dry DMF and added to the paper substrate. The setup was flushed with inert gas and subsequently irradiated with a terrarium light bulb emitting UVB-light in comparably high intensities, as the photoenol absorbs at approx. 350 nm and below. Thorough washing of the support results in products **5/5.1**.

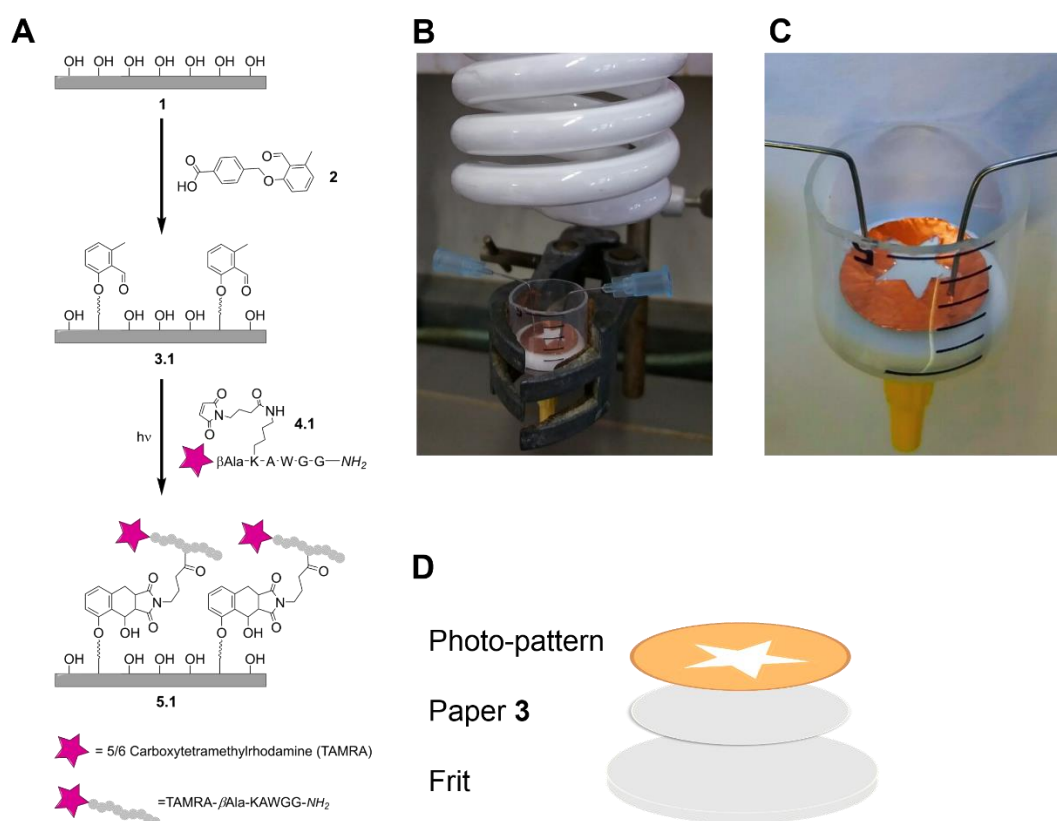


Figure 18: **A** Reaction scheme for the proof-of-concept experiment with the fluorescently labeled peptide **4.1**, which is coupled in a Diels-Alder reaction to material **3.1** under irradiation, resulting in product **5.1**. **B** Experimental setup for the preliminary studies comprising a photoreactor and a UV B terrarium lamp. **C** Enlarged image of a photoreactor. **D** Sketch of the photo-pattern sandwich. Modified after Hilberg et al.¹⁰⁰

Strategy 2: Peptide coupling via oxime ligation

The oxime ligation approach was the second strategy developed for efficient peptide conjugation. Like strategy 1, the oxime ligation approach is a strategy performed with a pre-synthesized and purified peptide. The decisive difference for this strategy; the peptide was

coupled to aldehydes in TEMPO-oxidized cotton linters fibers, compared to conversion of hydroxy groups from the first strategy. A robust oxime ether bond was formed under aqueous conditions at pH 4.5 between TEMPO-oxidized cotton linters fiber **13** with an aminooxy moiety bearing counterpart **14**, resulting in material **15** (Figure 19).



Figure 19: Oxime ligation of peptide **14** with TEMPO-oxidized fibers **13** resulting in fibers **15**.

The synthesis of the recognition peptide with the side chain modification of lysine in the center of the sequence **14** (Figure 20) was similar to peptide **4**, as both have the same backbone. In this case, the deprotected ϵ -amine was reacted with NHS-activated ethoxy-ethylidene protected aminooxyacetic acid and DIPEA for maximum one hour in DMF. After acidic global resin cleavage, the peptide was purified by preparative RP-HPLC and analyzed by analytical RP-HPLC and ESI-MS (see experimental section 7.4.4).

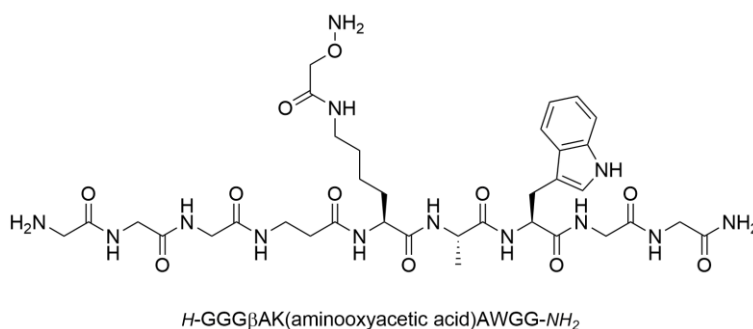


Figure 20: Recognition peptide **14**.

Strategy 3: Reductive amination as first step of peptide grafting

The third approach relies on reductive amination of TEMPO-oxidized cotton linters fibers with excess cadaverine. Then the peptidic sequence is completed by the coupling of a Boc-protected triglycine building block. Compared to the previous two methods, the peptidic sequence is not pre-synthesized but directly assembled on the fibers (Figure 21).

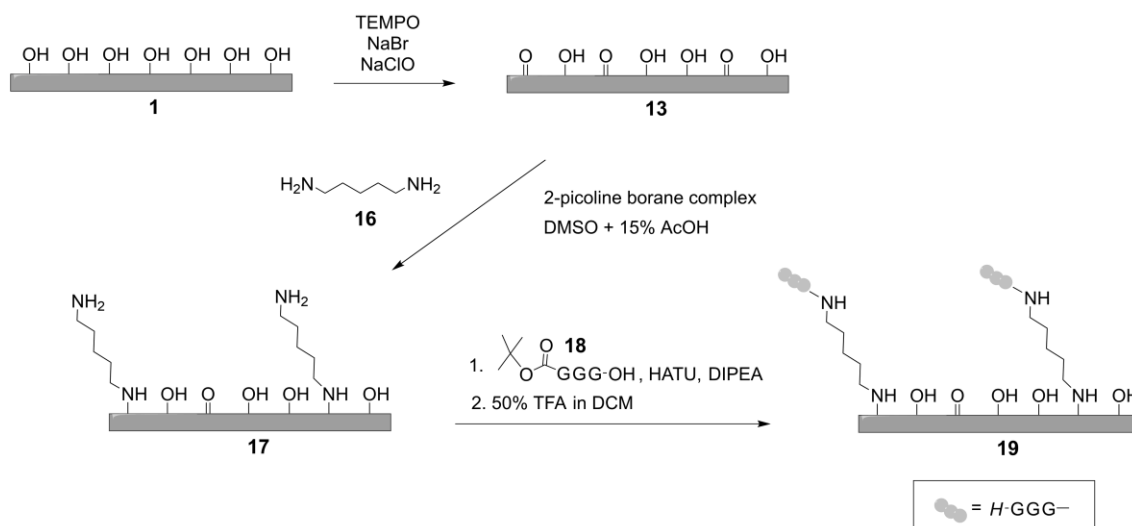


Figure 21: Build-up of the peptidic sequence after strategy 3. Cadaverine **16** is coupled with 2-picoline borane complex by reductive amination to TEMPO-oxidized fibers **13**. Subsequent coupling of Boc-GGG-OH **18** followed by Boc-deprotection results in fibers **19**.

TEMPO-oxidized cotton linters **13** were reacted with cadaverine **16** following reductive amination mechanism. Therefore, the oxidized fibers were incubated for two hours with 2-picoline borane complex and cadaverine **16** in DMSO with 15% acetic acid. Exhaustive excess of the reagents was used to avoid inter-fiber cross-linking with the unprotected cadaverine. Afterwards, product **17** was thoroughly washed and equilibrated with DMF. A commercially available *N*-Boc protected triglycine building block **18** was coupled under standard HATU/DIPEA activation. The fibers **19** were prepared by Boc-deprotection with 50% TFA in DCM.

Strategy 4: Esterification as first step of peptide grafting

For this last approach tested, initial coupling to cotton linters was performed employing the esterification reaction with EDC and DMAP as used in strategy 1 for the photoenol. The build-up of the recognition sequence was performed step by step on the fibers, similar as in strategy 3 (Figure 22).

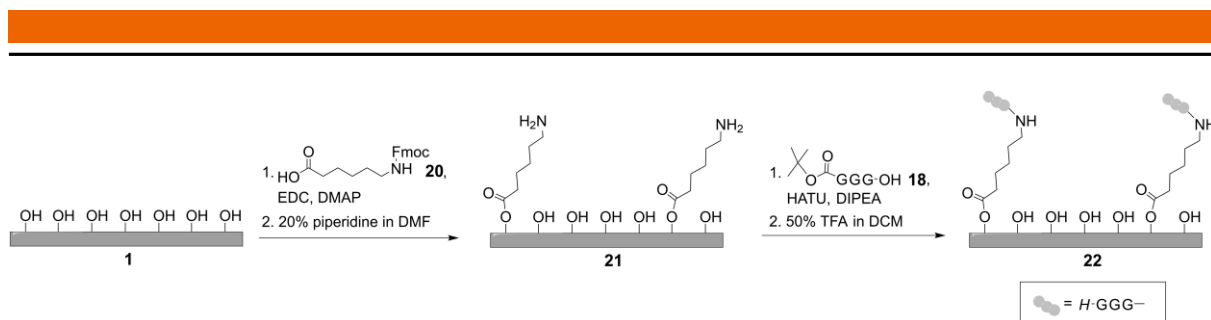


Figure 22: Build-up of the peptidic sequence under strategy 4. Fmoc-6-aminohexanoic acid **20** is coupled under HATU/DIPEA activation to fibers **1**. Subsequent Fmoc-deprotection with 20% piperidine in DMF results in **21**. Coupling of Boc-GGG-OH **18** followed by Boc-deprotection results in fibers **22**.

The first step is the carbodiimide-mediated esterification of hydroxyl groups from the cotton linters fibers **1** with Fmoc-protected 6-aminohexanoic acid **20**. A triglycine building block **18** is coupled to the free amine on intermediated **21** in a subsequent step, under standard SPPS conditions with HATU and DIPEA. Fibers **22** are prepared, as in strategy 3 by Boc-deprotection with 50% TFA in DCM.

3.1.4. Enzymatic ligations and protein design

The covalent and site-specific immobilization of a protein requires a sophisticated ligation strategy. Enzymatic ligation reactions allow for the connection of very specific counterparts under mild conditions. The herein reported toolbox relies on the potential of two very well characterized enzymes. Ligation products of part I (Figure 23) are inspected by fluorescence imaging of tGFP (see chapter 3.2.3), enzymatic assay for mTG or paper-based ELISA for ZZ-domain¹⁰⁸ (both see chapter 3.2.4). Ligation products of part II were analyzed after fluorescence imaging (see chapter 3.5.2 and 3.5.3) and CLSM (see chapter 3.5.4)

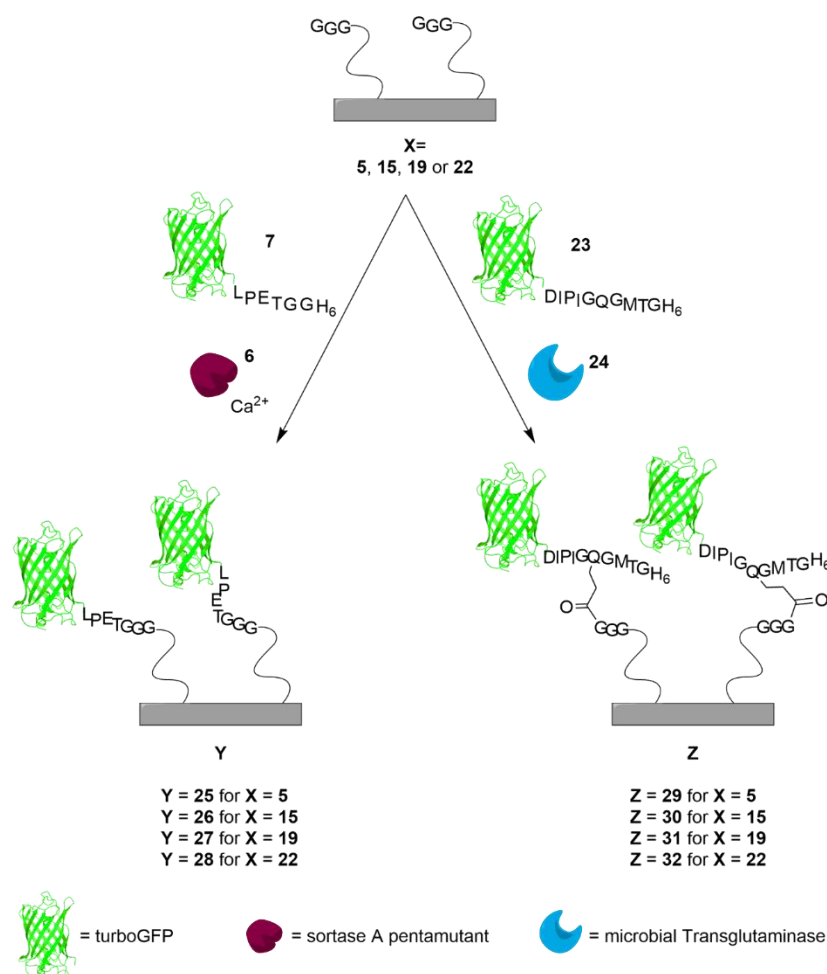


Figure 23: Sortase A (6) -mediated ligation of tGFP-LPETGGH₆ 7 with to GGG-modified cellulose X resulting in tGFP immobilized product Y is depicted. mTG (24)-mediated of tGFP-DIPIGQGMTGH₆ 23 to GGG-modified cellulose X resulting in tGFP immobilized product Y is depicted. Protein structure for visualization from PDB for tGFP (GFP; PDB-ID: 1EMA).⁹⁷

Sortase A ligation

Introduced in 2004, sortase A has shown its great potential in the immobilization of proteins on solid supports. Furthermore, improved variants regarding reaction rates or Ca²⁺ dependency were developed. The sortase A pentamutant is still a Ca²⁺ dependent variant, but ligates the same motifs as the wild-type enzyme, up to 120-times faster.⁵⁷ Thus, amino acid sequences of the model peptide or the functional proteins were decided to carry the C-terminal amino acid sequence -LPETG- for the studies of this work.

The matching part chosen for the immobilization on the paper fibers counts three subsequent N-terminal glycines, which is the minimum number of glycines reported to obtain competitive yields by ligation with sortase A.¹⁰⁹

Microbial transglutaminase ligation

Microbial transglutaminase is a transpeptidation enzyme that, in contrast to sortase A, is not restricted to the sequence's termini for efficient action. Instead, it forms an amide bond between a primary amine, such as lysine and a glutamine residue in a specified environment.⁸⁰ Thus, meaning not every glutamine residue in a protein sequence is suitable for transglutaminase-mediated reaction.

Consequently, the reported, very potent sequence -DIPIGQGMTG-⁸⁶ was introduced at the functional proteins C-terminus for the experiments performed within this work. Usually, lysine residues represent the amine substrate. Proteins usually present several lysine residues on their surface. Therefore, prior to being used for ligation on papers, the suitability of mTG as ligating enzyme is assessed, as oligomerization of the model protein presents a risk.

Additionally, it was shown, that mTG also effectively takes *N*-terminal glycine as the amine substrate.¹¹⁰ Thus, being somewhat flexible in terms of the amine substrate, for the mTG ligation experiments, the papers with the same peptide functionalization, as for the sortase A ligation experiments, were used.

3.2. Part I: Light-controlled peptide immobilization

3.2.1. Proof-of-concept studies

A reported procedure for the light-induced coupling of a model peptide onto a cellulose surface, was used as a starting point.^{94,106} However, the material, conditions and instrumentation used in the present work differed from the reported ones, as well as further subsequent modifications of the functionalized cellulosic support was carried out. Therefore, preliminary studies on commercially available filter papers were performed to verify the usability of the chosen method.¹¹¹

Evidence for effective coupling of the photoenol on paper with XPS and CLSM



Figure 24: Carbodiimide-mediated attachment of the photoenol moiety **2** to hydroxyl groups on cotton linters **1** resulting in product **3.1/3.2**.

The carbodiimide-mediated esterification of PE and accessible hydroxyl groups of the paper (Figure 24) was analyzed by X-ray photoelectron spectroscopy (XPS). A comparison of the spectra of modified paper (Figure 25 C) and a control sample, which is plain paper treated under the same conditions without the photoenol-moiety present (Figure 25 B), showed the introduction of PE was successful. Aromatic carbon ($E = 284.6$ eV) is elevated in modified paper and confirms the presence of the molecule on the surface. The content increased relatively to 6.91%, starting from 0.34 % in the control sample. Furthermore, the content of carboxylic groups ($E = 289.5$ eV) has risen from 3.57 % to 6.69 %, which is another indicator for successful functionalization. The outcome of the XPS analysis is in accordance with the previously reported work.⁹⁴ Based on this result, the EDC-mediated esterification on paper will be regarded as effective. Thus, for further carbodiimide-mediated esterification reactions on paper no more XPS analysis was performed.

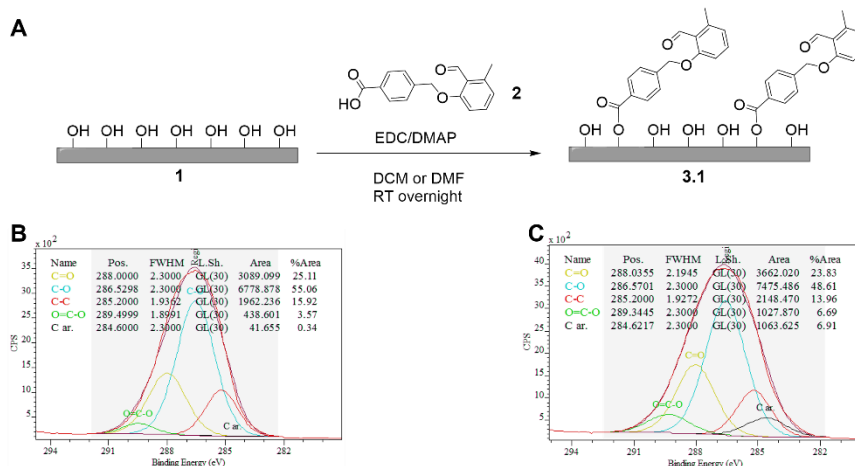


Figure 25: (A) Carbodiimide-mediated attachment of the photoenol moiety **2** to hydroxyl groups on cotton linters **1** resulting in product **3.1**. C 1s XPS spectra of paper **1** (B) and photoenol functionalized paper **3** (C). Modified after Hilberg et al.¹⁰⁰

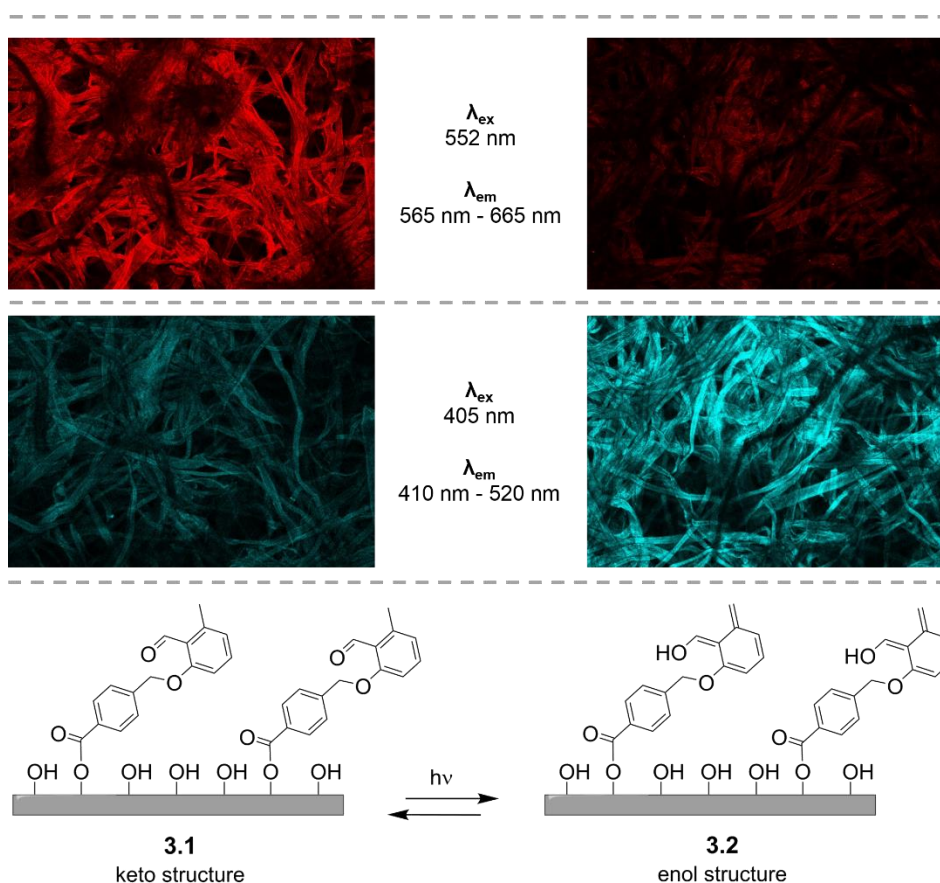


Figure 26: CLSM images visualizing the tautomers of a photoenol-functionalized cellulosic paper. Modified after Hilberg et al.¹⁰⁰

To generate the conditions for an effective peptide immobilization by Diels-Alder reaction in a subsequent step, the irradiation of the molecule **2** with UV-B light is necessary to trigger a tautomeric shift in the molecule, so the caged diene is exposed. This tautomeric shift was

observed with CLSM. A photoenol-modified paper was irradiated with UV-B intense light, while one part of the paper was shaded from above, thus generating the two tautomeric species on the same paper. To detect the existence of the two tautomeric forms (Figure 26) the different regions in the paper were irradiated at 405 nm or 552 nm. Indeed, the keto form emits stronger at an excitation wavelength of 552 nm, whereas the enol counterpart, the Diels-Alder reactive one, shows higher fluorescence upon excitation at 405 nm. Thus, imaging at these wavelengths offers a convenient method to distinguish between the two isomers and is another proof for the effective coupling of the photoenol on the cellulosic support.

Light-controlled Diels-Alder coupling of a fluorescently labeled peptide

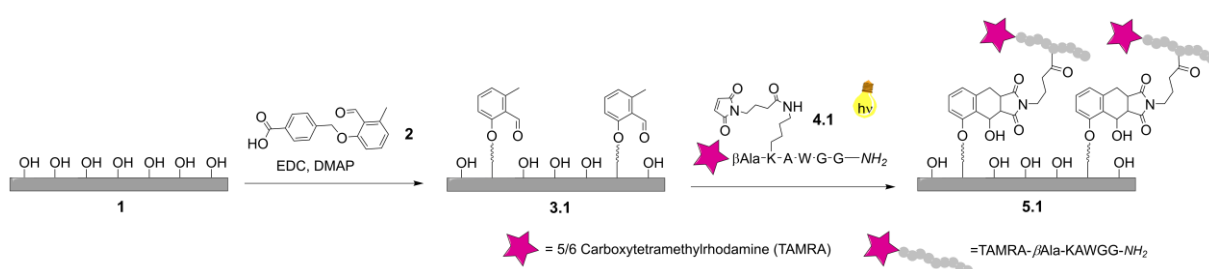


Figure 27: Reaction scheme for proof-of-principle experiment under strategy 1. Reaction starting with paper **1** via the PE-paper **3.2** to result in an immobilized fluorescently labeled peptide on paper (**5.2**) via Diels-Alder coupling. Modified after Hilberg et al.¹⁰⁰

After the verification for the effective PE functionalization of paper was given, the fluorescently labeled peptide 5/6-TAMRA-βAK(4-maleimidobutyric acid)AWGG-NH₂ was coupled in the subsequent proof-of-concept experiment (Figure 27), namely Diels-Alder reaction with the self-made photoreactor. As the results from XPS and CLSM analysis do not allow for a quantification of the photoactive moiety loaded on the paper, the peptide was taken in large excess. A star-shaped photo-pattern was placed between the photoenol functionalized paper and the light source. The peptide, dissolved in dry DMF, was filled in the photo-reactor, and purged with inert gas throughout the reaction. Coupling of the peptide was carried out successfully, as can be easily seen by the naked eye in the photograph (Figure 28).

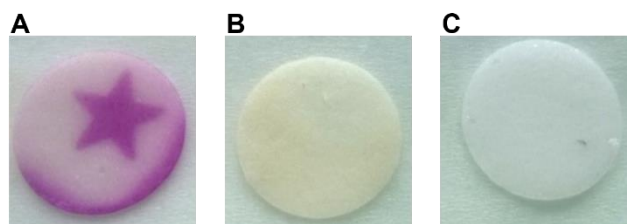


Figure 28: **A** Light-controlled Diels-Alder product **5.1** of photoenol-functionalized paper with a fluorescently labeled model peptide **4.1** in the self-made photoreactor. **B** Control reaction for CLSM of a photoenol-functionalized paper in the absence of the model peptide. **C** Control reaction for CLSM of unmodified filter paper in the presence of the model peptide. Modified after Hilberg et al.¹⁰⁰

As expected, due to the photo pattern, a spatial discrimination of areas with and without the colored peptide, is obtained. Not only the “star”, but the border of the paper is colored, too. As the copper stencil was a flexible foil, that was only fixated with two needles in the lower layers, this could be expected, as most probably light scattering occurred. Two control reactions were carried along as references, a photoenol-functionalized paper irradiated in the absence of the peptide and the adsorption control on unmodified paper, which was irradiated in the presence of the peptide. None of the controls shows the typical TAMRA color by visual inspection. There is only a light-yellow coloring of the PE-functionalized paper detectable compared to the adsorption control.

All materials, the desired one, as well as the controls were analyzed by CLSM with an excitation wavelength of $\lambda_{\text{ex}} = 552 \text{ nm}$ and a detection window of $\lambda_{\text{em}} = 570 \text{ nm} - 640 \text{ nm}$. The analysis of the CLSM images confirms, what could be seen by the naked eye (Figure 29). Completely unmodified paper (Figure 29 A), as well as PE-paper control without contact to the model peptide (Figure 29 B) are practically non-fluorescent under the chosen conditions during fluorescence imaging. The negative control, plain paper incubated with the model peptide and thoroughly washed afterwards, shows little fluorescence under the chosen imaging conditions, probably caused by adsorption of small amounts of the TAMRA-labeled peptide (Figure 29 C). The fluorescence intensity is equal to that of regions of the desired product, that were protected from UV light by the pattern (Figure 29 D). The fluorescence in the shaded region of the patterned material is therefore most probably also mainly caused by adsorption of small amounts of peptide. Furthermore, the described observations indicate, that the potential fluorescence of the photoenol detected in a prior experiment (Figure 26) does not interfere with the peptide's fluorescence emission and the effect is therefore irrelevant under the given conditions. The obtained results allow for the assumption, that the chosen method and instruments are suitable for the defined purpose.

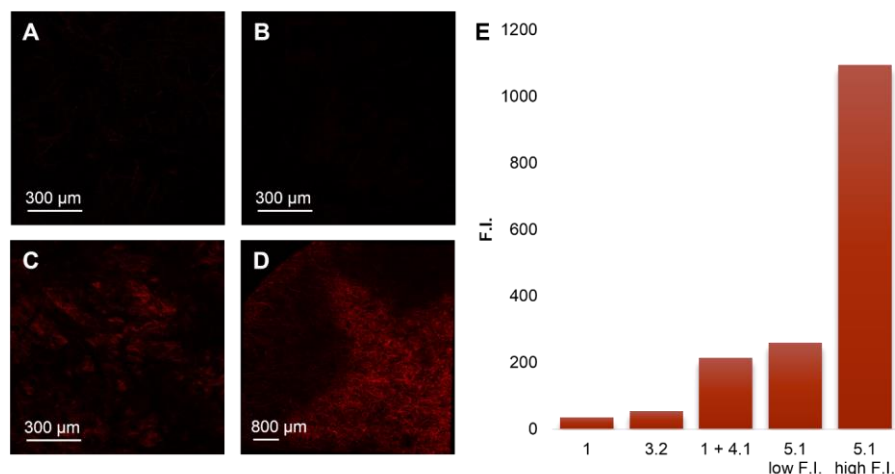


Figure 29: CLSM Images Ex: 552 nm, Em: 570-640 nm. **A** Plain filter paper **1**. **B** PE paper in the absence of the model peptide **3.2**. **C** Plain filter paper previously in contact with the model peptide (**1**+**4.1**). **D** Product **5.1**. **E** Analysis of the CLSM images. Fluorescence intensities are depicted as a mean of the whole image for images **A**-**C**. For image **D** the mean of three spots in the visually brightest (**5.1**, high fluorescence) and darkest regions (**5.1**, low fluorescence) was built.

Light-controlled Diels-Alder coupling of the recognition sequence and sortase A-mediated ligation of tGFP

Consequently, the next step was the immobilization of the enzyme recognition sequence **4** *H*-GGGβAlaKAWGG-NH₂ on paper (Figure 30).

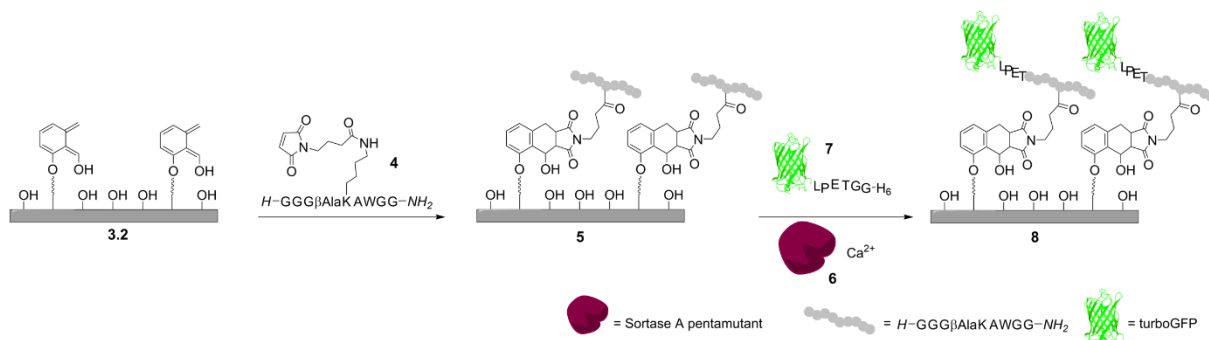


Figure 30: Reaction scheme for the subsequent immobilizations of the recognition peptide **4** to PE functionalized paper **3.2** resulting in peptide-functionalized paper **5**., and tGFP-LPETGGH₆ resulting in product **8**.

The peptide was immobilized in the star-shaped pattern (Figure 31). Experiments with fluorescence imaging showed that, when the full-length linker, consisting of the Diels-Alder product of the photoenol and the recognition peptide, is immobilized on the paper and is irradiated by UV-light at 365 nm, an emission is observed at around 595 nm (Figure 31 **B**). Subsequently tGFP⁹⁵ with the engineered C-terminal LPTEGG-tag⁴⁹ **7** was successfully immobilized with sortase A pentamutant **6** on paper **5** resulting in product **8** as depicted in

Figure 31 C. To ensure a successful conjugation, tGFP was used in large excess during sortase A-mediated ligation under physiological conditions (see experimental section 7.7.6). Thorough washing after the reaction time with 0.05% TWEEN-20 in PBS ensured the removal of adsorbed proteins. The images of the tGFP fluorescence and the autofluorescence of the Diels-Alder conjugate match very well in the overlay (Figure 31 D). The obtained result proves the suitability of the chosen strategy for site-specific protein immobilization with the addition, that the protein can be immobilized homogenously and in a localized fashion.

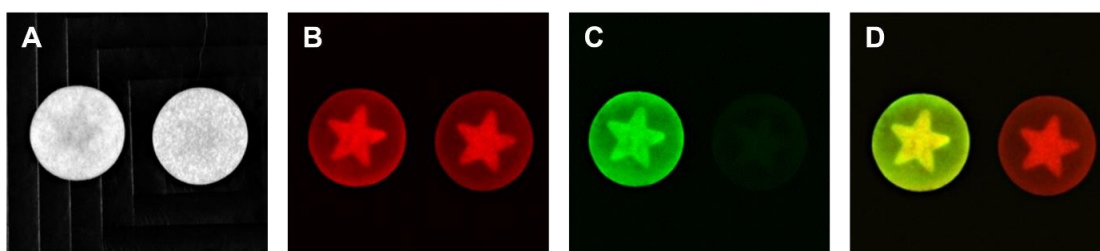


Figure 31: **A - D** PE (right) and a tGFP-functionalized paper (left) with a star-shaped-pattern. **A** White light photograph **B** Fluorescence image $\lambda_{\text{ex}} = 365 \text{ nm}$, $\lambda_{\text{em}} = 595 \text{ nm}$. **C** Fluorescence image for tGFP detection in product **8** $\lambda_{\text{ex}} = 480 \text{ nm}$, $\lambda_{\text{em}} = 535 \text{ nm}$. **D** Stacked mage of **B** and **C**. Modified after Hilberg et al.¹⁰⁰

3.2.2. Quantification of primary amines on paper

The next interesting question was about the loading density reached with the approach. In a first step the amount of immobilized peptide on the paper should be identified. The TNBS assay was developed for this purpose as an indirect quantification method. As the nitrogen in the primary amine at the peptide's *N*-terminus reacts as a nucleophile with the TNBS molecule, the aromatic compound gets substituted, the hydrogen sulfite ion is released and the product, the orange colored triphenyl amine is built (Figure 32). In solution this molecule can be analyzed in a UV-Vis spectrometer at 335 nm.

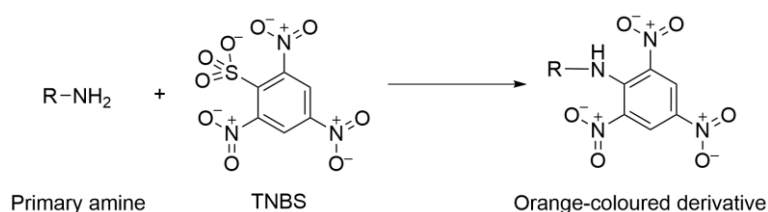


Figure 32: Nucleophilic aromatic substitution reaction underlying the TNBS quantification method.

As the analyte is attached to a solid support, the reaction was performed as an indirect quantification assay (see experimental section 7.6). Therefore, excess TNBS solution was added to the paper disc on which the peptide was immobilized. After the reaction time, a defined amount of the solution was taken out of the reaction and added to a standard solution with an excess of an amino acid (glycine or β -alanine) with known concentration. When the reaction time of this second step was up, the reaction was stopped by the addition of a stopping solution containing hydrochloric acid. The absorbance of the product was analyzed in a UV-Vis spectrometer at 335 nm. With the known parameters of the reagent and the standard solution, the actual amount of peptide, immobilized on the paper can be determined by back titration calculations.

To this end, the peptide was immobilized on standardized filter papers with a diameter of 0.5 cm, without the use of a stencil, with the afore described method (see experimental section 7.7.5). Using the back-titration method for these papers a surface loading of $7.8 (\pm 0.44) \mu\text{mol}$ peptide per gram of paper or $87.9 (\pm 5.0) \text{ nmol/cm}^2$ was calculated for the experiment performed in triplicate. This result is comparable to amounts reached with spot synthesis (1.8 to 280 nmol/cm^2) a multiple synthesis technique for the generation of peptide arrays on membranes including cellulose ones.¹¹²

3.2.3. Protein quantification of immobilized model protein tGFP

Based on the afore mentioned results, the obtained protein load was the next highly interesting question. Therefore, tGFP was chosen again as the model protein for immobilization on standardized peptide-paper discs. The big advantage of a fluorescent protein for this purpose is the direct readout of the fluorescence via a fluorescence imaging technique compared to e.g., using enzymes and their dedicated activity assay, which needs a special substrate, so that the readout would only be an indirect one.

To this end, tGFP was immobilized with sortase A on paper discs with 0.5 cm diameter without stencil (Figure 33 A). An adsorption control sample was carried along, in which no enzyme was added to the tGFP solution for reaction with the paper carrying the recognition sequence. Comparing fluorescence signals (CLSM images) of both samples clearly indicated a successful enzyme-mediated ligation of the tGFP to the paper, due to strong emitted fluorescence. Contrary, the control sample exhibited only a small signal, indicating that adsorption of the protein to the paper is negligible.

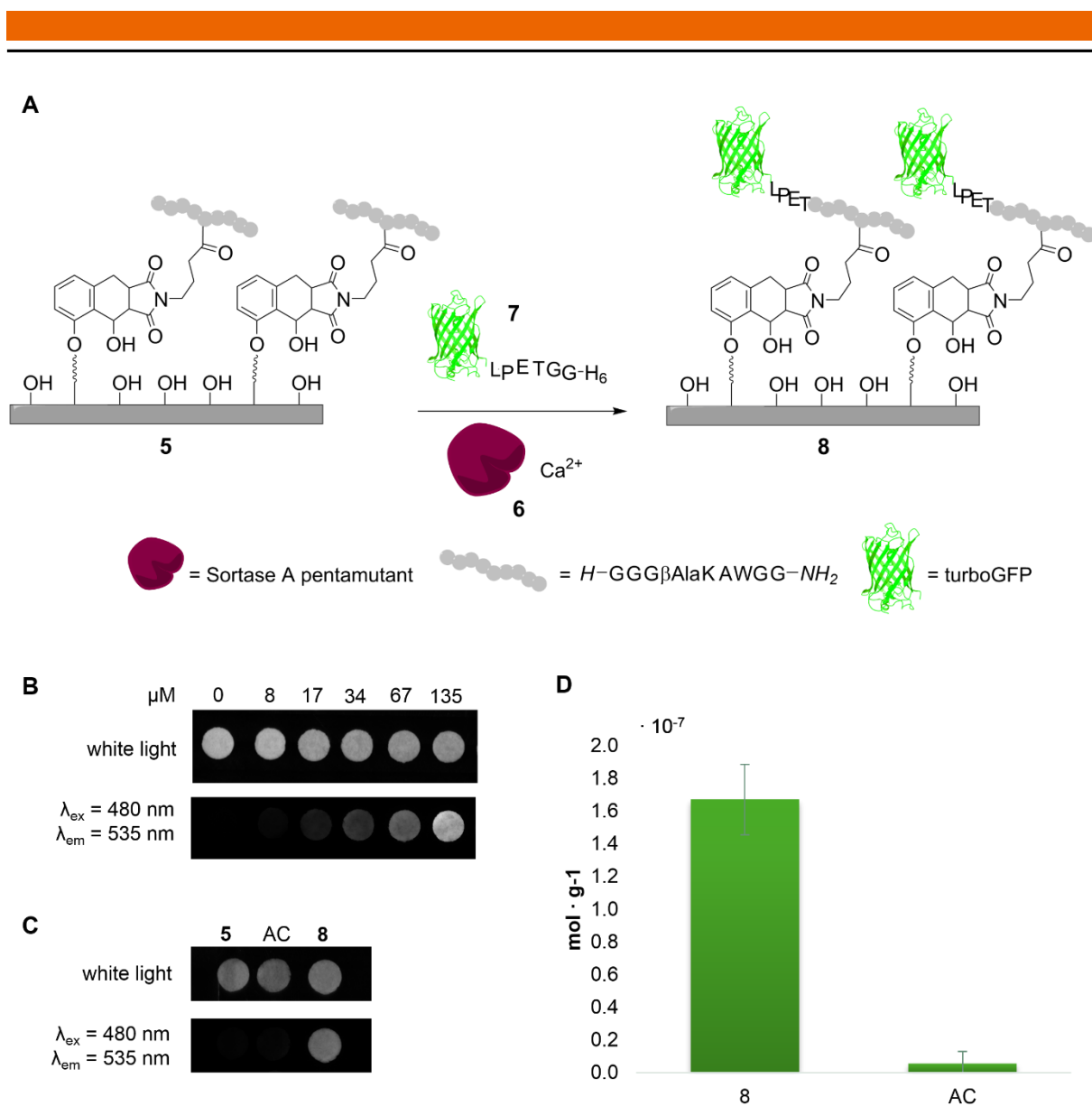


Figure 33: **A** Sortase A-mediated modification resulting in product **8**. **B** White light and fluorescence images of the standard curve. **C** White light and fluorescence images of one sample set consisting of a paper disc immobilized with peptide **5**, the adsorption control sample (AC) and the desired product **8**. **D** Result after comparison of the fluorescence intensities of the samples against the standard curve ($n = 9$). Modified after Hilberg et al.¹⁰⁰

For quantification of the immobilized protein, a standard curve was generated (Figure 33 **B**). Therefore, tGFP at different concentrations was dropped onto standardized, plain filter paper. The fluorescence signals (Figure 33 **C**) of the ligation products and the adsorption controls were compared to the freshly prepared standard curve. Samples **5** were carried along as blank correction. Obtained images were analyzed using Fiji software.¹¹³ Calculations based on the fluorescence signals suggest an amount of $0.17 (\pm 0.02) \mu\text{mol}$ tGFP immobilized per gram paper (Figure 33 **D**) or $19.4 (\pm 2.4) \text{ pmol/mm}^2$. The obtained results exceed the values for covalent immobilization on solid supports and approximate those achieved with non-covalent techniques.^{114–118} Very potent non-covalent immobilization strategies employ CBM,

carbohydrate binding modules, designed for specifically binding cellulose, and achieve binding capacities between 0.32 and 1.56 $\mu\text{mol/g}$.^{52,119,120} The methods are not entirely comparable, as steric hindrance during sortase A ligation near the ligation anchors close to the paper surface is probable. However, coming near those numbers for non-covalent approaches shows the potential of the afore demonstrated method.

3.2.4. Sortase A-mediated ligation of proteins with different biologic function

To show that the modular method is suitable for a broad range of proteins, further proteins with different biologic functions were immobilized and tested for activity. The enzyme microbial transglutaminase (mTG) was chosen, for which a well-established activity assay is available.¹²¹ Thus, evidence for functionality after immobilization was collected. Additionally, the ZZ-domain, a high affinity protein binding the Fc parts of a variety of IgG antibodies, derived from protein A,¹⁰⁸ was chosen to test a third type of protein. Therefore, a paper-based ELISA was chosen.

Transpeptidation enzyme: mTG

Catalyzing the formation of an isopeptide bond, mTG is established as a versatile tool in many different areas, from the food industry to hot scientific fields like engineering of antibody-drug conjugates.^{86,122} mTG is a highly efficient acyl transferase with low substrate discrimination.^{123,124} Therefore, the enzyme was immobilized as pro-peptide fusion, that ensures inhibition of the mTG activity throughout the sortase-mediated ligation. After immobilization of pro-mTG to standardized paper discs loaded with the recognition peptide, the pro-sequence was cleaved with dispase, a neutral protease.

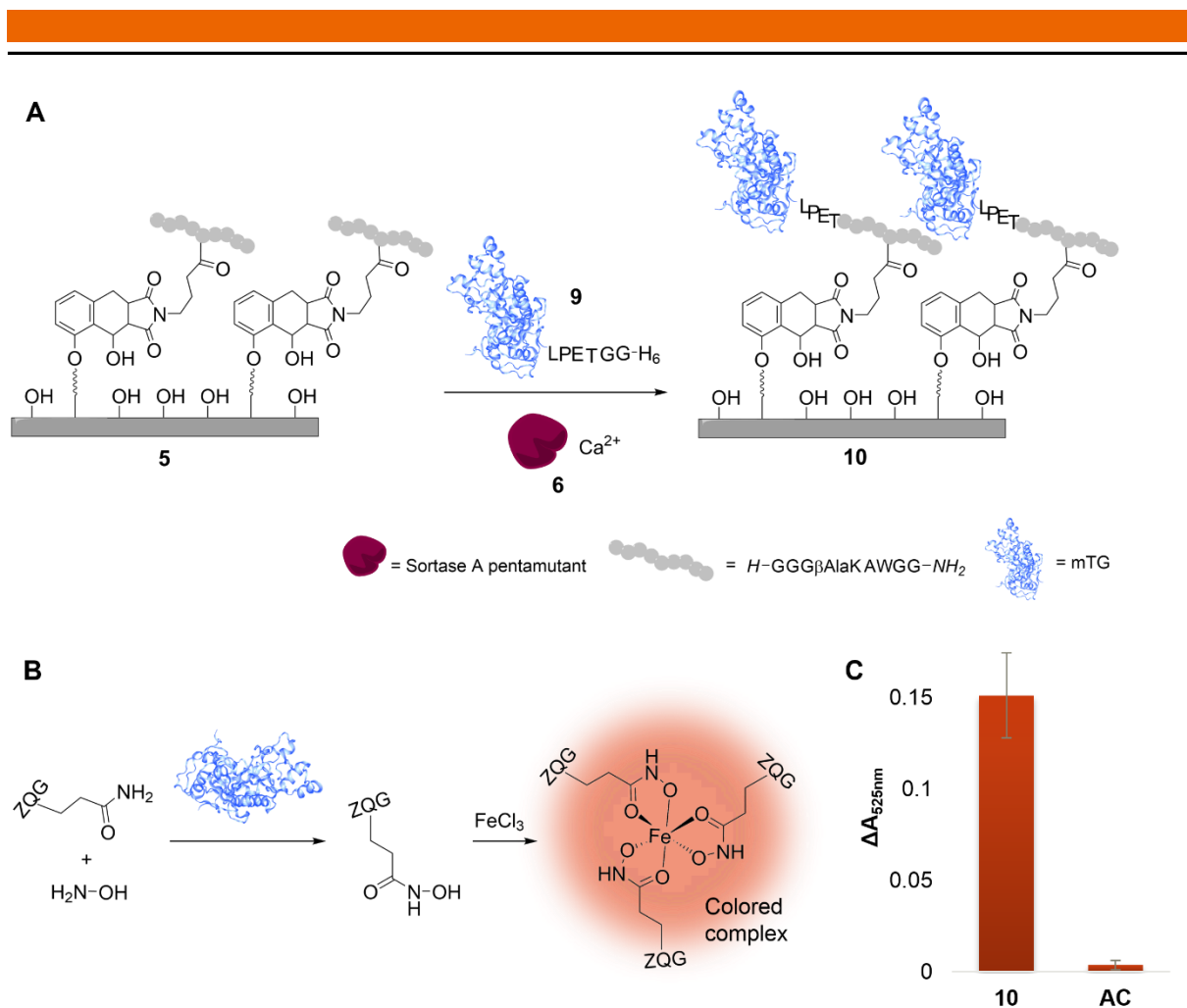


Figure 34: **A** Sortase A-mediated modification resulting in product **10**. **B** Reaction of the hydroxamate assay with the substrates ZG and hydroxylamine, which are converted by mTG catalysis. The product forms a colored complex with iron(III) which is detectable at 525 nm. **C** Semi-quantitative result of the readout of the hydroxamate assay with the desired product **10** and the adsorption control (AC). Protein structure for visualization from PDB for mTG (PDB-ID: 1IU4)⁹⁸. Modified after Hilberg et al.¹⁰⁰

The activity of the paper-immobilized mTG (Figure 34 A) was tested with the prevalent hydroxamate assay (Figure 34 B).^{121,125} Here, mTG catalyzes the reaction of hydroxylamine with the substrate Z-Gln-Gly-OH. Thus, the mTG-grafted papers were incubated in a solution containing the respective substrates for 10 minutes. Upon the addition of iron (III)-chloride in trichloroacetic acid to the reaction mixture a colored chelating complex was formed. For read-out the absorbance of the complex was detected by UV-Vis spectrometry at 525 nm. Figure 34 C shows the data plotted against an adsorption control, which did not comprise sortase A during the immobilization reaction. The figure indicates that the immobilized enzyme is active and that no, or only a negligible amount of mTG was bound by the paper due to adsorption.

High-affinity domain: ZZ-protein

As the active domain in protein A, Z-protein is able to bind the Fc part of several IgG antibodies by affinity interaction.¹⁰⁸ The repetitive unit ZZ-domain, is a convenient alternative to protein A, being producible in high yields combined with low-cost purification, and showing an efficiency comparable to that of protein A in immunoassays and affinity purification of IgG from serum.^{126,127} To show the effective immobilization of the ZZ-domain on peptide-modified paper (Figure 35 A) and to demonstrate its activity, the protein was immobilized using the presented method and assessed in a paper-based ELISA as modified from Whitesides et al.¹²⁸ (Figure 35 B).

ZZ-domain was immobilized on standardized paper discs of 0.5 cm in diameter. After the paper was dried at ambient temperature, it was blocked with a suspension containing 5 wt.-% of non-fat dry milk in PBS-T for 10 min. The paper was incubated with human IgG (hIgG) for 5 min at room temperature and thoroughly washed with PBS. Subsequently it was incubated for 5 min in a solution containing a horseradish peroxidase (HRP) coupled detection antibody derived from goat, meaning the detection antibody cannot be bound by the ZZ-domain, thus avoiding cross reactivity. The paper was thoroughly washed again and developed in a microtiter plate with a 4-chloro-1-naphthol/ H₂O₂ substrate solution, which forms a colored precipitate upon HRP turnover. Controls were performed simultaneously. For a readout the microplate was scanned and the obtained images were analyzed using the Fiji software.¹¹³ Comparing the signal intensities of the samples shows a significant coloring of the ZZ-functionalized paper to which all components of the assay were applied, while all controls exhibit only low signals compared to blank paper, indicating non-specific binding of the antibodies was successfully disabled (Figure 35 C).

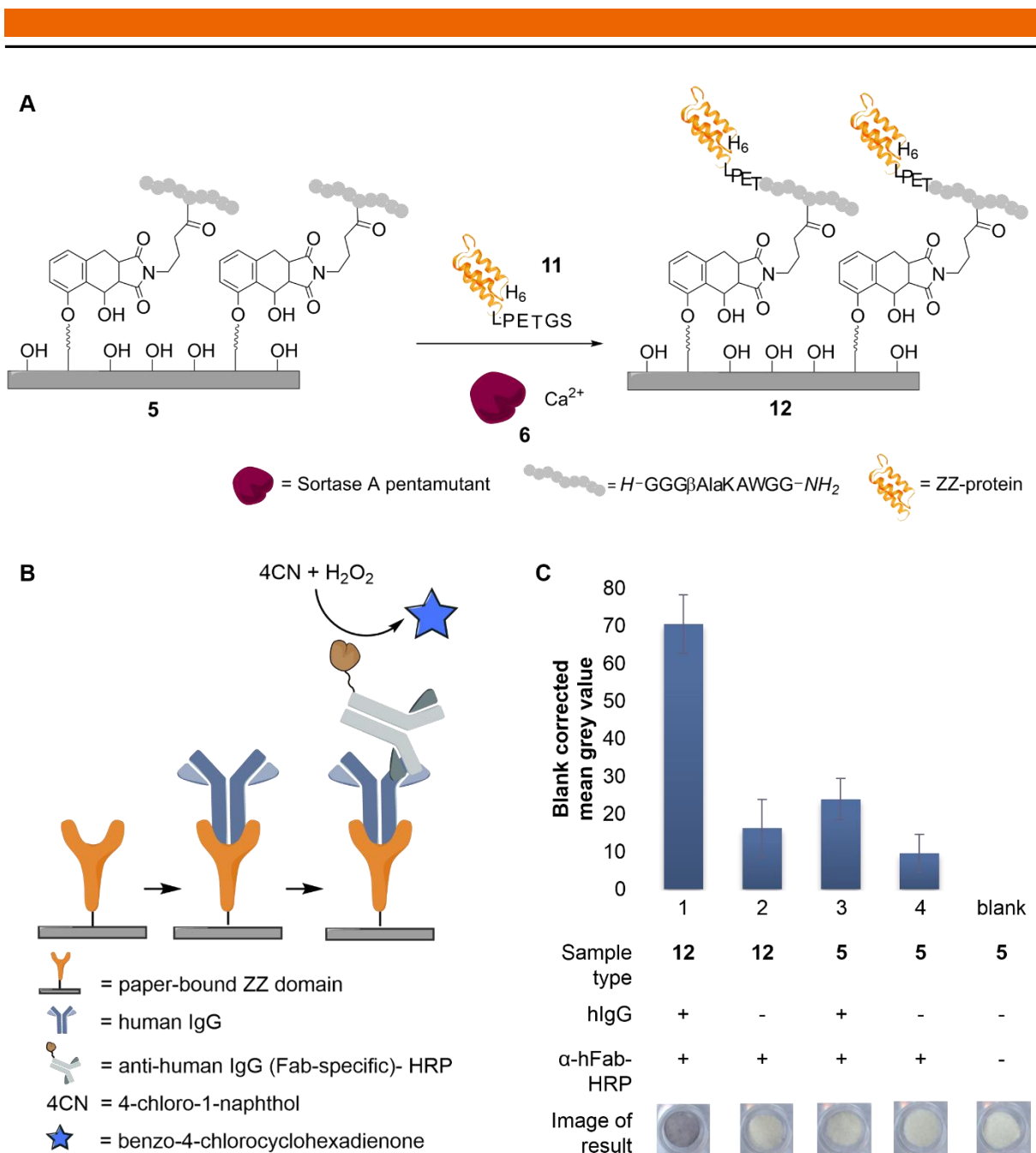


Figure 35: **A** Sortase A-mediated modification of **5** resulting in product **12**. **B** Scheme for the sequential procedure for the paper-based ELISA including the steps of analyte incubation, secondary antibody incubation and color development. **C** Result and overview of the performed paper-based ELISA with the respective controls ($n = 3$). "+" and "-" indicate whether the substance was added to the sample or not. "Image of result" represents an exemplary assay outcome. Modified after Hilberg et al.¹⁰⁰

3.3. Summary: Part I

In this part, the light-controlled approach was evaluated for suitability of the immobilization of proteins on cotton linters-based filter paper. In two steps, a linker was grafted to accessible hydroxyl groups of paper. The first step, the carbodiimide-mediated esterification of a photoenol, was successfully verified by XPS, which showed that especially the aromatic carbon content in the paper had increased due to the photoenol introduction. With CLSM, it was possible to visualize the shift of the enol tautomer, by excitation of UV light-irradiated or non-irradiated regions on a PE-functionalized paper, respectively. In a second step for the linker assembly, a fluorophore-labeled peptide was immobilized on the esterified paper with a stencil under irradiation with UV-B light in a self-made photoreactor in the frame of a proof-of-concept study. The positive result was observed by the naked eye and further confirmed applying a more detailed analysis of the fluorescence intensities from CLSM images. For the eventual protein immobilization, a peptide containing a recognition sequence was immobilized similar to the fluorophore-labeled peptide, with the stencil. Finally, a tGFP derivative compatible with sortase A, was immobilized using the enzyme-mediated conjugation in the “star” shape on paper. Both species, the linker, and the tGFP, could be distinguished from each other by fluorescence imaging.

Quantification strategies were developed for the determination of immobilized recognition peptide and fluorescent protein. The number of primary amines, respectively the amount of immobilized peptide in paper 5, was quantified indirectly using TNBS. The result is comparable to the reported amounts. tGFP was quantified via fluorescence imaging by comparing intensities of immobilized tGFP to a standard curve of tGFP at different concentrations adsorbed to standardized plain papers. Results are in the order of magnitude as obtained for very potent high-affinity binding employing CBM.

Two more functional proteins were immobilized using the presented strategy 1 and tested for functionality with specific assays. Pro-mTG was coupled on paper with sortase A to avoid mTG activity during the immobilization reaction. After the pro-sequence was cleaved, the mTG activity was successfully detected with the hydroxamate assay. ZZ-domain was chemoenzymatically immobilized on paper and the activity was successfully proven by a chromogenic paper-based ELISA.

3.4. Part II: Preliminary experiments for optimization and variations

Having evaluated the potential of the light-controlled strategy on filter papers, the optimization of strategy 1 and the broadening of the modular concept were consequent consecutive steps. To that end, the approach was transferred to lose cotton linters fibers for the immobilization of the peptidic sequence, instead of commercially available filter papers. A transfer to fibers might lead to denser peptide load corresponding to a greater reactive surface of single fibers compared to filter paper. Additionally, the above-described method is a very sophisticated one, which is the reason why it was pre-assessed. Hence, to expand the toolbox of chemoenzymatic coupling strategies on paper for possible applications, more and presumably simpler strategies were evaluated. Read-out of tGFP-conjugated samples was always performed at 480 nm for excitation and 535 nm for detection, if not indicated otherwise. For better comparison small papers were formed of the modified fibers with the help of a disposable syringe equipped with a frit (see experimental section 7.5).

3.4.1. Strategy 1: Optimization of the light-controlled strategy on fibers

Having found that the linker on paper **5** is fluorescent (see section 3.2.1), it was possible to detect the molecule more easily on paper. Therefore, to optimize the strategy, a set of different coupling conditions was examined. Different amounts of the photoenol in relation to the AGU and respective reactants were immobilized on cotton linters fibers and subsequently were reacted with equal amounts of peptide in the Diels-Alder reaction. Equal ratios of tGFP and srtA were used in the enzyme-mediated ligation for all attempts. Papers were formed after each step with the help of a disposable syringe equipped with a frit and disintegrated again before the next reaction step. The goal was to find with fluorescence imaging the most suitable PE/AGU ratio for the immobilization of the model protein tGFP.

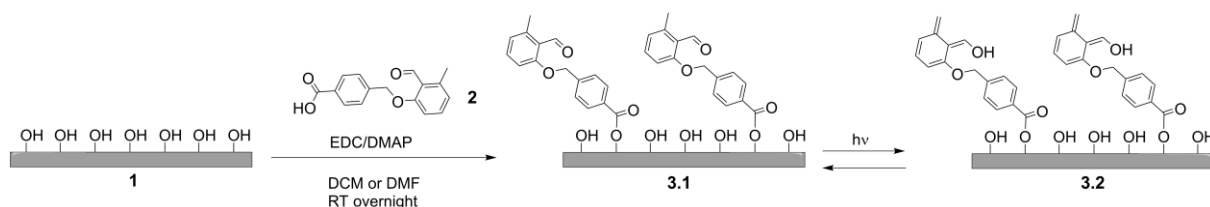


Figure 36: Synthetic approach to paper **5**.

Esterified samples (Figure 36) were analyzed via fluorescence imaging, under the assumption that not only the complete linker, but also the photoenol alone might be fluorescent at the

595 nm when excited at 365 nm and that the mean fluorescence intensity of a sample is dependent on the amount of photoenol coupled to the fibers.

Indeed, the values derived from the analysis of the fluorescence image (Figure 37) indicated that there might be a correlation between the amount of reactant used and the fluorescence at 595 nm (Ex: 365 nm). The fluorescence intensity increased nearly linearly from 0.125 over 0.25 to 0.5 eq. of PE. Interestingly, the trend was not observed further, and fluorescence intensity for 0.5 eq. was higher than for 1 eq. of PE per AGU in the esterification reaction. A possible explanation could be self-quenching of the molecules coupled by the “1 eq.” approach. The quenching effect could have multiple reasons resulting in reduced fluorescence, which is not further investigated at this point.¹²⁹ Furthermore, the fluorescence of the papers at 535 nm (Ex: 480 nm) was negligible, as all samples were almost as fluorescent as the blank under these conditions.

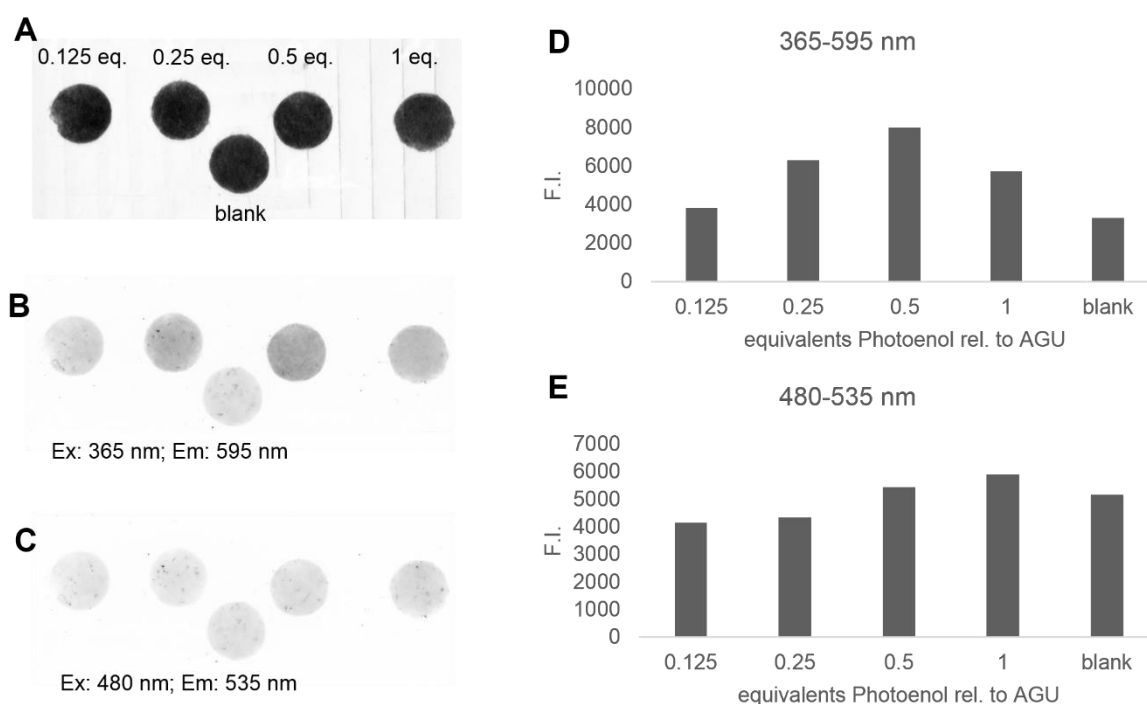


Figure 37: **A - C** (Fluorescence) images of PE coupled to cotton linters fibers and pressed to papers. **A** White light image. **B** Fluorescence image taken from the emission of the papers at 595 nm (Ex: 365 nm). **C** Image taken from the emission of the papers at 535 nm (Ex: 480 nm). **D** Image analysis of **B**. **E** Image analysis of **C**.

For the next step, the Diels-Alder peptide coupling (Figure 38), the papers from the first step were separately disintegrated again. After equilibration to DMF, all fiber slurries were reacted

with the same amount of recognition peptide, irradiated for 10 min, and washed thoroughly before papermaking.

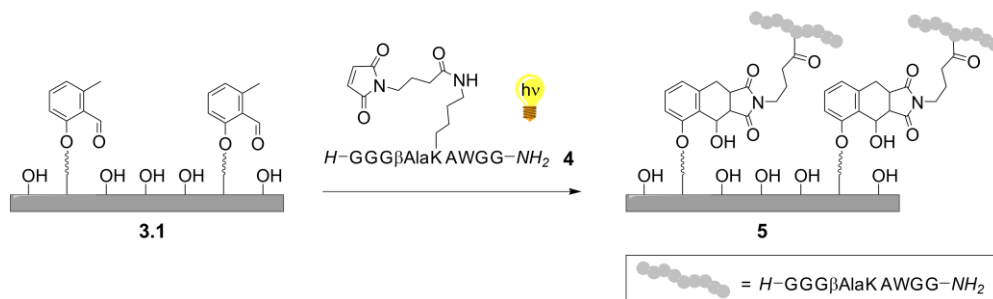


Figure 38: Diels-Alder reaction of fibers functionalized with PE 2 and maleimide-bearing peptide 4 resulting in functionalized fibers 5.

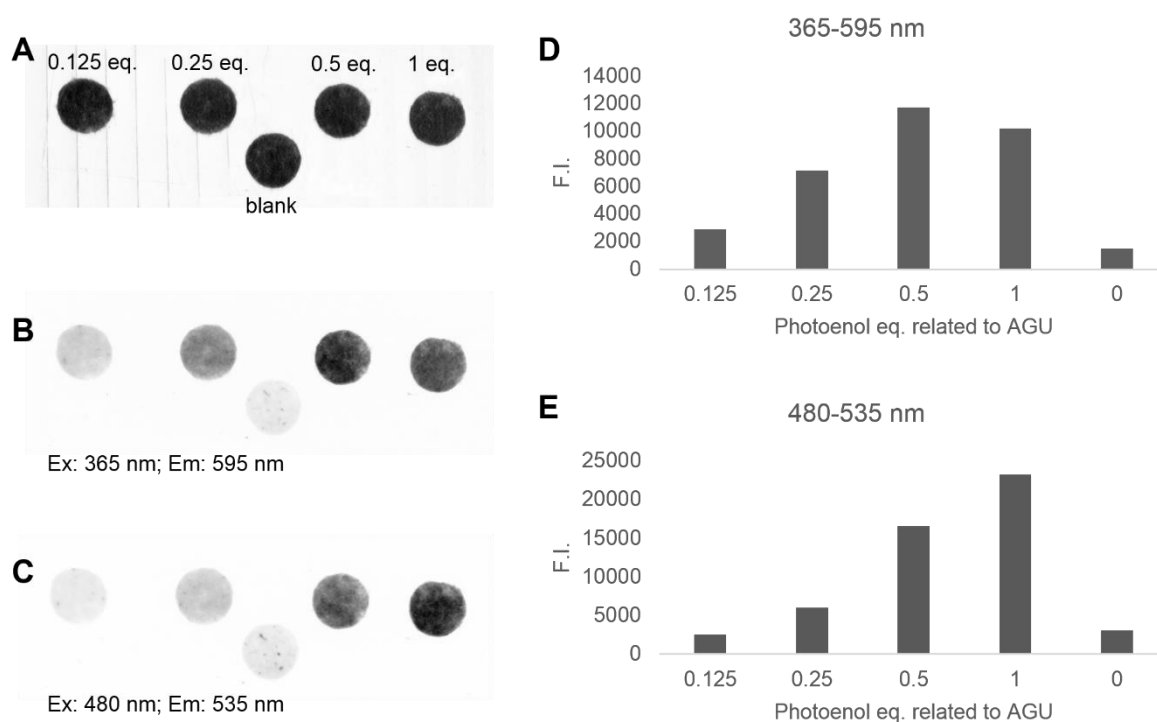


Figure 39: **A - C** (Fluorescence) images of PE and peptide 4 coupled to cotton linters fibers and pressed to papers. **A** White light image. **B** Fluorescence image taken from the emission of the papers at 595 nm (Ex: 365 nm). **C** Image taken from the emission of the papers at 535 nm (Ex: 480 nm). **D** Comparative image analysis of **B**. **E** Comparative image analysis of **C**.

Fluorescence intensities were analyzed. Figure 39 shows that the relative fluorescence intensities at 595 nm stayed approximately the same compared to the experiment before, with the difference that all signals increased compared to the blank. Besides, analyzing the emission

at 535 nm, a correlation between the fluorescence intensity and the amount of peptidic construct was observed, as the fluorescence intensity raised constantly. This is an interesting finding, as we have chosen tGFP as a model protein for all experiments, and the readout was performed at the shown wavelengths for excitation and emission.

For the sortase A-mediated ligation of tGFP with the peptidic fibers, the papers from step two were disintegrated again and conditioned to sortase A reaction buffer. Incubation of the fiber slurries followed for 2 hours at 22 °C in equal mixtures for each approach of tGFP-LPETG and sortase A (0.2 eq. of tGFP) in sortase A reaction buffer (Figure 40). The fibers were thoroughly washed with PBS and papers were formed.

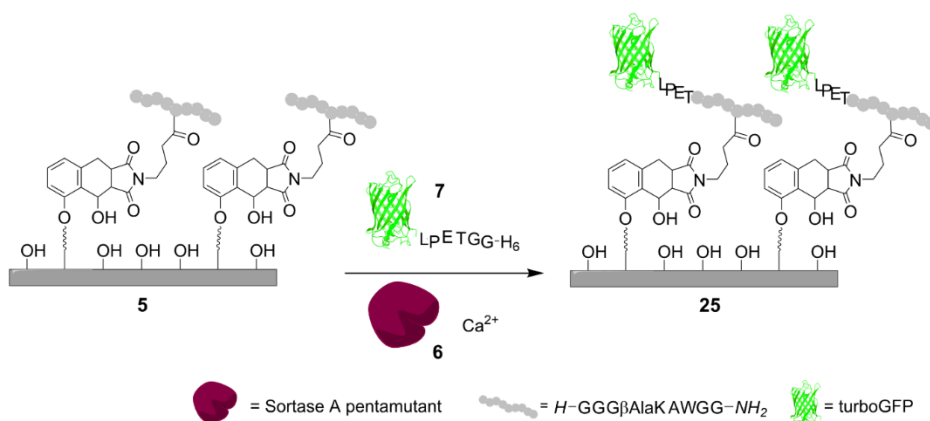


Figure 40: Reaction scheme for the immobilization of tGFP-LPETGGH₆ 7 to peptide-functionalized paper 5 resulting in product 25.

Figure 41 indicates that the fluorescence emission at 595 nm of the samples now increased almost linearly with the amount of photoenol used in the first step. A possible reason could be an interaction of the linker molecule with tGFP, that possibly compensates the effect observed before.

Furthermore, tGFP fluorescence was detected in the samples at 535 nm. Much shorter excitation times, so a less sensitive setup was used compared to the peptidic paper due to stronger tGFP fluorescence. Analyzing the images, the comparison shows that the signals of all samples, except for the blank, are almost equally intensive. However, some differences were observed. Thus, from 0.125 eq. of a photoenol in the underlying reaction to the 0.25 eq. sample, there was an increase in fluorescence signal intensity recognizable. However, the signal decreased again for 0.5 and 1 eq. Given the observation from the second step for these two samples (that the linker molecule consisting of the photoenol and the maleimido-peptide, is itself emitting fluoresce at

535 nm (Ex: 480 nm) to a higher extent) a quenching effect could also be imagined. However, the experiments were performed only once, and this effect was not further investigated. Therefore, the approach with the most promising tendencies, namely the 0.25 eq. one, was chosen for follow-up experiments. The peptide-papers made applying this approach have shown the best outcome of tGFP fluorescence after sortase A-mediated ligation and showed a comparably low self-fluorescence when emission at 535 nm (Ex: 480 nm) was detected.

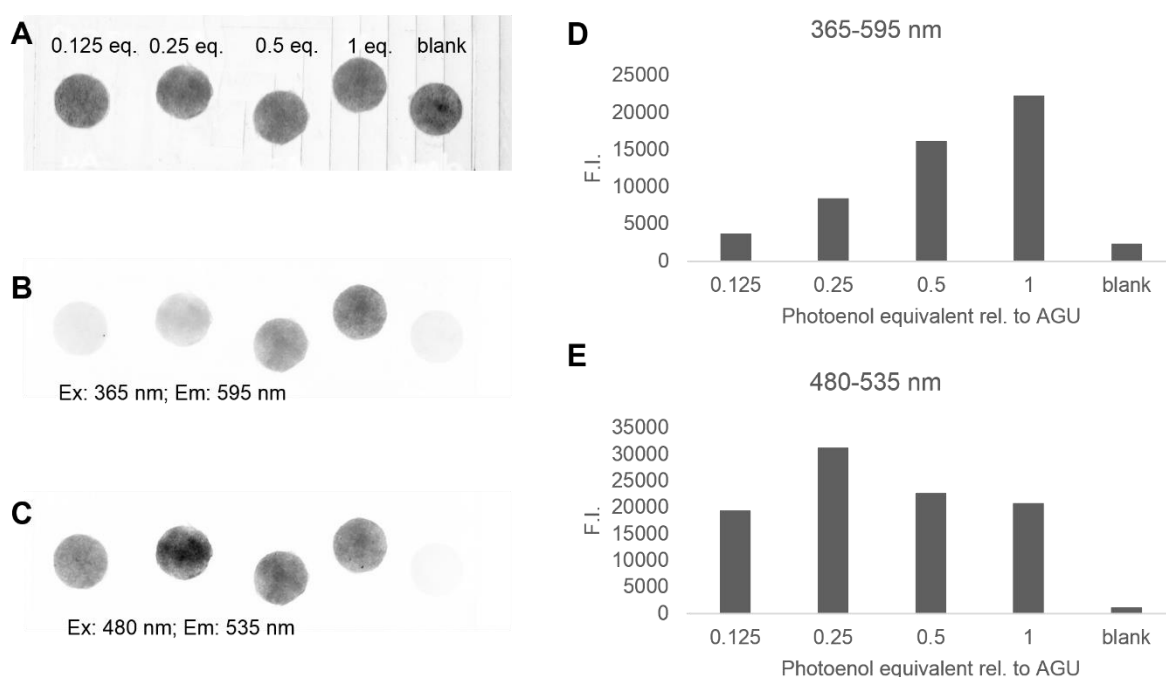


Figure 41: **A - C** (Fluorescence) images of PE and peptide **4** coupled to cotton linters fibers and pressed to papers with following GFP ligation. **A** White light image. **B** Fluorescence image taken from the emission of the papers at 595 nm (Ex: 365 nm). **C** Image taken from the emission of the papers at 535 nm (Ex: 480 nm). **D** Comparative image analysis of **B**. **E** Comparative image analysis of **C**.

3.4.2. Strategy 2: Oxime ligation as a strategy for peptide immobilization

The oxime ligation as an approach for peptide immobilization has been already successfully applied on crystalline nanocellulose (CNC).⁴⁹ However, CNC is structurally very different from cotton linters fibers. Therefore, as a very first experiment TEMPO-oxidized cotton linters were subjected to a reaction with fluorescein thiosemicarbazide, an aldehyde-reactive fluorescein derivative, to verify the accessibility of the aldehyde groups by chemical treatment (data not shown). Further tests were performed with TEMPO-oxidized cotton linters fibers with an aldehyde content of 122 μmol per gram fibers. The fibers were oxidized with 0.3 mmol NaClO

per gram fibers according to the protocol of Saito et al.⁴⁷; as they found this amount of a co-catalyst optimal to achieve the highest aldehyde yield.

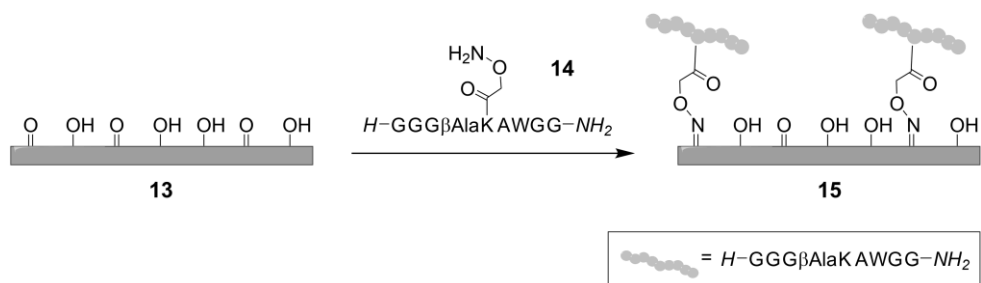


Figure 42: Oxime ligation of peptide **14** with TEMPO-oxidized fibers **13** resulting in fibers **15**.

Favorable reaction conditions for the oxime ligation were examined by using the peptide **14** (Figure 42). As the basic strategy shaking of the setup at ambient conditions in 0.1 M ammonium acetate buffer at pH 4.5 was chosen. In addition, experiments included the use of the catalyst aniline (100mM) or the freezing of the ligation setup without a catalyst at -20 °C, a strategy reported by Agten et al.¹³⁰. Within this comparison, increasing amounts of peptide were tested, ranging from 0.5 to 3 equivalents in relation to the aldehyde content of the fibers, within two hours after the start of the reaction. After thorough washing of the fibers, a standard tGFP/sortase A mixture was added to the slurries and allowed to react at 22 °C for 2 hours. The residual reagents were washed off, papers were manually pressed from the fibers, and the fluorescence was assessed.

Analysis (Figure 43) indicated a high effectiveness in all setups. Indeed, all ligation products have been seen with the naked eye. Minor tendencies towards the catalyzed approaches with aniline and towards higher amounts of applied peptide were detectable (Figure 43 D). Freezing of the samples did not seem to have a beneficial effect over the reaction at room temperature. Differences in the fluorescence intensities between the fluorescence intensities of samples made from larger amounts may also arise from different resulting paper masses. The latter were not determined in this experiment. Thus, a further study was performed, with and without 100 mM aniline in the reaction, at room temperature, applying 0.5 equivalents of peptide in relation to the aldehyde content in the fibers for the oxime ligation.

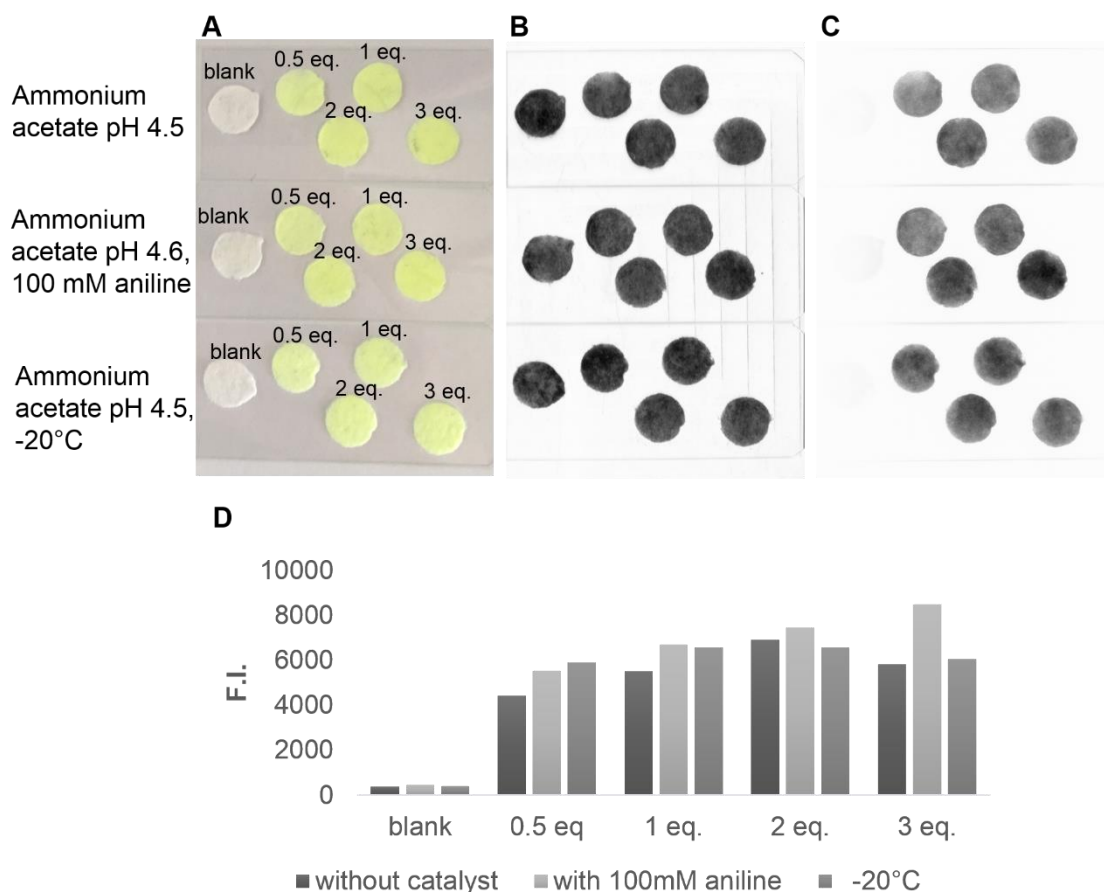


Figure 43: **A** Photographs, **B** white light images and **C** fluorescence images of the sortase A ligation products of the oxime ligation under three reaction conditions with different amounts of peptide. **D** Results of the fluorescence intensity analysis of images under **C**.

This time the kinetic outcome after 0.5, 2, 4, 8, 16 20 and 24 hours was evaluated. After oxime ligation, *srtA* ligation was performed on the fibers, and papers were pressed without applying heat. As usual, fluorescence was detected for read-out. Figure 44 **A** indicates an overall superior performance for the reaction conditions comprising the catalyst aniline. For both conditions, the reaction appeared to be nearly complete after 8 hours according to the trend.

However, further investigations showed that approaches relying on aniline catalysis, for reaction times exceeding 4 hours, have the tendency to develop a fluorescent response which can be detected at 535 nm, when the papers made from this material are irradiated at 480 nm (Figure 44 **B**) without tGFP coupled. This was also observable by a light-brown to yellow color of the resulting papers. Most probably, this effect that was not observed for the other variants without a catalyst, was arising from aniline that has been soaked up by the fibers and aged there. Indeed, not freshly distilled aniline has a red to brown color. Apparently, applied washing was not sufficient to remove the residual, aged catalyst. A revision of the protocol towards washing with organic solvents was not performed. Furthermore, this approach could be

considered as the only “green” approach, as no organic solvents were applied.¹³¹ Due to these reasons the decision was taken to perform the reaction without a catalyst. Further investigations were carried out with at least 2 equivalents of peptide in respect to the determined aldehyde content at pH 4.5 for at least 8 hours or in an overnight reaction.

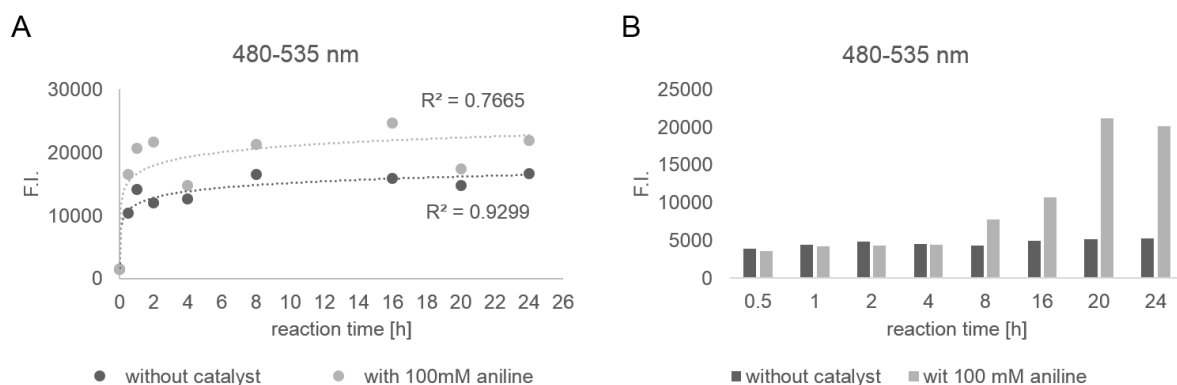


Figure 44: Kinetic assessments of the sortase A ligation resulting in product **26** based on the underlying functionalization with or without the catalyst aniline (A) and of the autofluorescence of the underlying peptide modified papers **15** at the respective emission wavelength (B).

3.4.3. Strategy 3: Reductive amination as strategy for peptide immobilization

Reductive amination as a covalent coupling strategy is present in the existing literature predominantly for coupling to CNC.^{132,133} To that end, the classic reagent used is sodium cyanoborohydride. However, to date its non-toxic alternative has become available, namely 2-methylpyridine borane complex, which was therefore chosen for the experiments.¹³⁴

Within the examined approach, coupling of 1,5-diaminopentane (cadaverine) was performed using a reductive amination of carbonyls on paper, followed by decoration of its free amine with a respective peptide by amidation (Figure 45). For the first step it was necessary to apply extremely high excess of cadaverine to prevent reaction of its two amino groups. Thereby, the attachment of only one of the amine residues to the fiber has been realized, making the second amine available for further modification. It is well known that sortase A requires a recognition sequence made of glycines, that is located *N*-terminally at the compound of interest. To evaluate if also solitaire cadaverine would be sufficient for sortase A coupling, a single experiment was performed with linkers of different length by varying amount of subsequent glycine residues in the sequence (zero (cadaverine only), one, and three glycines).

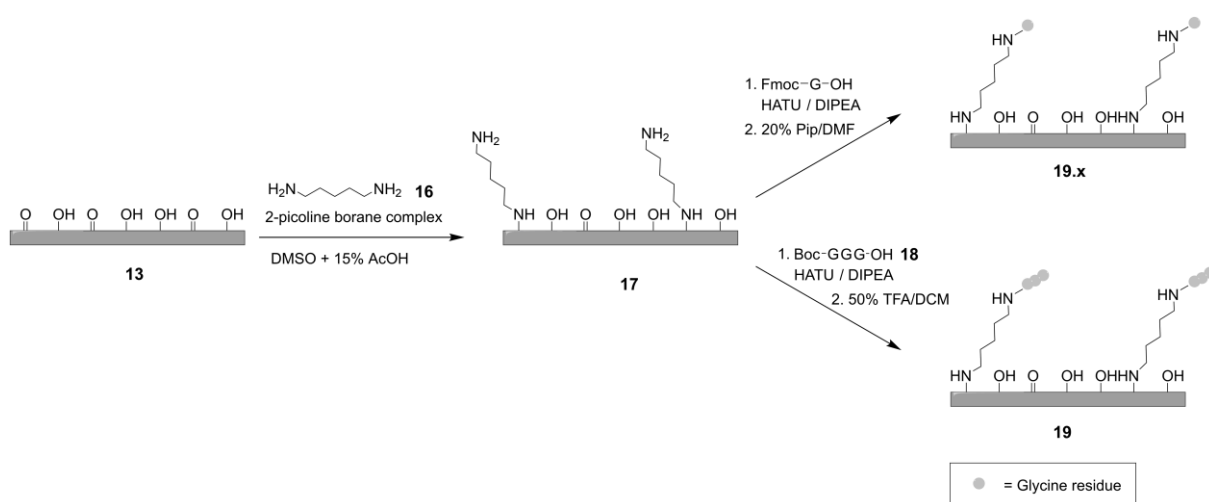


Figure 45: Introduction of the peptidic sequence under strategy 3. Cadaverine **16** is coupled with 2-picoline borane complex by reductive amination to TEMPO-oxidized fibers **13** resulting in amine-functionalized cotton linters fibers **17**. Subsequent coupling of **18** followed by Boc deprotection results in fibers **19**. Subsequent coupling of Fmoc-G-*OH* followed by Fmoc deprotection results in fibers **19.x**.

In a reductive amination, approximately 100 equivalent-excess of cadaverine and 2-methylpyridine borane complex were added to a mixture of TEMPO-oxidized cotton linters swollen in DMSO with 15% AcOH_{glacial}. The mixture was well shaken for 5 min and incubated at 65 °C for 2 hours. After thorough washing, the fiber slurries were stepwise equilibrated to DMF. For further reaction, Fmoc-Gly-*OH* or Boc-Gly-Gly-Gly-*OH* **18**, coupling reagent HBTU and DIPEA were pre-mixed in dry DMF and added to the fiber slurries. After 2 hours of reaction the fibers were thoroughly washed, and Fmoc/Boc deprotection followed, with thorough washing and drying of the fibers. Before sortase ligation with a standard mixture, the fibers were swollen in water and washed with sortase reaction buffer. Small papers were formed after ligation for better comparison, with the help of a disposable syringe equipped with a frit.

Figure 46 shows the fluorescence image of the different materials: paper with cadaverine **17**, with one additional glycine **19.x** or three additional glycines **19** after sortase A ligation and a blank (unmodified paper which was only incubated in sortase A reaction buffer). Fluorescence analysis showed an increase in fluorescence intensity from cadaverine only, over one additional glycine to three subsequent glycines. From these results, further experiments were performed using reductive amination of the fibers with large excess of cadaverine and a consecutive coupling of triglycine, which was found the best for sortase A ligation.

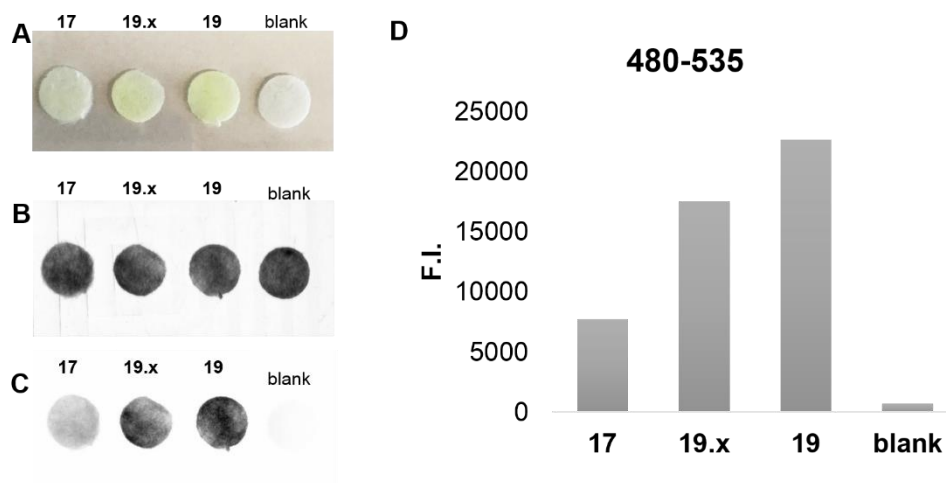


Figure 46: **A** Photograph of sortase A ligation products **17** (**1**), **19.x**, and **19** including blank. **B** White light and **C** Fluorescence image of the same samples. **D** Results of the fluorescence intensity analysis of image **C**.

3.4.4. Strategy 4: Esterification as initial peptide immobilization step

Immobilizing peptides of different size on conventional cellulose sheets via esterification is a well-known and straightforward strategy, e.g., in spot synthesis used for peptide-arrays. Using fibers, in the first step the surface was functionalized with amino groups, here using Fmoc-6-aminohexanoic acid (Fmoc-6ahx) in a carbodiimide-mediated esterification, followed by Fmoc cleavage. In the second step, the Boc-GGG-OH **18** building block was coupled under standard SPPS activation conditions. For Boc deprotection, the fibers were dried and kept in a mixture of 50% TFA in DMF for 30 min, thoroughly washed, and dried again. Figure 47 depicts the reaction schematically.

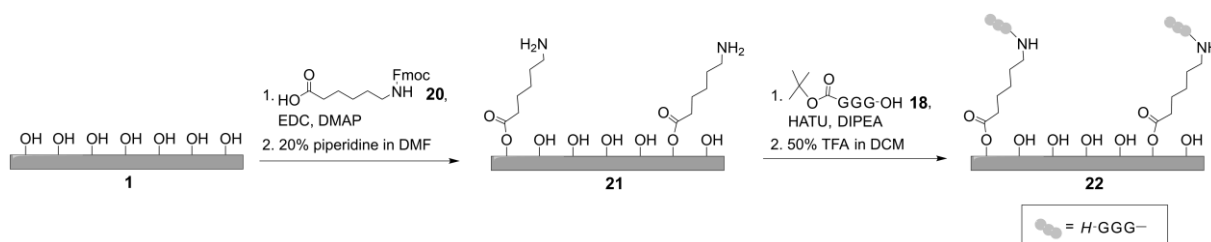


Figure 47: Introduction of the peptidic sequence under strategy 4. Fmoc-6-aminohexanoic acid **20** is coupled under HATU/DIPEA activation to fibers **1**. Subsequent Fmoc-deprotection with 20% piperidine in DMF results in product **21**. Coupling of **18** followed by Boc deprotection results in fibers **22**.

For a better understanding of the strategy, the esterification reaction was carried out applying varying amounts of Fmoc-6ahx in respect to the number of AGUs, starting with 0.25 over 0.5 to 1.0 equivalent (Figure 48). All fiber slurries were allowed to react with EDC/DMAP overnight

followed by washing, Fmoc cleavage and coupling of the building block **18** (1 eq.) under standard SPPS activation conditions for 2 hours. The results of the TNBS assay performed on papers made of these materials showed a rising content of primary amines on the fibers, corresponding to the rising amounts of Fmoc-6ahx used.

Another set of papers from the same batches was tested in sortase A ligation with tGFP-LPETGGH₆. Analysis of the papers showed fluorescence for all probes (Figure 48 **D**). Interestingly, the adsorption control of the “1eq. Fmoc-6-Ahx”-approach exhibited an equally strong fluorescence signal as the respective sortase A ligation product. The experiment was repeated, with the same observation. In some experiments also the 0.5 eq. approach showed this effect, but to a much smaller extent. Only the 0.25 eq. approach performed as expected.

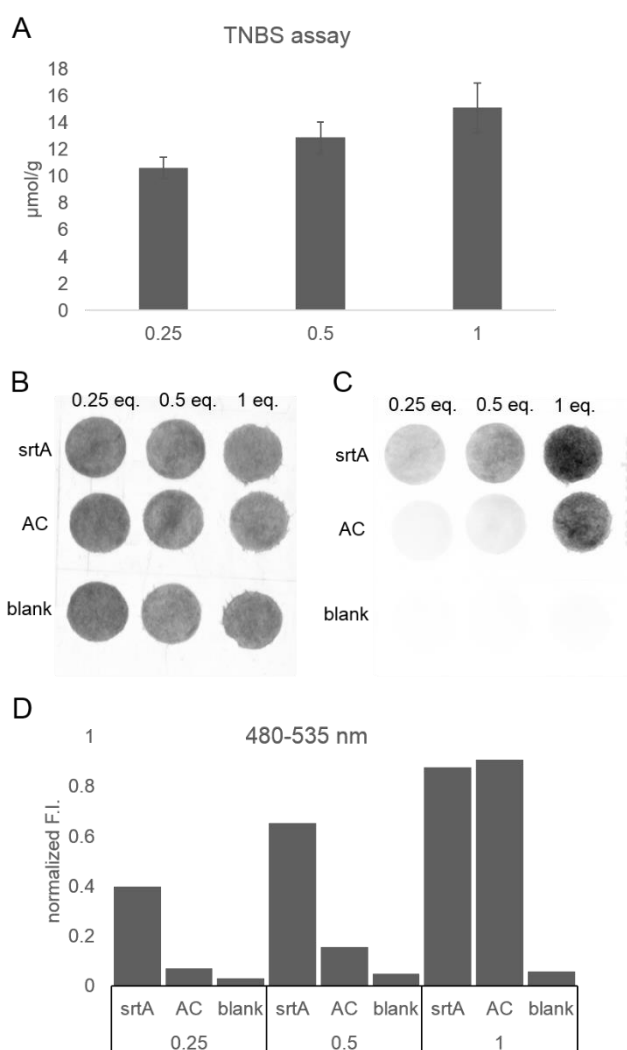


Figure 48: **A** TNBS assay of paper samples formed of the respectively functionalized fibers. $n = 3$, error bars depict the standard deviation. **B** White light image and **C** fluorescence image of the sortase A ligation including an adsorption control and blank. **D** Results of the fluorescence intensity analysis of image **C**.

Additionally, a factor worth considering in the decision which setup to follow was the handling of the fibers in the papermaking process. It was repeatedly observed in the experiments that fibers prepared with 0.5 and 1.0 equivalents Fmoc-6-ahx were attracted to the material of the disposable syringe, while the fibers were repelling each other, making it very difficult or almost impossible to generate regular papers with an equal mass. Figure 49 shows the average mass of dry fibers that was weighed in for paper making (“before”) and the resulting mass after paper making (“after”), for a single paper of 0.9 cm in diameter for the different approaches. The average and the standard deviation were generally calculated from $n = 9$.

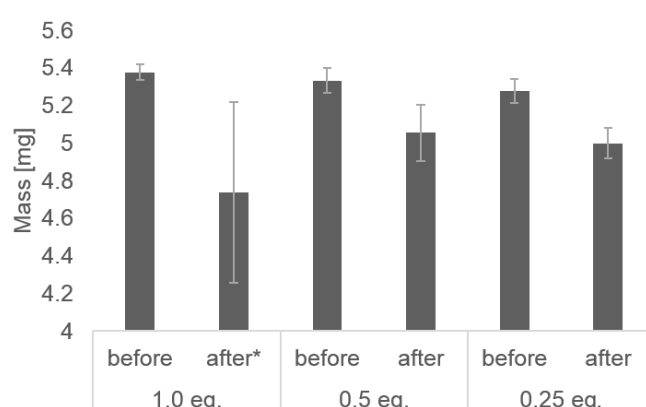


Figure 49: Masses of cotton linters fibers before and after papermaking. eq.: Equivalents Fmoc-6-aminohexanoic acid used in the initial coupling reaction related to AGU. $n = 9$, error bars depict the standard deviation.

It was crucial that all papers used in one fluorescence experiment had a standardized diameter, and possessed the same mass, to get comparable results. Obviously, fluorescence increases along with the level of functionalization. To achieve comparable results, it is therefore important to work with papers of approximately the same mass. Generating papers with a predictable and desired mass was continuously achieved only within the 0.25 eq. approach.

Due to the afore mentioned reasons, to avoid physical adsorption of the protein to the paper and to keep control over the resulting paper masses, it was decided to use 0.25 eq. of Fmoc-6-ahx and corresponding amounts of coupling reagents in further experiments, although it showed the lowest fluorescence intensity in the preliminary experiment.

3.4.5. Suitability of mTG as ligating enzyme

To apply mTG **24** for this purpose, it was necessary to pre-examine whether mTG causes oligomerization of the tGFP derivative **23** with the respective recognition tag. This would be a concern if surface-exposed lysine residues acted as amine donor substrates. SDS-PAGE inspection of the mTG overnight reaction with the related tGFP-variant in solution is depicted in Figure 50 and showed no additional bands for possible oligomers. Oligomers would appear above the original tGFP band in the separating or even the stacking gel. Thus, mTG was found suitable as ligating enzyme for protein conjugation to paper.

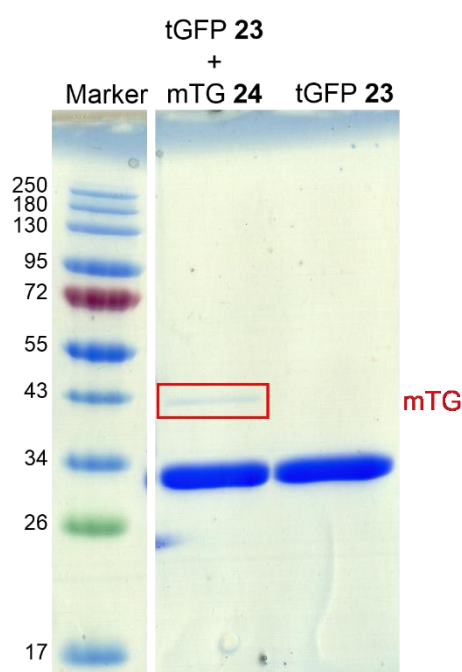


Figure 50: Coomassie blue stained SDS-PAGE after the overnight incubation at 37 °C of tGFP **23** with mTG **24**. For analysis a pre-stained protein ladder was used.

3.5. Part II: Comparison of the strategies

All the afore discussed strategies were subject to a side-by-side comparison. Papers have been prepared from fibers functionalized with the peptidic sequences and assessed for immobilization of the peptidic sequence using the indirect detection method with TNBS. Sortase A and mTG coupling efficiencies of tGFP derivatives as model proteins were examined after two hours of reaction. Further optimization of the strategies was necessary to enable a broader applicability. Furthermore, confocal laser scanning microscopy is employed for the evaluation of the homogeneity of the tGFP-immobilization and the distribution of the fluorescent protein. Read-out of tGFP-conjugated samples was always performed at 480 nm for excitation and 535 nm for detection, if not indicated otherwise. Finally, the incubation of one of the most promising ligation product with two different fluorescent CBM-fusion proteins, namely mKOκ-CBM28^{135,136} and mKOκ-CBM1Cel7a¹³⁷, was conducted to identify amorphous and crystalline cellulose regions and further characterize the binding of the modular strategy.

3.5.1. TNBS assay: Quantification of amine content

In general, paper sheets with a diameter of 0.9 cm and a mass of 5.0 (\pm 0,1) mg were pressed from the fiber slurries by using a disposable syringe equipped with a frit (Figure 51). The papers were removed from the syringe along with the plunger, pressed on blotting paper and dried at elevated temperatures between two glass slides. After conditioning the papers to the ambience, the density of primary amines in the paper was quantified per gram cellulose, using the TNBS assay. Here, the results are discussed, which are directly linked to assays performed under 3.5.3. Figure 13 in chapter 3.1.3 gives an overview of the resulting products. The results from three independent batches examined in triplicate show loading densities ranging from 9.5 to 12.3 $\mu\text{mol/g}$ paper, depending on the approach (Figure 52).

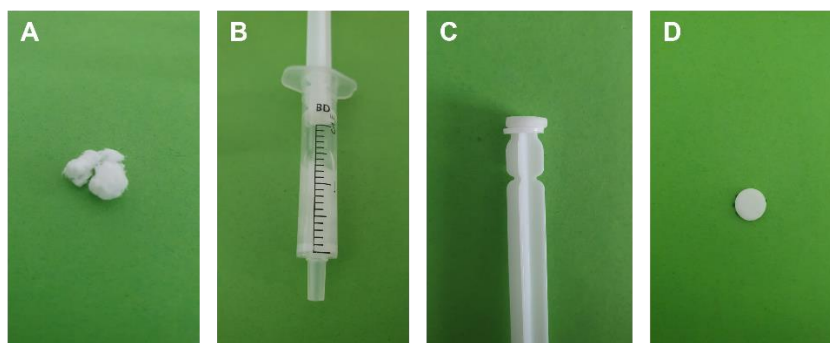


Figure 51: Essential steps of small-scale paper manufacturing: **A** Weighing of dry fibers. **B** Preparation of a fiber slurry. **C** Removing the paper along with the plunger. **D** Pressed paper.

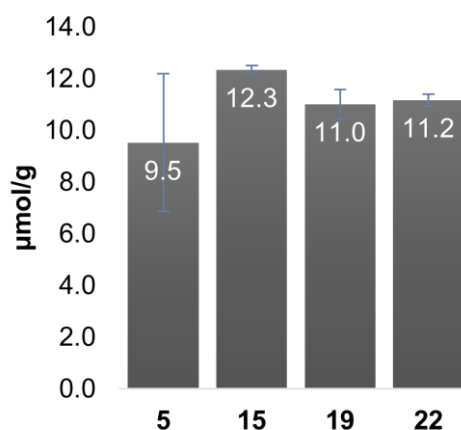


Figure 52: Indirect TNBS assay for functionalized fibers **5** (strategy 1), **15** (strategy 2), **19** (strategy 3) and **22** (strategy 4). Error bars depict the standard deviation. n = 9. Modified after Liebich et al.¹⁰¹

The loading appeared higher than that achieved using the light-controlled approach on ready filter paper ($7.8 \mu\text{mol/g}$ paper, 3.2.2). This result could be expected, as disintegrated cellulose fibers supply more approachable functional groups on the surface, and less hydroxy groups are involved in the interchain hydrogen bond network, than in the pre-made filter paper. Interestingly, similar coupling efficiencies were achieved, with all functionalization strategies examined after the afore discussed strategy optimization, with the light-controlled approach **5** being the only one with significant difference in loading. Indeed, the light-controlled strategy has been identified as the most sophisticated one in view of coupling steps and equipment, and at the same time the most sensitive to subtle changes of reaction conditions. This is probably the reason for the big standard deviation in the obtained results compared to the other strategies. However, it must be noted that with this determination only the primary amines can be quantified, which translate directly into the peptide load on the papers of strategies 1 and 2. For strategies 3 and 4 it cannot be discriminated between the primary functionalization of the fibers with cadaverine or 6-aminohexanoic acid (in the case of an incomplete last coupling step) and the attempted immobilized peptidic sequences.

3.5.2. Enzyme-mediated ligation: tGFP fluorescence comparison

Figures in chapter 3.1.1 can be used to get a global overview on the products.

Initial comparison of enzyme-mediated ligation

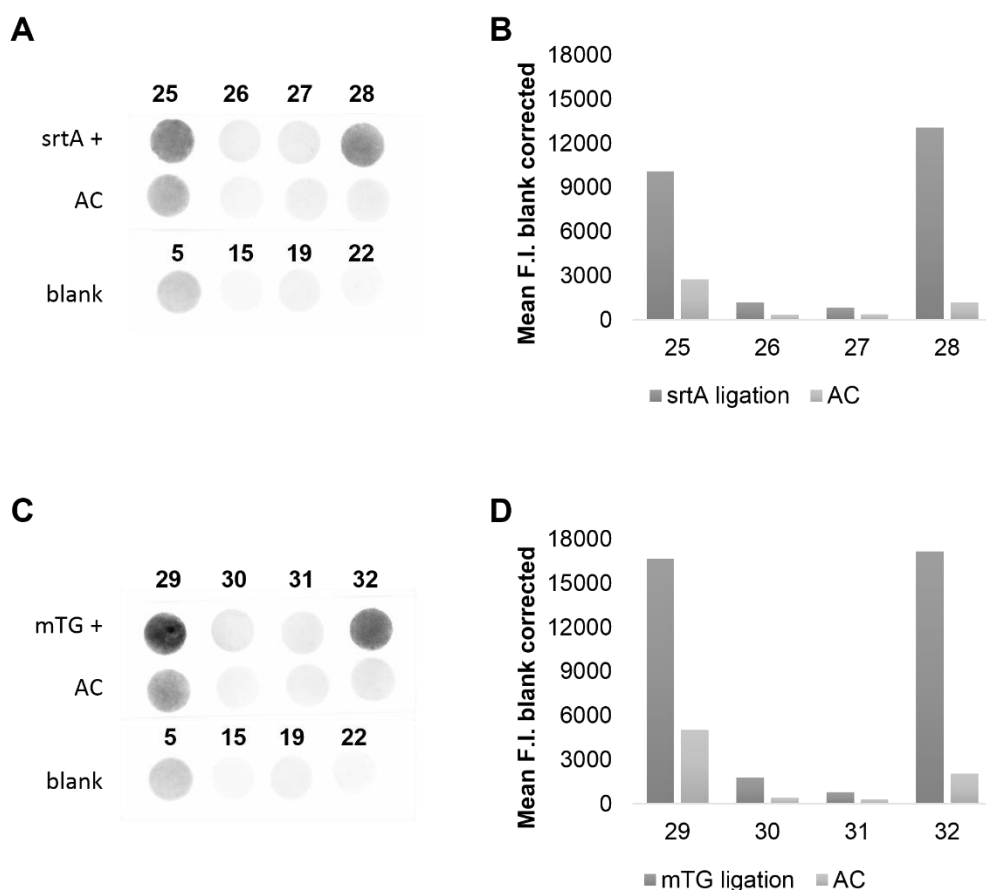


Figure 53: Fluorescence images of sortase A-mediated ligation (A) and mTG-mediated ligation (C) on peptidic papers 5, 15, 19 and 22 with the respective tGFP variant, including adsorption control (AC) and a blank for each approach. Blank corrected results from fluorescence analysis of the images for srtA ligation (B) and mTG ligation (D).

Enzymatic, site-specific protein conjugation on the papers was performed with the specific bond-forming enzymes sortase A and microbial transglutaminase (mTG). Therefore, papers with masses of 5.0 mg (\pm 0.1 mg) were prepared following all functionalization strategies as described above.

The enzymatic ligation of C-terminally modified tGFP, containing a recognition sequence for sortase A (LPETGG) or mTG (DIPIGQGMTG) respectively, was performed. Thus, dry papers were incubated in a standardized ligation mixture for two hours at 22 °C (srtA) or 37 °C (mTG). For detailed description see experimental section 7.9.5. Enzyme-mediated conjugation yields

were compared with those obtained by physical adsorption in absence of the conjugation enzyme. A typical fluorescence intensity analysis is depicted in Figure 53.

Results show that strategies 1 and 4 resulting in products **25/29** and **28/32** respectively, performed superior compared to strategies 2 and 3, products **26/30** and **27/31**, respectively. Additionally, unwanted physical adsorption was elevated only in strategies 1 and 4.

Strategies 2 and 3 did not perform as expected. That was surprising as these strategies, and especially the oxime ligation approach (strategy 2), performed extraordinary well in the preliminary experiments, where the tGFP fluorescence was visible with the naked eye.

A possible explanation of the weak performance of strategies 2 and 3 could be that the initial experiments using these strategies were performed not with dry papers, but with well-swollen fiber slurries, only pressed to papers right before fluorescence analysis. This has an influence on the accessibility of the functional groups on the single fibers. Due to the papermaking process (see Figure 51), most probably also the recognition sequences are integrated in the hydrogen bond network of the paper, reducing accessibility for the reacting proteins.

Furthermore, the ionic situation in the fibers might influence the accessibility of the recognition sequence arising from the nature of the underlying fibers of the two strategies. Both were performed on TEMPO-oxidized fibers. Based on the knowledge that cellulose itself is slightly negatively charged and the fact that through TEMPO oxidation further carboxy groups are introduced, an interaction with tGFP seems possible. In buffers at neutral pH or slightly above, during the enzymatic ligations, both the fibers and the tGFP (calculated pI = 5.49) might be negatively charged. Thus, it might appear that the fibers and tGFP repel each other. On the other hand, the *N*-terminus of the recognition sequence has an estimated pKa-value of 9.6 meaning it should be mostly protonated at neutral pH. Thus, an ionic interaction of the linker and the negatively charged cellulose should be also considered possibly stabilized through the papermaking process.

Papers vs fibers: A comparison

The results of the experiments with pressed, dried papers were compared with those performed on loose fibers from the same batches. The fibers were equilibrated in buffer before enzyme-mediated ligation and pressed to papers after ligation for better comparability. The images and graphs in Figure 54 clearly show that the ligation was more efficient for all types of functionalization when fibers instead of pressed papers were used.

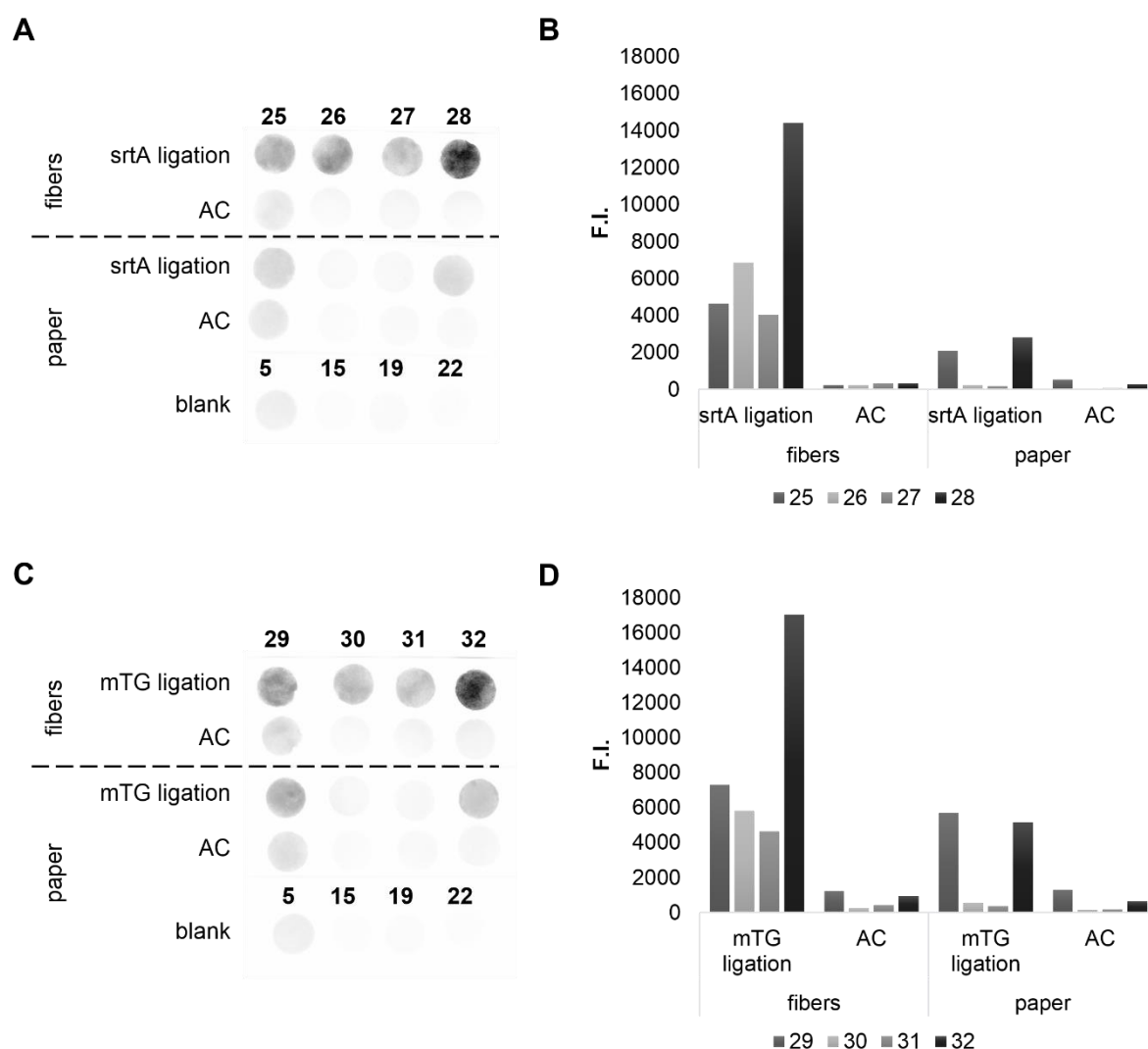


Figure 54: Fluorescence images of sortase A-mediated ligation (**A**) and mTG-mediated ligation (**C**) on peptidic fibers and papers **5**, **15**, **19** and **22** with the respective tGFP variant, including adsorption control (AC) and a blank for each approach. Blank corrected results from fluorescence analysis of the images for srtA ligation (**B**) and mTG ligation (**D**) from a single determination.

Interestingly, strategies 1, 2 and 3 performed almost equally well, while strategy 4 worked superior and exhibited a 3 times increased fluorescence intensity, compared to the other approaches. The obtained result for strategy 4 would be in accordance with the discussion above, however. Unmodified cellulose, the basis for strategy 4 keeps a minimum of negative charge, compared to TEMPO oxidized fibers, and *N*-termini with a positive charge would attract negatively charged tGFP, probably resulting in beneficial proximity of the two substrates.

Nevertheless, it must be noted that paper masses of the “fiber” approaches, obtained after drying of the enzyme-mediated ligation products, showed rather inhomogeneous results. Papers

pressed from the “fiber approaches” of strategies 1 and 4 had lighter masses than those of strategies 2 and 3, which has an impact on the comparability of the fluorescence results.

Comparison of TEMPO fibers with different aldehyde/carboxy content

To gain further insight, a comparison on strategy 3 between two differently oxidized fiber batches was performed, as through TEMPO oxidation not only aldehyde groups but also carboxyl groups are generated. The difference between Batch 1 and Batch 2 was the amount of a co-catalyst sodium hypochlorite used in the oxidation. Batch 2 was oxidized with half the amount, compared to Batch 1, resulting equally in half of the total aldehyde content and surface carboxylate content in Batch 2 compared to Batch 1 (see chapter 7.1.3). For peptide functionalization of fibers, equal amounts of reactants were used for both batches (the excess of reactants should be secured) and fibers were functionalized as described for strategy 3. Papers were pressed of the fibers and TNBS assay was carried out. Sortase A ligation was performed on dried papers for 1 h at 22°C. Fluorescence images were taken, as well as of adsorption controls (Figure 55 A).

Results of the TNBS assay revealed comparable amine load for both batches. Results of the fluorescence comparison are shown in Figure 55 B. Fluorescence intensity of papers from Batch 2 was determined to be twice as strong as for papers of Batch 1, as assessed from two independent experiments. This result indicates that a lower degree of oxidation might be indeed beneficial for increasing the protein immobilization on strategies based on TEMPO-oxidized fibers. However, this two-times increased fluorescence intensity is still low compared to strategies 1 and 4, as can be seen from Figure 54 B. Thus, if the effect is of ionic nature, this could probably also be overcome by pre-incubation of the papers in buffer or increasing the ionic strength of the reaction milieu.

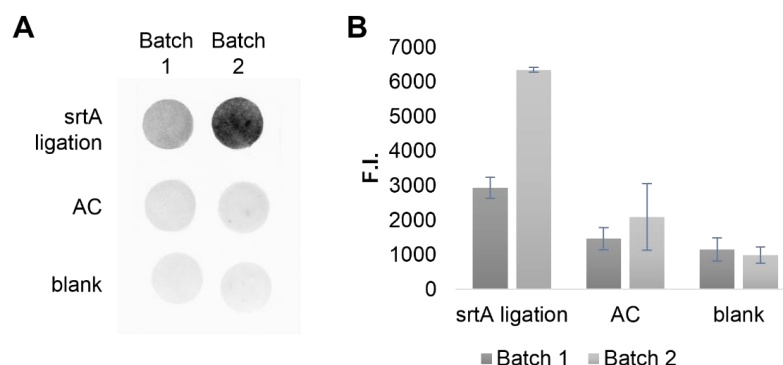


Figure 55: **A** Fluorescence image of sortase ligation products **27** on TEMPO-oxidized fibers with different aldehyde and carboxyl content, adsorption control (AC) and blank **19**. **B** Analysis of mean fluorescent intensities of two independent experiments. Standard deviations are depicted with error bars.

3.5.3. BSA blocking towards improved ligation

Based on the discussed results, papers were preincubated in ligation buffer containing bovine serum albumin (BSA, 3%). We have assumed that the salts in the buffer should enable the ligation for strategies 2 and 3, as its Na^+ -ions should act as counterions for cellulose carboxylates. Additionally, the BSA is applied to block “sticky” sites on the functionalized papers to avoid unwanted physical adsorption in the samples for all strategies, but especially for the 1 and 4. Unspecific adsorption often possesses the risk of protein bleeding upon long-term incubation, which is important for possible applications. BSA has a partial hydrophobic surface, which serves in its natural function to transport non-polar compounds. It has been successfully applied in nitrocellulose applications for the blocking of unspecific protein adsorption. Thus, papers were incubated in a solution of 3 wt.-% BSA in tris-buffered saline (TBS) for 25 minutes and were washed with Milli-Q® and TBS before the enzymatic ligation mixture was added. After two hours under preferred conditions for the respective enzyme, samples were washed and analyzed by evaluation of fluorescence images (Figure 56). The experiment was performed in triplicate.

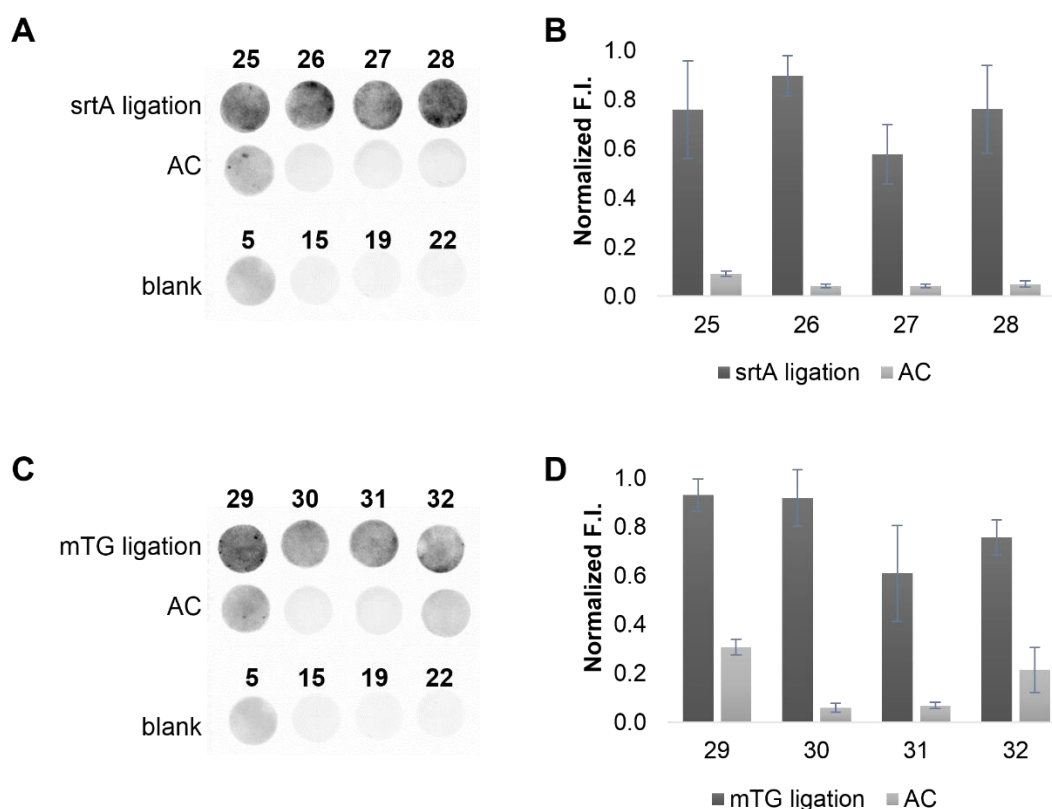


Figure 56: Exemplary fluorescence images of sortase A-mediated ligation (**A**) and mTG-mediated ligation (**C**) on BSA-blocked peptidic papers **5**, **15**, **19** and **22** of the same batch for both enzymatic ligations. Performed with the respective tGFP variant, including adsorption control (AC) and a blank for each approach. Blank corrected results from fluorescence analysis of the images for srtA ligation (**B**) and mTG ligation (**D**) from a triple determination. Each result was normalized to the sample with the strongest fluorescence at 535 nm. Average values were built upon normalized figures ($n = 3$). Modified after Liebich et al.¹⁰¹

Results of blank corrected and normalized figures show that all the examined approaches performed almost equally efficient under the chosen conditions, with some deviation. The difference between the results was not significant. Unspecific binding of tGFP due to adsorption could be almost completely suppressed for sortase A ligation, while for the mTG one it was still pronounced in strategies 1 and 4. As strategies 2 and 3 obviously worked as good as strategies 1 and 4, the preincubation in BSA containing buffer seems to be a good approach in making more recognition sites available for reaction. On the other hand, strategy 4 that was often superior in preliminary experiments, has an average or slightly lower performance now. This could also be an effect of BSA incubation, as according to the findings above BSA, with a pI of 4.7 to 5.1¹³⁸ it is negatively charged under the reaction conditions. Considering that the surface of paper in Strategy 4 might bear a positive charge, BSA may get adsorbed easily, being able to block reaction sites.

This indeed could indicate that ligation conditions need an adjustment regarding reaction time and substrate input, as this could be a solution to overcome a potential blocking of recognition

sites and will most probably increase protein immobilization. In a first experiment, sortase A ligation was performed as before for 2 h at 22 °C on papers for all approaches and prepared to capture fluorescence images. In a consecutive step, a fresh ligation solution was added to the samples, which were then kept for further 16 h at 22 °C. Fluorescence images were captured anew. For analysis mean fluorescence intensities were normalized to the blanks separately for each approach, as this appeared to be the most straightforward strategy to evaluate if fluorescence intensity increased in one of the approaches. Figure 57 presents the results of the analysis.

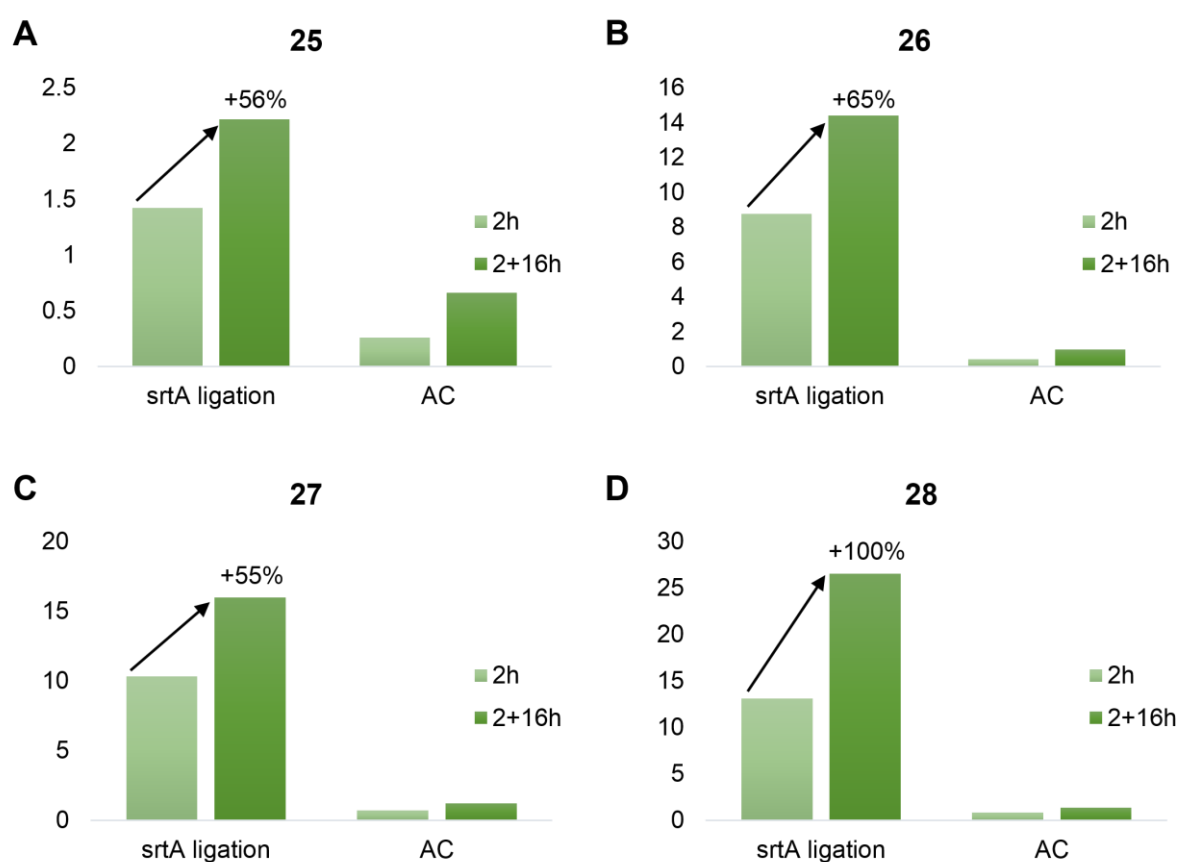


Figure 57: Analysis of two fluorescence images consecutively taken after 2 and additional 16 hours of sortase A ligation leading to products **25** (A), **26** (B), **27** (C) and **28** (D) including adsorption controls (AC) and blanks. Blanks were used for initial normalization of the image's fluorescence intensities separately for each strategy. Single determination.

Thus, fluorescence intensity increased in all the approaches, with the increase ranging from about +55% in strategies 1 and 3, over +65% in strategy 2 to +100% in strategy 4. Since no additional time points were examined between 2 h and 18 h, this result leaves it unclear,

whether the endpoint of the enzymatic ligation has been reached within this time, and thus the possible potential of the strategies remains to be discovered.

3.5.4. CLSM of the tGFP-conjugated fiber networks

Previous investigations with the fluorescence imager already showed a rather homogeneous disposition of the tGFP on a macroscopic scale. To further investigate the homogeneity and specificity of the tGFP immobilization throughout the paper network and on single fibers confocal laser scanning microscopy (CLSM) was employed. Figure 58 shows several false color images at different resolutions exemplarily for product **28**. In general, the spreading throughout the papers is very homogenous (Figure 58 A) for all tested approaches. Similarly, regarding close-up images, the functionalization is especially prominent along the fiber's fibrils, no matter which approach has been inspected (Figure 58 B and C). The lumen is not filled with the fluorescent protein under the tested treatment conditions (Figure 58 D). This would be the case if tGFP was soaked in by the fibers, indicating undesired adsorption of the protein or inefficient washing of the paper after the ligation reaction. As this seems not to be the case, this is another proof for the effectiveness of the methods for covalent immobilization.

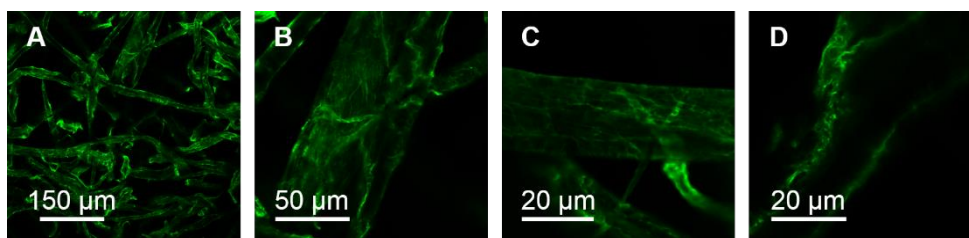


Figure 58: Exemplary CLSM images of product **28**. **A** Global view of overlapping cotton linters fibers. **B** and **C** showing pronounced immobilization along fibrillar structures. **D** The lumen of the cotton linters fibers is not filled by tGFP. After Liebich et al.¹⁰¹

A final experiment was performed to identify whether the covalent immobilization strategy 4 discriminates between crystalline and amorphous parts of the fibers. To that end, a paper product **28** was divided into two parts. One was incubated with mKOK-CBM28, a fluorescent fusion protein of carbohydrate binding module (CBM) marking amorphous parts of cellulose. The other piece was incubated in mKOK-CBM1Cel7a, marking crystalline parts of cellulose, respectively. Incubation was performed at a concentration of 40 $\mu\text{g/mL}$ for 5-10 min at room temperature. The overlays of false color images obtained with CLSM of tGPF ($\lambda_{\text{ex}} = 488 \text{ nm}$, $\lambda_{\text{em}} = 505\text{-}525 \text{ nm}$) in green and the CBM fusion protein ($\lambda_{\text{ex}} = 552 \text{ nm}$, $\lambda_{\text{em}} = 560 - 590 \text{ nm}$) in

red of either co-localization, indicate that the functionalization is successful on both, crystalline and amorphous parts of the cotton linters fibers (Figure 59). Overlaying regions are depicted in yellow. A third experiment of a co-incubation with both fusion proteins on the same piece of paper showed, that green areas remained where no CBM-fusion protein has been bound. As cotton linters fibers consist of several different organic molecules, of which cellulose is only making the biggest part, this result is within the expectations. Other compounds like pectin or lignin carry addressable hydroxyl groups, that are probably not discriminated in frames of a chemical transformation.

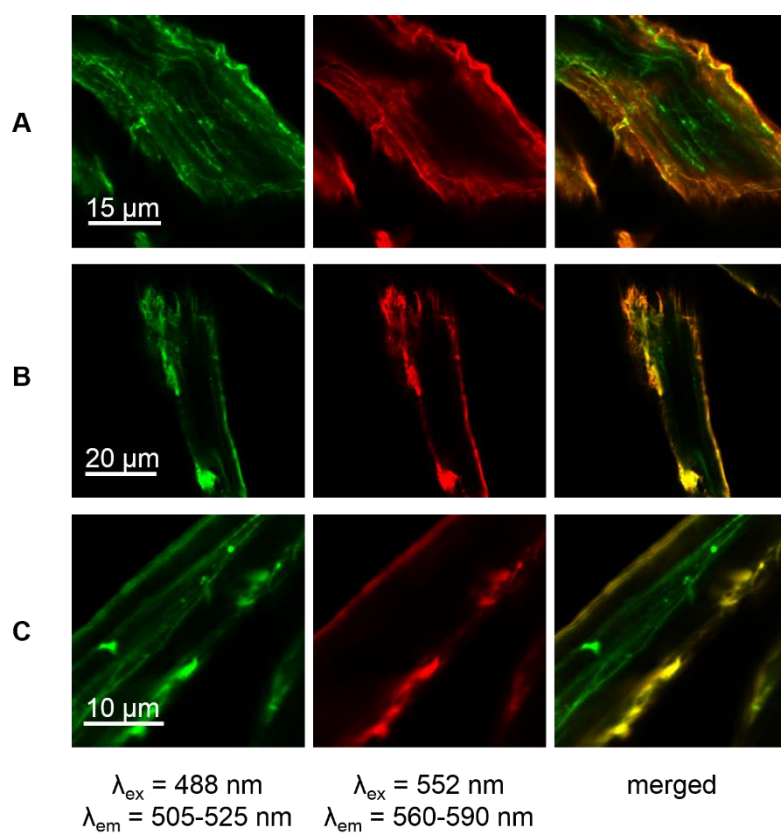


Figure 59: CLSM: False color images of product **28**. Immobilized tGFP was co-localized with **A** mKO κ -CBM28 to identify amorphous cellulose, **B** mKO κ -CBM1Cel7a to identify crystalline cellulose, **C** and both CBM fusion proteins to identify additional binding sites in cotton linters fibers.

3.6. Summary: Part II

The second part of this work started with orienting experiments regarding optimization of strategy 1 and the development of alternative strategies 2 to 4. For strategy 1, the esterification of cotton linters fibers with 0.25 equivalents of the photoenol moiety related to AGU content was identified as most suitable for the chosen attempt. For strategy 2, the oxime ligation of the pre-synthesized peptide was examined under three different conditions. Although the aniline catalysis showed the best performance, an aging of the catalyst in the fibers has led to visible impurities. Thus, due to the potential of the strategy without a catalyst (that can be considered as a “green” approach) it was decided to follow this approach but enhance reaction time towards an overnight process. For strategy 3, different linker lengths were tested to find out whether in this setup a solitaire primary amine of immobilized cadaverine would be sufficient to be recognized by sortase A. In accordance with literature, a triglycine peptide performed best, therefore it has been chosen for both strategies 3 and 4 as a recognition unit. For strategy 4, the esterification was optimized regarding the ratio of Fmoc-6-aminohexanoic acid input per AGU. Analysis of the sortase A ligation by fluorescence imaging showed a strong adsorption effect of papers with high peptide load. This has probably arisen due to a presumably positive net charge of the fibers, which resulted in attracting negatively charged proteins. Equally to strategy 1, the ratio of 0.25 equivalents of AGU was chosen for initial functionalization of the fibers, as they showed the best behavior regarding unwanted adsorption and handling of the fibers during the papermaking process.

Based on these predeveloped strategies, the primary amine content was determined indirectly using TNBS assay. The functionalization reactions resulted in comparable amine loads, with slightly lower density for strategy 1. For strategies 1 and 2, this amine load translates directly into peptide content, whereas for strategies 3 and 4 the number is the sum of primary amines from the initial functionalization of the fibers and the full peptidic linker.

The comparison of enzymatic ligation efficiencies using sortase A and mTG as coupling enzymes employing fluorescence imaging, first showed a clear preference for strategies 1 and 4. This was turned into almost equally efficient conjugations for all strategies due to further optimization, which mainly included an incubation of the papers in a 3-wt% BSA solution in TBS applied to loosen up ionic interactions between fibers and to block unwanted adsorption. However, adsorption controls from the mTG ligation showed still slightly elevated signals for strategies 1 and 4. Additionally, it was suspected that the enzymatic ligation needs further optimization as blocking with BSA could not only affect unwanted adsorption but also “close” conjugation sites. The fluorescence image of a 2-hour reaction was compared with a ligation that proceeded 16

hours longer. An increase in the fluorescence intensity was detected for all ligation products, being the most pronounced for strategy 4. However, the endpoint was not identified, yet.

An CLSM inspection of the sortase A ligation products for all approaches revealed a homogeneous distribution of the tGFP throughout paper and fibers and confirmed sufficient washing after ligation, as the lumen was not filled with protein. A co-incubation of products from strategy 4 with a CBM-fluorescent protein fusion emitting at wavelengths compatible with tGFP-fluorescence showed a functionalization of both crystalline and amorphous cellulose parts, thus having revealed additional binding sites. The latter were assigned to hydroxyl groups from other cotton linters compounds.

4. Graphical summary

The following graphic and table (Figure 60 and Table 1) summarize the performed work.

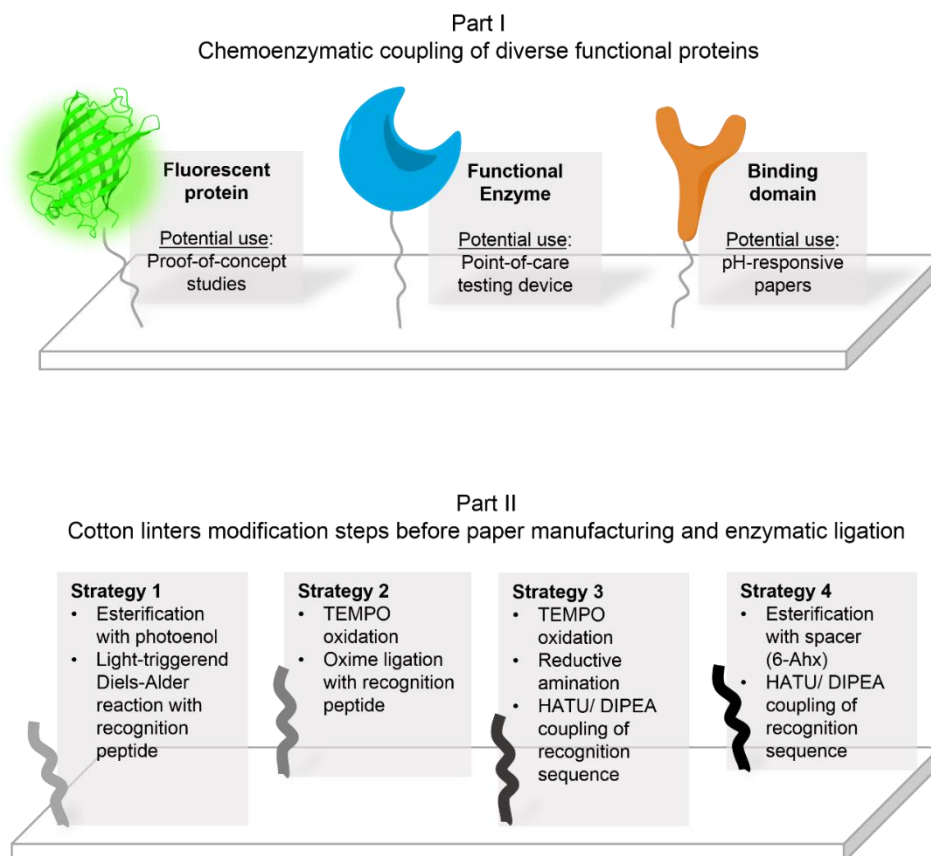


Figure 60: Graphical summary of work performed in this thesis. Potential applications described in the upper part I are not limited to the suggestions made.

Table 1: Immobilization strategies used within the two parts of the work.

	Part I: Proof-of-concept			Part II: Expanding the toolbox							
	Installation of recognition motif			Installation of recognition motif							
Cellulose support	commercial filter paper			cotton linters fibers							
Strategy	light-controlled			Strategy 1		Strategy 2		Strategy 3		Strategy 4	
Reaction	light-activated Diels-Alder reaction			light-activated Diels-Alder reaction		oxime ligation		reductive amination, then amidation		amidation	
Preliminary modification of paper	esterification with photoenol			esterification with photoenol		generation of aldehydes by TEMPO oxidation		generation of aldehydes by TEMPO oxidation		esterification with Fmoc-6-aminohexanoic acid	
Recognition motif	sortase A-addressable peptide			sortase A- and mTG-addressable peptide		sortase A- and mTG-adressable peptide		sortase A- and mTG-adressable oligoglycine		sortase A- and mTG-adressable oligoglycine	
	Coupling of a biomolecule			Coupling of a biomolecule							
Functional protein	tGFP	mTG	ZZ-Protein	tGFP	tGFP	tGFP	tGFP	tGFP	tGFP	tGFP	tGFP
Recognition motif	LPETGG	LPETGG	LPETGS	LPETGG	DIPIGQGMTG	LPETGG	DIPIGQGMTG	LPETGG	DIPIGQGMTG	LPETGG	DIPIGQGMTG
Coupling enzyme	sortase A pentamutant (Mut5)			sortase A Mut5	wild type mTG	sortase A Mut5	wild type mTG	sortase A Mut5	wild type mTG	sortase A Mut5	wild type mTG
	Activity examination			Activity examination							
Assay type	Fluorescence	Enzyme activity assay	ELISA	Fluorescence							
Detection type	Quantitative	Qualitative	Qualitative	Semi-quantitative							

5. Conclusion and outlook

Within this PhD research, the fundamental questions listed in the chapter Objectives were successfully addressed. The goal of this PhD thesis was to establish a generally applicable method for the directed conjugation of bioactive proteins to paper fibers with the potential for high protein charge. The basic approach included a pre-functionalization of paper fibers with thermostable peptides, that survive a papermaking process under applying heat, as conjugation anchors. The ultimate strategy was designed to assure the formation of a stable covalent bond site-specifically and under mild reaction conditions, while the biomolecule's function must be preserved. A number of conjugation strategies were successfully studied with the goal to generate a versatile toolbox. Being reproducible, modular, and straightforward, the strategies open new avenues towards the generation of tailor-made bioactive papers, with ramifications for use in low-instrumented diagnostics.

The proof-of-concept study demonstrated the possibility to attach functional peptides and proteins on paper in competitive amount and density in a two-step chemoenzymatic approach using strategy 1. It was shown that the combination of highly efficient light-triggered Diels-Alder reaction with a follow-up enzyme-promoted site-specific conjugation can be efficiently applied to functionalization of paper supports. Thus, three functionally different proteins, among them a fluorescent one, an enzyme, and a high affinity domain, were loaded on paper without compromising their biological function.

Four unique strategies were elaborated to attach peptidic sequences required for a further enzyme recognition, on paper materials. Efficient, mild, and site-directed protein ligation was demonstrated for all of them. The formation of a covalent and site-specific bond was assured applying two bond-forming enzymes, namely sortase A and mTG. All four strategies revealed various advantages or disadvantages concerning the suitability in future applications.

Strategy 1 relying on light-induced introduction of a recognition peptide followed by enzymatic ligation, showed high efficiency and performance, especially considering the fact that the peptide load can be directly calculated from the amine content measured by TNBS assay, as the full-length peptide is immobilized in one step. However, the assumed interference of the linker with the tGFP fluorescence makes it difficult to assess the real potential using tGFP for (semi)-quantification. As shown in section 3.4.1 the tGFP fluorescence intensity detected may be underestimated in the chosen setup and fluorescence might be more pronounced. To overcome this obstacle, another quantification method should be established in future research. Additionally, this strategy is rather sophisticated. Thus, and due to economic reasons, the

usability of the strategy is probably limited to applications requiring the functionalization of defined areas in paper.

The second strategy based on oxime ligation for peptide immobilization also demonstrated high efficiency and performance. As for strategy 1, the peptide immobilization load equals the amine content as determined with TNBS. Furthermore, the strategy performed excellent on fibers and when papers were incubated in BSA prior to enzymatic ligation. With aniline as a catalyst, the outputs may be improved. In terms of sustainability, this approach, as carried out, is highly favorable, since all the conjugation steps are performed in water, without the need for washing with organic solvents. Supplemented with water-based peptide synthesis¹³¹, the approach would be completely “green”, and thus a good choice for further research and future applications.

The third strategy relied on cadaverine as initial functionalization of cotton linters and was found slightly weaker performing than the compared strategies. Nevertheless, the difference is not significant in the results from BSA preincubated papers, that were comparable to the other strategies. However, it possessed a slight drawback in terms of a fact that the immobilized peptide loading cannot be directly quantified. Only the combined amount of unreacted cadaverine residues and the Boc-deprotected triglycine can be displayed together, indicating that the overall peptide load could be smaller than for the compared strategies 1 and 2. The potential of strategy 3 could be further increased, due to optimization of chemical reaction times for linker binding.

The fourth strategy based on esterification of the Fmoc-6-aminohexanoic acid as initial functionalization of cotton linters, shows very good results overall. The strategy is very promising, as it delivers good results in reactions with fibers, on dry as well as on BSA/TBS incubated paper. However, the peptide amounts immobilized must be regulated in an attentive manner, as papers with a very high peptide content seem to excessively adsorb protein. On the other hand, a high peptide amount hampers the papermaking process, as it was performed in this research by generating steady paper masses, as fibers seem to repel each other. As both effects might be connected, this finding may be interesting to study further. As a drawback, like strategy 3, only the combined amount of potentially unreacted immobilized 6-aminohexanoic acid residues and the full linker can be determined together in the TNBS assay. Nevertheless, this peptide immobilization strategy is the least demanding among all methods examined. All compounds are easily accessible, starting with unmodified cotton linters fibers to standard SPPS building blocks and standard reaction steps. In combination with the highly promising results,

especially for sortase A ligation, this approach appears to be a very promising method for future applications.

As next steps towards potential applications, several further properties should be studied. First, the surface charge of the resulting fibers should be determined to achieve an efficient optimization of buffer conditions, protein substrate input, and duration of the ligation in the following steps. The afore discussed studies were performed in a buffer solution standardized for each enzyme and a relatively low target protein concentration for 2 hours. An evaluation of the suggested parameters will allow reaching the endpoint of the ligation in an acceptable time range, thus enabling a quantification of the maximum possible protein load reached upon the respective strategy. Furthermore, paper specifics, such as porosity, fleece density, as well as hydrophobicity and sorption characteristics should be evaluated of the papers obtained from peptide functionalized fibers. Knowledge of these properties would allow for the decision of the most suitable method or the tuning of the paper characteristics regarding the requirements of the targeted application.¹³⁹

6. Zusammenfassung

Bioaktive Papiere sind von stetig wachsendem Interesse für Point-of-Care-Tests, die keine umfangreiche analytische Ausrüstung erfordern und spätestens mit Covid-19 gerade ihren Weg in jedermanns Haushalt gefunden haben. Die Herstellung solcher Papiere, die in ihrer einfachsten Form ein an Papier adsorbiertes, bioaktives Protein enthalten, kann typischerweise auf vier sehr unterschiedlichen Protein-Immobilisierungsprinzipien beruhen, die sich in kovalente/nicht-kovalente und ortsspezifische/nicht ortsspezifische Strategien unterteilen lassen. Kovalente, ortsspezifische Strategien sind erforderlich, wenn eine gleichmäßige, ortsgerichtete Verteilung des Biomoleküls auf dem Papiersubstrat und eine stabile Bindung erreicht werden sollen. Modulare, chemoenzymatische Ansätze ermöglichen die Bildung solcher Bindungen.

Chemoenzymatische Ansätze für die Immobilisierung funktioneller Proteine auf Materialien auf Baumwoll-Linters-Basis wurden bisher nicht untersucht. Daher soll in dieser Arbeit ein vielseitiger Werkzeugkasten von Strategien für die effiziente und zuverlässige Herstellung bioaktiver Papiere entwickelt werden. Die synthetischen Strategien zur Peptidimmobilisierung auf Linters beruhen auf:

- 1) hocheffizienter, räumlich kontrollierbarer licht-induzierter Cycloaddition,
- 2) nahezu "grüner" Oxim-Ligation,
- 3) reduktiver Aminierung mit anschließender Amidierung, oder
- 4) direkter Veresterung einer Aminosäure mit anschließender Amidierung,

gefolgt von einer ortsspezifischen Sortase A- oder mikrobiellen Transglutaminase-katalysierten Transamidierung. Diese vier verschiedenen Konjugationsstrategien für die Peptidimmobilisierung wurden im Hinblick auf Reproduzierbarkeit und Faserbeladungseffizienz bewertet. Die beiden für die Proteinkonjugation eingesetzten Enzyme konnten denselben Oligoglycin-Peptidanker verwenden.

Der grundlegende Ansatz beinhaltet eine Vorfunktionalisierung von Papierfasern mit thermostabilen Peptiden, als Konjugationsanker, die einen Papierherstellungsprozess unter Hitzeeinwirkung überstehen. Die Strategie sollte die Bildung einer stabilen, kovalenten Bindung, ortsspezifisch und unter milden Reaktionsbedingungen sicherstellen, wobei die Funktion des Biomoleküls erhalten bleiben soll. Da die Strategien reproduzierbar und modular sind, eröffnen sie neue Wege zur Herstellung maßgeschneiderter bioaktiver Papiere.

Die Proof-of-Concept-Studie im ersten Teil der Arbeit hat gezeigt, dass es möglich ist Peptide und funktionelle Proteine in konkurrenzfähiger Menge und Dichte in einem zweistufigen chemo-enzymatischen Ansatz an Papier zu binden. Es konnte gezeigt werden, dass die Kombination einer hocheffizienten Licht-induzierten Diels-Alder-Reaktion mit einer anschließenden Enzym-katalysierten, ortsspezifischen Konjugation zur Funktionalisierung von Papierträgern eingesetzt werden kann. So konnten drei funktionell unterschiedliche Proteine, darunter ein fluoreszierendes Protein, ein Enzym und eine hochaffine Domäne, auf Papier aufgebracht werden, ohne ihre biologische Funktion zu beeinträchtigen.

Im zweiten Teil der Arbeit wurden alle vier Strategien zur Papierfunktionalisierung mit Peptiden getestet und zunächst hinsichtlich ihrer Effizienz optimiert, das fluoreszierende Modellprotein *turboGFP* über Enzym-vermittelte Konjugation zu binden. Ein Vergleich der optimierten Proteinkonjugationsstrategien zeigte, dass die Inkubation in Puffer und das Absättigen von unspezifischen Konjugationsstellen mit Rinderserumalbumin vor der Enzym-vermittelten Proteinanbindung, die erfolgversprechendste Vorgehensweise ist. Die Strategien zeigten darüber hinaus verschiedene Vor- und Nachteile hinsichtlich ihrer Eignung für zukünftige Anwendungen und weiteren Optimierungsbedarf.

Die erste Strategie basierte auf der Licht-induzierten Einführung eines Erkennungspeptids und anschließender enzymatischer Bindung. Diese zeigte eine hohe Effizienz und Leistungsfähigkeit. Die Peptidbeladung kann direkt aus dem ermittelten Amingehalt bestimmt werden, da das Peptid in voller Länge in einem Schritt immobilisiert wird. Die angenommene Wechselwirkung während der Fluoreszenzmessung des vollständigen Linkers mit tGFP macht es jedoch schwierig, das tatsächliche Potenzial der Verwendung von tGFP für die (Semi-) Quantifizierung zu beurteilen. Möglicherweise wird die ermittelte tGFP-Beladung in dem gewählten Aufbau unterschätzt. Weiterhin ist diese Strategie recht anspruchsvoll. Aus wirtschaftlichen Gründen ist die Verwendung dieser Strategie daher wahrscheinlich auf Anwendungen beschränkt, die eine Funktionalisierung definierte Bereiche im Papier erfordern.

Die zweite Strategie basierte auf der Oxim-Ligation zur Peptidimmobilisierung. Wie bei Strategie 1 entspricht die Peptidbeladung dem mit TNBS bestimmten Amingehalt. Die Strategie hat unter verschiedenen Bedingungen hervorragende Ergebnisse erzielt. Mit Anilin als Katalysator könnten die Ergebnisse noch verbessert werden. In Bezug auf die Nachhaltigkeit ist dieser Ansatz, so wie er durchgeführt wurde, allerdings sehr vorteilhaft, da alle Konjugationsschritte in Wasser durchgeführt werden, ohne dass ein Waschen mit organischen Lösungsmitteln erforderlich ist. Ergänzt durch eine Peptidsynthese auf Wasserbasis wäre der

Ansatz vollständig "grün" und unter dem Aspekt der Nachhaltigkeit damit eine gute Wahl für weitere Forschung und künftige Anwendungen.

Die dritte Strategie stützte sich auf Kadaverin als anfängliche Funktionalisierung von Baumwoll-Linters und erwies sich zunächst als weniger effizient im Hinblick auf die Proteinkonjugation als die verglichenen Strategien. Dennoch ist der Unterschied bei den Ergebnissen der mit BSA vorinkubierten Papiere, nicht signifikant. Ein kleiner Nachteil ist jedoch die Tatsache, dass die immobilisierte Peptidbeladung nicht direkt quantifiziert werden kann. Nur der kombinierte Gehalt des Triglycins und nicht umgesetzter Kadaverinreste kann dargestellt werden. Das Potenzial von Strategie 3 könnte durch die Optimierung der Reaktionszeiten für die Linkerbindung noch weiter gesteigert werden.

Die vierte Strategie basiert auf der Veresterung der Fmoc-6-Aminohexansäure als initiale Funktionalisierung von Baumwoll-Linters. Die Strategie ist sehr vielversprechend, da sie gute Ergebnisse bei Reaktionen mit Fasern, sowohl auf trockenem als auch auf BSA-inkubiertem Papier, liefert. Die immobilisierten Peptidmengen müssen jedoch sorgfältig gesteuert werden, da Papiere mit einem sehr hohen Peptidgehalt anscheinend sehr gut Proteine adsorbieren. Andererseits behindert ein hoher Peptidgehalt die Herstellung von vergleichbaren Papieren. Wie bei Strategie 3 ist nur die kombinierte Menge der potenziell nicht umgesetzten immobilisierten 6-Aminohexansäurereste und des vollständigen Linkers im TNBS-Test quantifizierbar. Diese Peptid-Immobilisierungsstrategie, stellt die am wenigsten anspruchsvolle unter allen untersuchten Methoden dar. Alle Edukte sind leicht zugänglich, angefangen bei unmodifizierten Baumwoll-Linters-Fasern bis hin zu Standard-SPPS-Bausteinen und -Reaktionsschritten. In Kombination mit den vielversprechenden Ergebnissen, scheint dieser Ansatz eine sehr vielversprechende Methode für zukünftige Anwendungen zu sein.

Die Untersuchung weiterer Eigenschaften ist für die Verwendung in zukünftigen Applikationen notwendig, darunter eine Optimierung der Reaktionsbedingungen und die Bestimmung der Papierspezifikationen. Die Kenntnis dieser Eigenschaften wird es ermöglichen, die ideale Methode mit den Anforderungen an die angestrebte Anwendung abzustimmen.

7. Experimental section

7.1. General

7.1.1. Solvents

Solvents were obtained from *Carl Roth GmbH & Co. KG* (Karlsruhe, Germany), *Fisher Scientific GmbH* (Schwerte, Germany) or *Merck KGaA* (Darmstadt, Germany) and used without further purification unless specified otherwise.

7.1.2. Reagents

Chemicals were obtained from *Fisher Scientific GmbH* (Schwerte, Germany), *Merck KGaA* (Darmstadt, Germany), *Carl Roth GmbH & Co. KG* (Karlsruhe, Germany), *Agilent Technologies, Inc.* (Santa Clara, US), *Bachem Holding AG* (Bubendorf, Switzerland), *Fluochem Ltd.* (Derbyshire, United Kingdom), and *TCI Deutschland GmbH* (Eschborn, Germany).

Protected amino acids and building blocks were purchased from *Carbolution Chemicals GmbH* (St. Ingbert, Germany), *Carl Roth GmbH & Co. KG* (Karlsruhe, Germany), or *Iris Biotech GmbH* (Marktredwitz, Germany).

All reagents were applied without further purification or drying.

7.1.3. Supported materials

TAMRA-NHS was supported by members of Kolmar working group (TU Darmstadt).

Unmodified cotton linters fibers (Grade 225 HSR-M, Buckeye Technologies) and TEMPO-oxidized ones were supported by Laura Hillscher (Biesalski's working group, TU Darmstadt). Results of TEMPO-oxidations are listed in Table 2.

Table 2: Specifications of TEMPO-oxidized fibers.

Batch	n(NaClO) per gram fibers [mmol/g]	surface carboxyl content [$\mu\text{mol/g}$]	total aldehyde content [$\mu\text{mol/g}$]
blank fibers	NA	NA	22 (± 1.3)
1	0.3	10.33 (± 1.4)	122 (± 1.3)
2	0.15	5.39 (± 0.4)	64.9 (± 3.3)

7.1.4. Removal of organic solvents

Organic solvents were removed under reduced pressure with a *Rotavapor R-300* rotary evaporator (*BÜCHI Labortechnik AG*, Flawli, Switzerland)) combined with either a *MD4C* membrane pump (*VACUUBRAND GmbH & Co. KG*, Wertheim, Germany) or a *trivac D4A* high vacuum pump (*Leybold GmbH*, Köln, Germany) with a *MC2L* Unicryo cooling trap (*UniEquip Laborgerätebau und Vertriebs GmbH*, Martinsried bei München, Germany).

7.1.5. Lyophilization

Lyophilization was performed on a *Christ Alpha 2-4 LSC* freeze dryer (*Martin Christ Gefriertrocknungen*, Osterode am Harz, Germany) furnished with an *Ilmvac Type 109012* high vacuum pump (*Gardner Denver Thomas GmbH*, Fürstentfeldbruck, Germany).

7.1.6. Storage

Protected amino acids, building blocks and activation reagents were stored at -18 °C. All other substances were stored as recommended by the supplier. The photoenol **2** was stored at -20 °C. The tGFP variants were stored at 4 °C. Sortase A and microbial transglutaminase were stored as -80°C. Peptide loaded resins were stored *in vacuo*; cleaved peptides were stored in reaction tubes at -20 °C. Buffers were stored at room temperature or 4 °C. Fibers in aqueous suspension were stored at 4 °C. Dried fibers and papers were stored at ambient conditions.

7.2. Characterization

7.2.1. NMR spectroscopy

¹H and ¹³C spectra of liquid samples were recorded on an *Avance III* or an *Avance II* NMR Spektrometer at 300 MHz (*Bruker BioSpin GmbH*, Rheinstetten, Germany). All samples were dissolved in chloroform-d or DMSO- δ 6 (*Sigma-Aldrich Chemie GmbH* now *Merck KGaA*, Darmstadt, Germany).

The spectra were recorded by the NMR department at the chemistry faculty at TU Darmstadt.

7.2.2. X-ray photoelectron spectroscopy

Analysis was performed on an SSX 100 ESCA Spectrometer (Surface Science Laboratories, Inc., Singapore) equipped with a radiant source emitting monochromatic Al K α X-rays (9kV).

XPS spectra were recorded by members of Hess' working group at the chemistry faculty at TU Darmstadt

7.2.3. High performance liquid chromatography (HPLC)

Analytical RP-HPLC

Analytical reversed-phase high performance liquid chromatography (RP-HPLC) was performed using an *Agilent LC 1100 series* (Agilent Technologies, Inc., Santa Clara, US) with an *Agilent Eclipse Plus* RP column (C18, 100 \times 4.6 mm, 3.5 μ m, 95 Å) at a 0.6 mL/min flow rate.

Eluents A (0.1 % aqueous TFA) and B (90 % acetonitrile, 10 % water including 0.1 % TFA) were used for sample elution. Absorption was measured at 220 nm, 280 nm and/or 554 nm.

Semi-preparative RP-HPLC

An Interchim PuriFlash 4250 (Interchim, Montluçon, France) equipped with a *Prep-LC column* (*Uptisphere Strategy C18-HQ*, 5 μ m, 250 \times 21,2 mm) was used with a flow rate of 18 mL/min.

Eluents A (0.1 % aqueous TFA) and B (90 % acetonitrile, 10 % water including 0.1 % TFA) were used for sample elution. Absorption was measured at 220 nm and 280 nm.

7.2.4. Mass spectrometry

Electrospray-ionization mass spectrometry (ESI-MS) was performed on a *Shimadzu LCMS-2020* (Shimadzu Deutschland GmbH, Duisburg, Germany) combined with a *Phenomenex Synergy 4 u Fusion-RP 80* column (C-18, 250 \times 4.6 mm, 2 μ m, 80 Å; Phenomenex Ltd. Deutschland, Aschaffenburg, Germany). Eluents A (0.1 % formic acid in LC-MS-grade water) and B (0.1 % formic acid in LC-MS-grade acetonitrile) were used for substance elution.

7.2.5. UV-Vis spectroscopy

UV/Vis spectra were either obtained using a *Shimadzu UV-1650 PC* or a *Shimadzu UVmini 1240* device. Using either *Qarzglas Suprasil* quartz cuvettes (10 mm pathlength; *Hellma Analytics*, Müllheim, Germany) or *semi-micro cuvettes* (PS, 10 mm pathlength; *Sarstedt AG & Co. KG*, Nümbrecht, Germany).

7.2.6. Fluorescence imaging

Fluorescence images were recorded on a *Fusion FX7 Edge* chemiluminescence and fluorescence imager (*VILBER LOURMAT Deutschland GmbH*, Eberhardzell, Germany) equipped with a CCD-camera. Either LED white-light epi-illumination or LED epi-fluorescence-illumination in the UVA- (365 ± 20 nm), blue- (480 ± 20 nm) or green- (530 ± 20 nm) light regions was used. For detection either no filter, a green filter (F-535, 505 - 565 nm) or an orange filter (F-595, 560 - 630 nm) was used. Exposure times were adjusted to the dynamic of the individual image.

7.2.7. Confocal laser scanning microscopy

A *Leica TSC SP8* confocal microscope (*Leica Microsystems CMS GmbH*, Wetzlar, Germany) furnished with a *HC PL FLUOTAR 10×/0.30 DRY* objective was used to capture CLSM images with a protocol after Bump et al.¹⁴⁰ Imaging of the samples was obtained by sequential excitation of each pixel line of the confocal scan with a 405 nm and 488 or 552 nm laser, corresponding to an appropriate excitation for the expected fluorescence derived from cellulose,¹⁴⁰ tGFP,¹⁴¹ TAMRA or mKOκ,¹⁴¹ respectively.

The images were recorded by members of Biesalski's working group at the chemistry faculty at TU Darmstadt.

7.3. Biological materials and methods

7.3.1. Materials

The heterologously expressed proteins sortase A pentamutant **6**,¹⁰⁰ mTG **24**,¹⁴² mTG derivative **9**,¹⁰⁰ ZZ-domain **11**,¹⁰⁰ as well as the plasmids to produce tGFP **7**⁴⁹ and **23**¹⁰¹ were provided by members of AG Kolmar, TU Darmstadt. Their production is described in the cited references.

mKOκ-CBM fusion proteins were kindly provided by Markus Langhans, TU Darmstadt.

Purchased materials were obtained from *Fisher Scientific GmbH* (Schwerte, Germany), *Merck KGaA* (Darmstadt, Germany), *Carl Roth GmbH & Co. KG* (Karlsruhe, Germany), *GE Healthcare Europe GmbH* (Solingen, Germany), *New England Biolabs GmbH* (Frankfurt am Main, Germany) and *Thermo Fisher Scientific* (Schwerte, Germany).

7.3.2. Bacterial strain for tGFP expression

Escherichia coli BL21(DE3): F-ompT hsdS_B(r_B-m_B-) gal dcm λ(DE3)

7.3.3. Culture media and buffers

Culture media

dYT-medium (double yeast tryptone medium)	1 % (w/v) Yeast extract 1.6 % (w/v) Tryptone/Peptone from casein pancreatic digested 0.5 % (w/v) NaCl
--	---

Buffers

PBS buffer (10×), pH 7	1.37 M NaCl 100 mM Na ₂ HPO ₄ 27 mM KCl 18 mM KH ₂ PO ₄
PBS buffer (1×), pH 7	137 mM NaCl 10 mM Na ₂ HPO ₄ 2.7 mM KCl 1.8 mM KH ₂ PO ₄
PBS-T buffer, pH 7	137 mM NaCl 10 mM Na ₂ HPO ₄ 2.7 mM KCl 1.8 mM KH ₂ PO ₄ 0.1% Tween® 20
TBS buffer (10×), pH 7.5	500 mM Tris/HCl 1.5 M NaCl
TBS buffer (1×), pH 7.5	50 mM Tris/HCl 150 mM NaCl
TBS-T buffer (1×), pH 7.5	50 mM Tris/HCl 150 mM NaCl 0.1% Tween® 20
Lysis buffer, pH 8.0	50 mM Tris/HCl 150 mM NaCl 1 mM EDTA 1 mg/mL lysozyme (added after suspension)
IMAC A (loading)	50 mM Tris/HCl 600 mM NaCl 20 mM Imidazole

IMAC B (elution) buffer, pH 7.5	50 mM Tris/HCl 600 mM NaCl 500 mM Imidazole
Sortase A reaction buffer (10×), pH 7.5	500 mM Tris/HCl 1.5 M NaCl 50 mM CaCl ₂
mTG reaction buffer (10×), pH 8.0	250 mM Tris/HCl 1.5 M NaCl
SDS-PAGE 4 × running gel buffer	3 M Tris/HCl pH 8.85 4 mg/mL SDS
SDS-PAGE 4 × stacking gel buffer	0.5 M Tris-HCl pH 6.8 4 mg/mL SDS
SDS-PAGE 5 × loading buffer (reducing)	0.25 M Tris/HCl pH 8 7.5% (w/v) SDS 25% (v/v) Glycerin 0.25 mg/ml Bromophenol blue 12.5% (v/v) 2-mercaptoethanol
SDS-PAGE running buffer	50 mM Tris/HCl pH 8.8 190 mM Glycine 1 mg/mL SDS

Solutions

Coomassie destaining solution 1	10% (v/v) AcOH _{aq.} 25% (v/v) Isopropanol
Coomassie destaining solution 2	10% (v/v) AcOH _{aq.}
Coomassie staining solution	0.2% (w/v) Coomassie Brilliant Blue R-250 0.2% (w/v) Coomassie Brilliant Blue G-250 30% (v/v) Isopropanol 7.5% (v/v) AcOH _{aq.}

7.3.4. Immobilized metal ion affinity chromatography (IMAC)

IMAC was performed to purify tGFP derivatives with a hexa-His-tag. The stable complex of Ni²⁺-loaded nitrilotriacetic acid (NTA) immobilized to the column matrix. The matrix further binds the hexa-His-tag of recombinantly produced proteins by complexation of histidine imidazole rings. Proteins were purified using gravity flow chromatography or an ÄKTA Purification System (GE Healthcare) with a HisTrap™ 1 ml HP column (GE Healthcare). For the latter the elution of the protein of interest was performed by applying a continuous gradient of imidazole. Purity of the fractions was determined by SDS-PAGE.

7.3.5. Sodium dodecyl sulfate polyacrylamide gel electrophoresis (SDS-PAGE)

SDS-PAGE was used to assess the purity of protein samples and the formation of by-products in mTG ligation as described in chapter 3.4.5. Protein samples are hereby assessed due to their molecular weight. A pre-stained protein standard, a mixture of proteins with known molecular weight was applied to one line of the SDS gel. To identify the molecular weight of tested protein mixtures samples were diluted in a 5× loading buffer containing β -mercaptoethanol to reduce disulfide bonds. Samples were heated to 98 °C for 5-10°C to ensure full denaturation. Cooled samples were centrifuged and applied to the SDS polyacrylamide gel (composition see Table 3) in an electrophoresis chamber. The gel was covered with running buffer and electrophoresis was carried out at 40 mA for 1 h. Gels are stained with Coomassie staining solution under microwave heating for 1 minute to color protein bands. Incubation in destaining solutions 1 and 2 followed for the removal of excess background staining.

Table 3: Composition of 15% separation and stacking gel. Volume for 5 gels.

Stock solution	Separation gel	Stacking gel
ROTIPHORESE 30% acrylamide-bisacrylamide solution	13 ml	2.4 ml
4× separation gel buffer	6.5 ml	/
4× stacking gel buffer	/	3.6
water	6.5 ml	8.4 ml
APS-Stock 10 % (w/v)	195 μ l	129.6 μ l
TEMED	9.75 μ l	10.8 μ l

7.3.6. Production and purification of tGFP-derivatives 7 or 23

The respective expression plasmid (pET16btGFP-LPETGGH₆⁴⁹ or pET16btGFP-DIPIGQGMTGH₆¹⁰¹) was transformed into *E.coli* BL21 (DE3) via electroporation. Therefore, 50 μ l of a cell suspension were mixed with 1-5 μ l of the respective DNA. The mixture was pipetted in an electroporation cuvette and a voltage pulse was applied (2500 V, 25 μ F, 200 Ω) using a *BioRad Gene Pulser*. The cells were spread on ampicillin (0.1 % v/v) containing dYT-plates. After overnight incubation at 37 °C a single colony was suspended in dYT medium (50 mL) containing ampicillin (0.1 % v/v) and incubated again at 37 °C overnight. dYT medium (1 L) with ampicillin (0.1 % v/v) was inoculated to an OD_{600nm} of 0.1 from the overnight culture. At an OD_{600nm} of 0.5 protein production was induced by the addition of IPTG (1 mM). The culture was incubated in the dark at 18 °C overnight. The supernatant was removed by centrifugation. Cells were suspended in IMAC A or lysis buffer, sonicated and centrifuged. The supernatant was

filtrated (0.45 μm) and supernatant proteins were separated on HisTrap HP (1 ml, GE Healthcare) using a linear gradient of imidazole on an Äkta purification system (GE Healthcare). Pure fractions were combined and dialyzed (MW cut-off 3.5 kDa) overnight against 50 mM Tris-HCl pH 7.4, 300 mM NaCl.

The protein's concentration in solution was determined by the specific absorption at 280 nm. The molar extinction coefficient of a protein, along other protein parameters can be calculated by its primary sequence. Calculations were performed using *Expasy ProtParam*.¹⁴³ Subsequently, the protein concentration can be calculated using Lambert-Beer-law. Photometrical determination of the protein concentration was performed using *BioSpec Nano™ Microvolume UV-Vis Spectrophotometer* (Shimadzu).

tGFP 7: Molecular weight: 27521.36 g/mol; Theoretical pI: 5.49; Molar extinction coefficient: ϵ (280 nm) = 17880 $\text{M}^{-1} \text{cm}^{-1}$; c = 269 μM

tGFP 23: Molecular weight: 26469.34 g/mol; Theoretical pI: 5.64; Molar extinction coefficient ϵ (280 nm) = 17880 $\text{M}^{-1} \text{cm}^{-1}$; c = 325 μM

7.4. Solid phase peptide synthesis (SPPS)

7.4.1. General procedure for manual SPPS

The synthesis was carried out manually using standard Fmoc-SPPS on an *AmphiSpheres™ 40* RAM resin (0.37 $\text{mmol} \cdot \text{g}^{-1}$, Agilent Technologies)

The resin (0.125 or 0.25 mmol) was swollen in DCM for 30 min and successively in DMF for 30 min under agitation. Fmoc deprotection was carried out with 20% piperidine in DMF for 15 minutes, followed by washing with DMF (5 \times 5-10 mL).

Canonical amino acids were attached by double coupling (Table 4): A solution of the respective Fmoc-protected amino acid (4 eq.), with N, N-diisopropylethylamine (DIPEA, 8 eq.), and HBTU (3.97 eq.) in a minimal amount of DMF was prepared and added to the deprotected resin. The suspension was shaken for 40 min at RT. After washing with DMF (5 \times 5-10 mL), the procedure was repeated. The solution was removed by filtration and the loaded resin was washed with DMF.

In the case of Fmoc-Lys (Dde)-OH and Boc-GGG-OH 2 eq. of the amino acid, 1.97 eq. of HATU and 4 eq. of DIPEA were used.

ESI-MS: measured m/z: 924.5 $[M+H]^+$

Backbone synthesis was performed as stated but stopped for peptide **4.1** with the introduction of β -Alanine. After final Fmoc deprotection TAMRA was introduced to the peptide backbone using (5/6)-TAMRA-NHS (4 eq.) and DIPEA (8 eq.) in a minimum of DMF. The solution was shaken at RT for 24 h and washed thoroughly with DMF. Lysine side chain deprotection was performed as explained. 4-maleimidobutyric acid (4 eq.), HBTU (4 eq.) and DIPEA (4 eq.) in a minimum of DMF, were added to the resin and shaken for 3 h at ambient temperature. After washing with DMF, DCM and ether, the resin was dried under reduced pressure.

The peptide was cleaved from the dry resin using a mixture of TFA, anisole, triethylsilane (TES) and H₂O (94:2:2:2, V:V:V:V, 10 mL).

The peptide was purified by preparative RP-HPLC and analyzed by analytical HPLC and LC-MS.

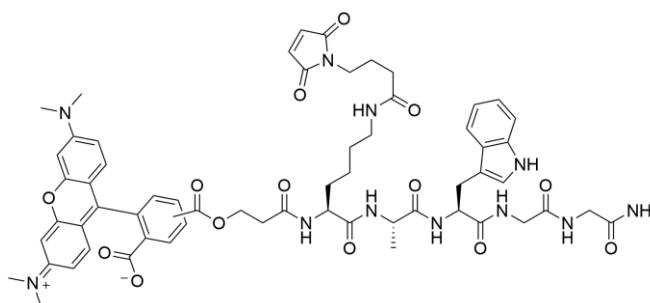


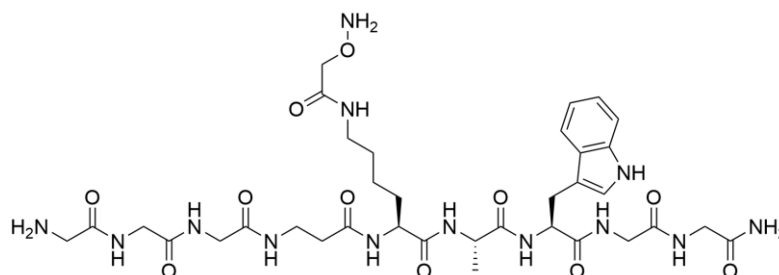
Figure 62: Structure of peptide **4.1**. MW = 1165.5 g·mol⁻¹

ESI-MS: $m/z = 1164.7$ $[M+H]^+*$ ¹

*1Additionally to $m/z = 1164.7$ $[M+H]^+$ a value of $m/z = 1275.8$ $[M+H]^+$ was found. Due to the treatment of resin bound TAMRA-peptide with hydrazine, a chemical conversion of TAMRA occurred. The resulting peptide was still a fluorescent chromophore; thus, it was used for the proof-of-concept experiments. CLSM parameters were adjusted accordingly.

Backbone synthesis and lysine side chain deprotection were performed as explained. The deprotected peptide-resin was washed with DMF, and subsequently N-(1-ethoxyethylidene)-2-aminooxyacetic acid N-hydroxysuccinimidylester (Eei-Aoa-NHS, 2 eq.) and DIPEA (1.92 eq.) in

The peptide was purified by preparative RP-HPLC and analyzed by analytical HPLC and LC-MS.

ESI-MS: $m/z = 832.5$ $[M+H]^+$

For one paper sheet 5.2 ± 0.2 mg fibers were homogenously suspended in water in a 2 mL BD syringe equipped with a PET frit (~ 0.9 cm inner diameter). With the help of the syringe plunger the water was pressed out and the paper was removed from the syringe along with the syringe plunger. The wet paper was pressed on blotting paper and dried between two glass slides for 10 min on a heating block at 97°C unless indicated otherwise. Dried papers were allowed to equilibrate to ambient conditions overnight.

Primary amines were quantified with a 2,4,6-trinitrobenzenesulfonic acid (TNBS) containing reaction solution with a protocol adapted as follows. 250 μ L of a 0.01% solution of TNBS in sodium bicarbonate 0.1 M (pH8.5) was added to each paper sample and blank (unmodified cotton linters papers). The papers were allowed to react for 2 h at 37°C. For samples: 200 μ L of the reaction solutions were added to 400 μ L of a 200 μ M glycine or β -alanine standard. For blanks: 200 μ L of the reaction solutions were added to 400 μ L of a standard solution ranging from 0 to 200 μ M. The preparations were allowed to react for 2 h at 37 °C. The reaction was

stopped by the addition of 300 μ L of a 2:1 mixture of 10% aqueous SDS and 1 M HCl. Absorbance was detected at 335 nm.

7.7. Part I

7.7.1. Pretreatment of paper discs 1

Filter paper samples (MN 616, Machery Nagel) were standardized to circles of 0.5 or 1.6 cm in diameter by employing a hole puncher. The paper pieces were placed in aqueous NaOH (10 wt-%) and kept under gentle agitation overnight. The discs were washed with ethanol until a neutral supernatant (pH 6-8) was obtained and stored in ethanol until further use.

7.7.2. Synthesis of 4-((2-formyl-3-methylphenoxy)methyl)benzoic acid 2

The synthesis followed slightly modified protocols published by Oehlenschlaeger et al. ^[57] and Pauloehrl et al. ^[58].

2-methoxy-6-methylbenzaldehyde

To a mixture of acetonitrile and water in equal parts (330 mL), 4.59 g (1 eq.) 2,3-dimethyl anisole, 8.9 g (1.06 eq.) CuSO₄ 5 H₂O and 26.7 g (2.93 eq.) K₂S₂O₈ were added. The suspension was intensely stirred and heated to 90 °C, until all the starting material had been consumed as indicated by thin layer chromatography. When the mixture cooled to room temperature, the non-dissolved copper salt was removed by filtration. DCM (100 mL) was added, and the phases were allowed to separate. The aqueous phase was extracted with DCM (65 mL) twice and the combined organic layers were dried over MgSO₄. The solvent was removed under reduced pressure. The crude product was purified by flash chromatography (silica gel, hexane/ethyl acetate 5:1 (V:V) 3 L, 1:1 (V:V) 1 L, 1:2 (V:V) 1 L).

Yield: 2.45g (49.7 %), yellow solid.

¹H NMR (300 MHz, CDCl₃) δ (ppm): 10.63 (s, 1H), 7.40 – 7.32 (m, 1H), 6.80 (t, *J* = 8.8 Hz, 2H), 3.88 (s, 3H), 2.55 (s, 3H).

R_F = 0.3

2-hydroxy-6-methylbenzaldehyde

2.4 g (1 eq.) of 2-methoxy-6-methylbenzaldehyde (Step 1) were dissolved in DCM (22 mL) before 6.4 g, (1 eq.) of AlCl_3 were added to the yellow solution. The mixture was stirred at room temperature overnight. The color changed from yellow to dark brown. Deionized water was cautiously added to quench excess of AlCl_3 , and further to dissolve the solid residual. The phases were separated, and the aqueous layer was extracted with DCM (3×30 mL). The combined organic layers were dried over MgSO_4 . The solvent was removed under reduced pressure.

Yield: 2.22 g (100 %), dark yellow oil.

The crude product was used without further purification.

^1H NMR (300 MHz, CDCl_3) δ (ppm): 11.88 (s, 1H), 10.31 (s, 1H), 7.35 (t, $J = 7.9$ Hz, 1H), 6.74 (dd, $J = 30.8, 7.9$ Hz, 2H), 2.59 (s, 3H).

Methyl 4-((2-formyl-3-methylphenoxy)methyl)benzoate

2.2 g (1 eq.) of 2-hydroxy-6-methylbenzaldehyde and 3.78 g (1.02 eq.) of 4-(bromomethyl) benzoate were dissolved in dry acetone (112 mL). 3.37 g (1.5 eq.) K_2CO_3 and 67 mg (0.015 eq.) 18-crown-6 were added to the solution and the color changed instantly from yellow to black. The mixture was stirred at 40 °C overnight. The suspension was filtrated, and the solvent was removed under reduced pressure. The residue was dissolved in equal parts of DCM and deionized water (80 mL) and acidified with HCl (1 M). The aqueous layer was extracted with DCM (2×40 mL) and the combined organic layers were dried over MgSO_4 . The solvent was removed under reduced pressure. Impurities were dissolved with n-hexane/ethyl acetate (7:1 (V:V), 100 mL). The product was dried under reduced pressure.

Yield: 2.76 g (60 %), yellow powder.

^1H NMR (300 MHz, CDCl_3) δ (ppm): 10.74 (s, 1H), 8.05 (d, $J = 8.3$ Hz, 2H), 7.48 (d, $J = 8.2$ Hz, 2H), 7.34 (t, $J = 8.0$ Hz, 1H), 7.24 (s, 1H), 6.83 (dd, $J = 7.9, 3.5$ Hz, 2H), 5.21 (s, 2H), 3.91 (s, 3H), 2.57 (s, 3H).

4-((2-formyl-3-methylphenoxy)methyl)benzoic acid

1.01 g (1 eq.) of methyl 4-((2-formyl-3-methylphenoxy)methyl)benzoate were dissolved in DCM (50 mL). 440 mg (3 eq.) of NaOH dissolved in 10 mL methanol were added. The reaction mixture was stirred overnight at ambient temperature. The solvents were removed under

reduced pressure. The residue was dissolved in equal parts of DCM and water (100 mL). The organic layer was extracted with deionized water (3 × 20 mL). The combined aqueous layers were acidified with HCl (1 M) to pH 3. The aqueous phase was subsequently extracted with DCM (3 × 50 mL). The combined organic layers were dried over MgSO₄, followed by solvent removal under reduced pressure.

Yield: 0.88 g (91.6%), white powder.

¹H NMR (300 MHz, DMSO-*d*₆) δ(ppm): 10.63 (s, 1H), 7.97 (d, *J* = 8.3 Hz, 2H), 7.61 (d, *J* = 8.3 Hz, 2H), 7.52 – 7.44 (m, 1H), 7.13 (d, *J* = 8.4 Hz, 1H), 6.89 (d, *J* = 7.6 Hz, 1H), 5.34 (s, 2H), 2.48 (s, 3H).

UV-Vis: λ_{max} < 350 nm

7.7.3. PE-functionalization of paper 1 resulting in paper 3

Pretreated paper discs **1** were placed in DCM for solvent exchange and subsequently in a solution of 37 mg (0.135 mmol, 1 eq.) 4-((2-formyl-3- methylphenoxy)methyl)benzoic acid (PE), 65 mg (0.34 mmol, 2.5 eq.) 1-ethyl-3-(3-dimethylaminopropyl)carbodiimide (EDC) and 4 mg (0.034 mmol, 0.25 eq.) 4-dimethylaminopyridine (DMAP) in anhydrous DCM (10 mL). The mixture was flushed with inert gas for 2 min and gently shaken at ambient temperature overnight. The paper **3** was washed with DCM, THF, deionized water, and again THF (each 10 mL for at least 20 min) and kept in THF until further use.

7.7.4. Diels-Alder reaction of PE-functionalized paper with maleimido-peptides **4** or **4.1** using a stencil to produce papers **5** or **5.1**

Paper **3** (Ø=1.6 cm) was placed in the sample holder comprising a 20 mL syringe with a frit, shortened at the 5.5 mL labeling, and closed at the outlet. A stencil in a copper foil was pinned on the paper with two sterile cannulas. The respective peptide **4** or **4.1** (1 mg/mg paper) was dissolved in dry DMF (2 mL) and added to the paper. The setup was purged with inert gas for 20 min before irradiation from approximately 5 cm distance for 2.5 h using an Exo Terra UVB200 lamp (25 W, KG HAGEN Deutschland GmbH & Co.). The sample was washed by gentle shaking in DMF overnight and after for 1 h in deionized water.

7.7.5. Diels-Alder reaction of PE-functionalized paper with GGG-maleimido-peptide 4 for quantification and further ligations of 5

Paper samples **3** ($\varnothing=0.5$ cm) were placed in a small glass petri dish. The respective peptide **4** or **4.1** (1 mg/mg paper) was dissolved in dry DMF (2 mL) and added to the paper. The setup was purged with inert gas for 20 min before irradiation from 5 cm distance for 2.5 h using an Exo Terra UVB200 (KG HAGEN Deutschland GmbH & Co.) reptile lamp (25 W). The samples were washed by gentle shaking in DMF overnight and after for 1 h in deionized water.

7.7.6. SrtA-mediated ligation of filter papers 5 with stencil and tGFP 7

A paper disc **5** ($\varnothing=1.6$ cm functionalized with stencil) was equilibrated in sortase A reaction buffer (1 \times) for 5 min and ligation was performed with tGFP **7** (16.95 nmol) and sortase A pentamutant (1.695 nmol) for 2 h at 22 °C. Adsorption controls were performed with milliQ® water instead of the enzyme. The product was washed 3 \times with TBS-T and 3 \times with TBS.

7.7.7. SrtA-mediated ligation of GGG-photoconjugates 5 with proteins 7, 9 or 11

Paper discs **5** ($\varnothing=0.5$ cm) were equilibrated in sortase A reaction buffer (1 \times) and ligation was performed with the respective protein tGFP **7**, pro-mTG **9** or ZZ-domain **11** (0.5 eq.) and sortase A pentamutant (0.05 eq.) for 2 - 4 h at 22 °C. Adsorption controls were performed with milliQ® water instead of the enzyme. The product was washed three times with PBS-T and three times with PBS.

7.7.8. Quantification of protein load using tGFP fluorescence

For quantification of the immobilized tGFP **7**, a standard curve was generated by dropping 4 μ L of the tGFP **7** solution in a specified concentration onto standardized, plain Whatman® Grade 40 filter paper ($\varnothing = 0.5$ cm, m = 2.2 mg). The fluorescence signals of the ligation products and the adsorption controls were compared to the freshly prepared standard curve. Samples **5.1** were carried along for blank correction.

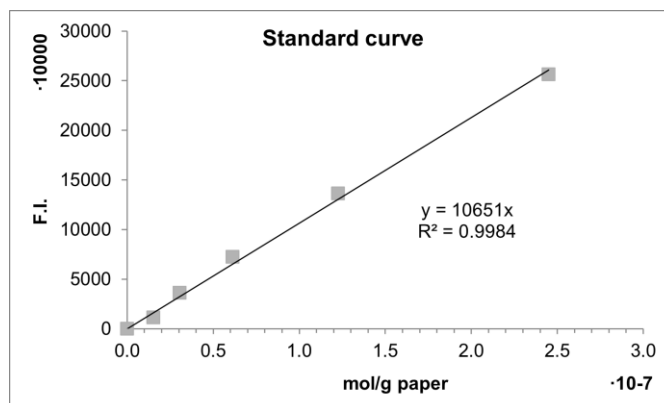


Figure 64: Standard curve for tGFP quantification.

Table 5: Utilized concentrations of tGFP 7 calculated into loading on paper.

Concentration [μM]	Loading [μmol/g]
134.75	0.245
67.38	0.123
33.69	0.061
16.84	0.031
8.42	0.015
0	0

7.7.9. Hydroxamate assay: microbial transglutaminase activity test

Prior to activity testing the pro-sequence was cleaved off the paper samples **10** and adsorption controls by incubation in a solution containing the neutral protease dispase at 1.2 – 2.0 U/mL for 30 min at 37°C. The papers were thoroughly washed, with TBS, PBS-T and again TBS until no more foam was built.

For one activity test, a paper sample **10** and the respective adsorption control were each placed in 200 μL of a reaction mixture consisting of hydroxylamine hydrochloride (100 mM), glutathione (reduced, 10 mM) and N-benzyloxycarbonyl-L-glutaminyglycine (Z-QG, 35.6 mM) in Tris-acetate buffer (pH 6.0 at 37 °C). The samples were kept on a shaker at 37 °C for 10 min. To stop the reaction 500 μL of trichloroacetic acid and 500 μL of a FeCl₃ solution (5% in 0.1 M HCl) were added and mixed. For readout, absorption of the supernatants was measured at 525 nm with an ELISA reader (CLARIOstar, BMG LABTECH GmbH, Germany).

7.7.10. ZZ-conjugation test: paper-based ELISA

Table 6: Required Materials for paper-based ELISA

Substrate	Human IgG (1.4 mg/mL)
Blocking solution	Milk powder, 5-wt% in PBS-T
Detection antibody	goat anti-hIgG(Fab-specific)-HRP (1:5000 in PBS-T)
HRP-substrate solution	1 mL PBS 0.1 mL 4-chloro-1-naphthol (6mg/mL in EtOH) 0.01 mL H ₂ O ₂ (3 vol.-%)

The assay was performed following the steps:

1. Drying of paper **12** at RT
2. Blocking: 3 μ L blocking solution, 10 min, RT
3. Incubation with substrate: 5 μ L, 5 min
4. Washing: 3 \times 15 μ L with PBS-T on blotting paper
5. Incubation with detection antibody: 5 μ L, 5 min
6. Washing: 3 \times 15 μ L with PBS-T, 3 \times 10 μ L with PBS on blotting paper
7. Colorimetric assay: 150 μ L substrate solution, 20 min, RT
8. Washing: 2 \times 100 μ L water
9. Readout: Scanning with standard desktop scanner

Analysis of grey values was performed using Fiji^[2] a distribution of ImageJ.^[1, 3]

7.8. Part II: Preliminary experiments

7.8.1. Optimization of strategy 1 regarding PE input

For each sample 5 mg (1 eq. AGU) of cellulose linters fibers **1** (Grade 225 HSR-M, Buckeye Technologies) were soaked in deionized water and successively in DMF for solvent exchange. Stock solutions of PE **2** (0.12 M), EDC (0.3 M) and DMAP (0.4 M) were prepared separately in DMF. Related to the PE input a ratio of 2.5 eq. was used for EDC and 0.1 eq. for DMAP. Table 7 summarizes the volumes given to the different samples from the stocks. Solutions were filled up to approx. 1 mL purged with inert gas shortly and kept on a shaker at RT overnight. The resulting fibers **3** were washed thoroughly with DMF, DCM and deionized water before papermaking. The dried papers were analyzed by fluorescence imaging.

Table 7: Overview of the reactants input for esterification of paper with PE 2

Sample	eq. PE per AGU	V _{PE 2, stock} [μ L]	V _{EDC, stock} [μ L]	V _{DMAP, stock} [μ L]
1	1.0	251	257	7.5
2	0.5	125	129	3.8
3	0.25	62.7	64.3	1.9
4	0.125	31.3	32.2	0.9

The papers were disintegrated again. From a stock solution of the recognition peptide **4** (15.6 mM) dissolved in dry DMF 89 μ L were given to each sample. The suspensions were shortly purged with nitrogen and subsequently irradiated for 10 min from approximately 5 cm distance with the Exo Terra UVB200 lamp. The suspension was mixed, purged again, and irradiated again for 10 min. The reaction solution was removed, and the fibers were washed thoroughly with DMF and deionized water before papermaking. The dried papers were analyzed by fluorescence imaging.

Before sortase A-mediated ligation the fibers were disintegrated and washed with sortase reaction buffer (1 \times). tGFP-LPETGGH₆ **7** (80 μ M) and sortase A pentamutant **6** (16 μ M, 0.2 eq. of tGFP) in 100 μ L sortase ligation buffer were added. The fibers were incubated for 2 h at 22 °C in the reaction mixtures. The samples were washed with PBS to stop the reaction. Papers were made without applying heat and analyzed by fluorescence imaging.

7.8.2. Preliminary experiments of strategy 2 regarding oxime ligation

Comparison of reaction conditions with and without catalyst

A stock solution of peptide **14** (13.8 mM) was prepared in 0.1 M ammonium acetate pH 4.5 (solution A) and in 0.1 M ammonium acetate containing 100 mM aniline, pH 4.6 (solution B). To each sample of 5 mg TEMPO-oxidized fibers **13** (aldehyde content: 122 μ mol per gram paper) the respective amount of peptide stock solution, as noted in Table 8, was given to the samples, and filled up to 1 mL with the corresponding ammonium acetate solution. Two samples for each testing point were prepared in solution A, and one in solution B. One series of samples prepared with solution A and the samples prepared in solution B were kept at RT for 2 h. The second series prepared with solution A was kept at -20°C until frozen. After the conditions were reached, the samples were washed with solution A and PBS.

Table 8: Overview of the peptide **14** input for oxime ligation.

Sample	eq. of peptide 14 per aldehyde	V _{Peptide 14, stock} [μ L]
1	0	0.0
2	0.5	23.4
3	1	46.8
4	2	93.6
5	3	140

Fibers were washed with sortase reaction buffer (1 \times). tGFP-LPETGGH₆ **7** (80 μ M) and sortase A pentamutant **6** (16 μ M, 0.2 eq. of tGFP) in 100 μ L sortase ligation buffer were added. The fibers were incubated for 2 h at 22 °C in the reaction mixtures. The samples were washed with PBS to stop the reaction. Papers were made without applying heat and analyzed by fluorescence imaging.

Kinetic evaluation of oxime ligation

Samples of 5 mg TEMPO-oxidized fibers **13** (aldehyde content: 121 μ mol per gram paper) were prepared according to the previous experiment with 0.5 eq. peptide **14**. One series each was prepared for both solutions A and B to keep samples for 0.5, 1, 2, 4, 7, 16, 20 or 24 hours at RT before stopping the reaction by washing with solution A and PBS. Papers were made without applying heat and analyzed by fluorescence imaging. Afterwards sortase A ligation was performed as described in the previous experiment. Papers were made without applying heat and analyzed by fluorescence imaging.

7.8.3. Preliminary experiments on strategy 3

Evaluation regarding linker length

5 μ L 1,5-diaminopentane (cadaverine; 39.1 μ mol) were dissolved in 1.08 mL 15% AcOH in DMSO. 4 mg 2-picoline borane complex (37.4 μ mol) were dissolved in 1.0 mL 15% AcOH in DMSO. 250 μ L of either solution was added to each sample of 5 mg TEMPO-oxidized fibers **13** (aldehyde content: 121 μ mol per gram paper) intensively shaken for 5 min and incubated at 65 °C for 2 h. After cooling to ambient temperature, the samples were washed with DMSO, water, ammonium acetate and water.

In case of further reaction, solvent exchange to DMF was performed.

For the coupling of one glycine to a 5 mg fiber sample **17** 1.16 mg Fmoc-Gly-OH (3.89 μ mol), 1.46 mg HBTU (3.84 μ mol) and 1.35 μ L DIPEA (7.78 μ mol) were dissolved in approx. 1 ml DMF and allowed to react for 2 h. Fmoc-deprotection followed for 15 min with 20 % piperidine in DMF resulting in product **19.x**. The sample was thoroughly washed with DMF, DCM and ether.

For the coupling of three subsequent glycine residues to a 5mg fiber sample **17** 1.12 mg Boc-Gly-Gly-Gly-OH (3.89 μ mol), 1.46 mg HBTU (3.84 μ mol) and 1.35 μ L DIPEA (7.78 μ mol) were dissolved in approx. 1 ml DMF and allowed to react for 2 h. Boc-deprotection followed for 40 min with 50 % TFA in DCM resulting in product **19**. The sample was thoroughly washed with DMF, DCM and ether.

For subsequent srtA ligation samples **17**, **19.x** and **19** were washed with water and sortase A reaction buffer (1 \times). tGFP-LPETGGH₆ **7** (80 μ M) and sortase A pentamutant **6** (16 μ M, 0.2 eq. of tGFP) in 100 μ L sortase ligation buffer were added to each of the samples, which were incubated for 2 h at 22 °C in the reaction mixtures. Samples were washed with PBS to stop the reaction. Papers were made without applying heat and analyzed by fluorescence imaging.

Evaluation regarding degree of oxidation of TEMPO-oxidized cotton linters

For each of the TEMPO-oxidized fibers (0.3 or 0.15 NaOCl approaches): 50 mg TEMPO-oxidized fibers **13** were swollen in water and successively in DMSO. 11.5 μ L (0.098 mmol) cadaverine **16** were mixed with 15% AcOH in DMSO (5 mL) containing 10 mg (0.094 mmol) 2-methylpyridineborane complex and added to the fibers. The suspension was intensively shaken for 5 min and incubated for 2 h at 65°C. Fibers **17** were washed with 15% AcOH in DMSO, DMSO and deionized water, followed by solvent exchange to DMF for further reaction.

A solution of 11.2 mg (0.039 mmol) Boc-GGG-OH **18**, 14.6 mg (0.038 mmol) HBTU and 13.5 μ L (0.077 mmol) DIPEA in DMF was added to the fibers **17** and allowed to react for 2 h. The fibers were washed thoroughly with DMF, DCM and Et₂O, rinsed with EtOH and acetone and dried at 37 °C overnight. 50% TFA in DCM (5 mL) was added to the dry fibers for Boc deprotection and allowed to incubate for 30 min. Fibers **19** were washed thoroughly with Et₂O, rinsed with acetone, and dried at 37°C overnight.

Papermaking of 5 mg papers was performed as described under 7.5.

For subsequent srtA ligation tGFP-LPETGGH₆ **7** (15 μ M) and sortase A pentamutant **6** (3 μ M, 0.2 eq. of tGFP) in 250 μ L sortase ligation buffer were added to each of the samples, which

were incubated for 1 h at 22 °C in the reaction mixtures. Supernatant was removed, samples were transferred to blotting papers and washed with TBS-T 3× and TBS 3×.

7.8.4. Preliminary experiments on strategy 4 regarding primary functionalization

Approx. 52 mg of fibers **1** per approach (Table 9) were swollen in water overnight. Solvent exchange to DMF was performed. 192 mg Fmoc-Ahx-OH (0.542 mmol), 260 mg EDC (1.36 mmol) and 16.5 mg DMAP (0.135 mmol) were dissolved in 10 mL dry DMF. Volumes of this reaction mixture were given to the approaches according to Table 9, filled up to 5 mL with dry DMF and suspended. Slurries were purged with inert gas for 2 min and shaken at RT overnight. Fibers were washed thoroughly with DMF. Fmoc deprotection followed with 20% piperidine in DMF for 15 min. Slurries were again thoroughly washed with DMF.

Table 9: Overview of the reaction mixture input for esterification of paper **1** with compound **21**.

Sample	eq. PE per AGU	V _{mix, stock} [mL]
1	1.0	5.0
2	0.5	2.5
3	0.25	1.25

360 mg Boc-GGG-OH (1.25 mmol), 459.8 mg HATU (1.21 mmol) and 430 µL DIPEA (2.47 mmol) were dissolved in 8 mL DMF. 2 ml of this reaction mixture were added to each approach, filled up to 5 mL with DMF and allowed to react for 2 h. All slurries were washed thoroughly with DMF, DCM, ether, acetone and dried at 37 °C overnight. Boc deprotection was performed for 30 min with 4-5 mL 50% TFA in DCM on each sample. Fibers were washed with ether and acetone and dried at 37 °C overnight.

Papermaking of 5 mg papers and TNBS assay were performed as described under 7.5 and 7.6.

For subsequent srtA ligation tGFP-LPETGGH₆ **7** (20 µM) and sortase A pentamutant **6** (4 µM, 0.2 eq. of tGFP) in 200 µL sortase ligation buffer were added to each of the samples, which were incubated for 2 h at 22 °C in the reaction mixtures. Supernatant was removed, samples were transferred to blotting papers and washed with TBS-T 3× and TBS 3×.

Samples were analyzed by fluorescence imaging.

7.9. Part II: Comparison experiments

7.9.1. Synthesis of fibers 5

75 mg (1 eq. AGU) of cellulose linters fibers **1** (Grade 225 HSR-M, Buckeye Technologies) were soaked in deionized water and successively in DMF for solvent exchange. A solution of 31.3 mg PE **2** (0.116 mmol, 0.25 eq. relative to cellulose AGU), 55.5 mg EDC (0.289 mmol, 0.63 eq.), and 3.54 mg DMAP (0.0289 mmol, 0.06 eq.) in anhydrous DMF (5-7 mL) was added to the fibers. The suspension was flushed with inert gas for 2 min and shaken at ambient temperature overnight. The resulting fibers **3** were washed thoroughly with DMF before further reaction.

21.4 mg of the recognition peptide **4** (*H*-GGGβAK(4-maleimidobutyric acid)AWGG-NH₂, 0.0231 mmol, 0.05 eq.) were dissolved in 5 mL dry DMF and added to the non-dried fibers. The suspension was shortly purged with nitrogen and subsequently irradiated for 10 min in an open glass container from approximately 5 cm distance with a UV-B intense terrarium bulb (Exo Terra UVB 200). The suspension was purged, mixed and irradiated again for 10 min. The reaction solution was removed, and the fibers were washed with DMF and deionized water under gentle shaking for 1 h each. Fibers **5** were rinsed with ethanol (2×) and acetone and dried at 37°C overnight.

Papermaking of 5 mg papers and TNBS assay were performed as described under 7.5 and 7.6.

7.9.2. Synthesis of fibers 15

75 mg of TEMPO-oxidized cotton linters fibers **13** (aldehyde loading 64.9 μmol/g) were swollen in water and washed with ammonium acetate (pH 4.5). A solution of 19.3 mg of peptide **14** (*H*-GGGβAK(aminooxyacetic acid)AWGG-NH₂, 0.0231 mmol, 4.8 eq.) dissolved in ammonium acetate (pH 4.5, 5 mL) was added to the fibers. The fibers were suspended and kept at ambient temperature overnight. Fibers **15** were thoroughly washed with deionized water, rinsed with ethanol and acetone, and dried at 37°C overnight.

Papermaking of 5 mg papers and TNBS assay were performed as described under 7.5 and 7.6.

7.9.3. Synthesis of fibers 19

75 mg TEMPO-oxidized fibers **13** (aldehyde loading 64.9 μmol/g) were swollen in water and successively in DMSO. 54.2 μL (0.463 mmol, 95 eq.) cadaverine **16** were mixed with 15% AcOH in DMSO (5 mL) containing 49 mg (0.58 mmol, 94 eq.) 2-methylpyridineborane complex and

added to the fibers. The suspension was intensively shaken for 5 min and incubated for 2 h at 65°C. Fibers **17** were washed with 15% AcOH in DMSO, DMSO and deionized water, followed by solvent exchange to DMF for further reaction.

A solution of 134 mg (0.463 mmol, 95 eq.) *Boc*-GGG-*OH* **18**, 167 mg (0.44 mmol, 90 eq.) HATU and 1.36 μ L (0.926 mmol, 190 eq.) DIPEA in DMF was added to the fibers **17** and allowed to react for 2 h. The fibers were washed thoroughly with DMF, DCM and Et₂O, rinsed with EtOH and acetone and dried at 37 °C overnight. 50% TFA in DCM (7 mL) was added to the dry fibers for Boc deprotection and allowed to incubate for 30 min. Fibers **19** were washed thoroughly with Et₂O, rinsed with acetone, and dried at 37°C overnight.

Papermaking of 5 mg papers and TNBS assay were performed as described under 7.5 and 7.6.

7.9.4. Synthesis of fibers **22**

85 mg cellulose linters fibers **1** (Grade 225 HSR-M, Buckeye Technologies) were swollen in water and solvent exchange to DMF was performed. A solution of 46.4 mg (0.131 mmol, 0.25 eq.) Fmoc-6-Ahx-*OH* **20**, 62.9 mg EDC (0.328 mmol, 0.63 eq.), and 4.0 mg DMAP (0.0328 mmol, 0.06 eq.) in dry DMF (5 mL). The suspension was flushed with inert gas shortly and shaken at ambient temperature overnight. The fibers were washed thoroughly with DMF. 20% piperidine in DMF (10 mL) were added and the suspension was shaken for 15 min for Fmoc deprotection. Fibers **21** were washed afterwards with DMF.

A solution of 152 mg (0.525 mmol, 1 eq.) *Boc*-GGG-*OH* **18**, 190 mg (0.498 mmol, 0.95 eq.) HATU and 183 μ L (1.05 mmol, 2 eq.) DIPEA in DMF were added to fibers **21** and allowed to react for 2 h. The fibers were washed thoroughly with DMF, DCM and Et₂O, rinsed with EtOH and acetone and dried at 37 °C overnight. 50% TFA in DCM (7 mL) were added to the dry fibers and allowed to incubate for 30 min for Boc deprotection. Fibers **22** were washed thoroughly with Et₂O rinsed with acetone and dried at 37°C overnight.

Papermaking of 5 mg papers and TNBS assay were performed as described under 6.5 and 6.6.

7.9.5. Enzyme-mediated ligation of tGFP **7** or **23** onto papers

Peptide-functionalized paper discs (Ø 0.9 cm) were either tested dry or pre-incubated in 200 μ L of 3 wt-% BSA in TBS for 20 min. If incubated, the papers were washed with Milli-Q® water and sortase A reaction buffer (1 \times) before ligation.

For sortase A-mediated ligation: tGFP-LPETGGH₆ **7** (20 μ M) and sortase A pentamutant **6** (4 μ M, 0.2 eq. of tGFP) in 200 μ L sortase ligation buffer were added. The papers were incubated for 2 h at 22 °C in the reaction mixtures.

For mTG-mediated ligation: tGFP-DIPIGQGMTGH₆ **23** (20 μ M) and mTG **24** (0.3 μ M, 1/60 eq. of tGFP) in 200 μ L mTG reaction buffer (1 \times) were added. The papers were incubated for 2 h at 37 °C in the reaction mixtures.

For the adsorption controls Milli-Q[®] water was used instead of the enzyme. To stop the reaction the supernatant was removed, and the papers were washed with TBS (3 \times).

7.9.6. Co-localization with CBM fusion proteins

A paper **28** was cut in two and each half was incubated in a solution of either mKO κ -CBM28 or mKO κ -CBM21Cel7a at a final concentration of approximately 40 μ g/mL in double distilled water for 5-10 min. The papers were washed with water and analyzed in the CLSM.

For the co-localization with both CBM fusion the mKO κ -CBM28 sample was incubated with mKO κ -CBM21Cel7a at a final concentration of approximately 40 μ g/mL in double distilled water for 5-10 min. The papers were washed with water and analyzed in the CLSM.

8. Supporting information

8.1. Spectra of photoenol 2

8.1.1. NMR spectra

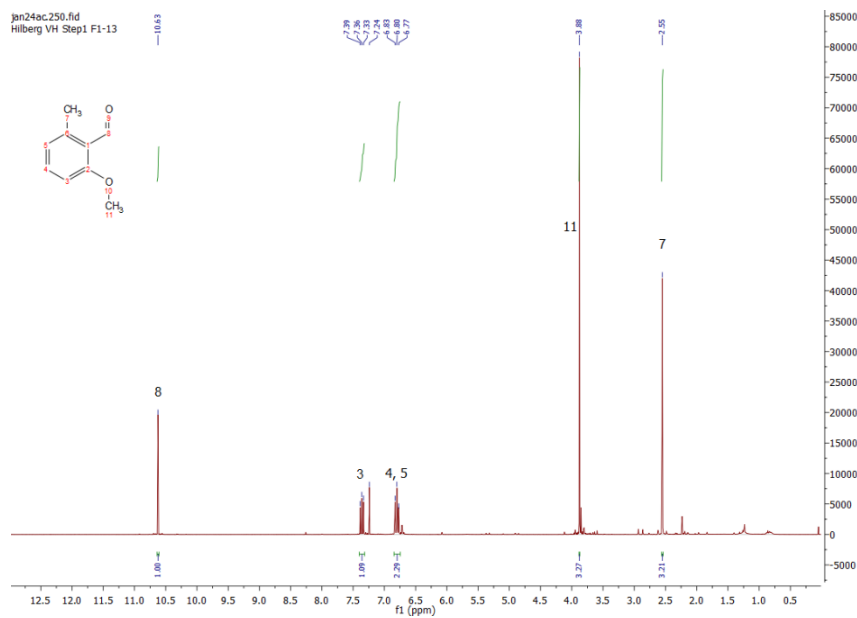


Figure 65: ^1H -NMR spectrum of 2-methoxy-6-methylbenzaldehyde.¹¹¹

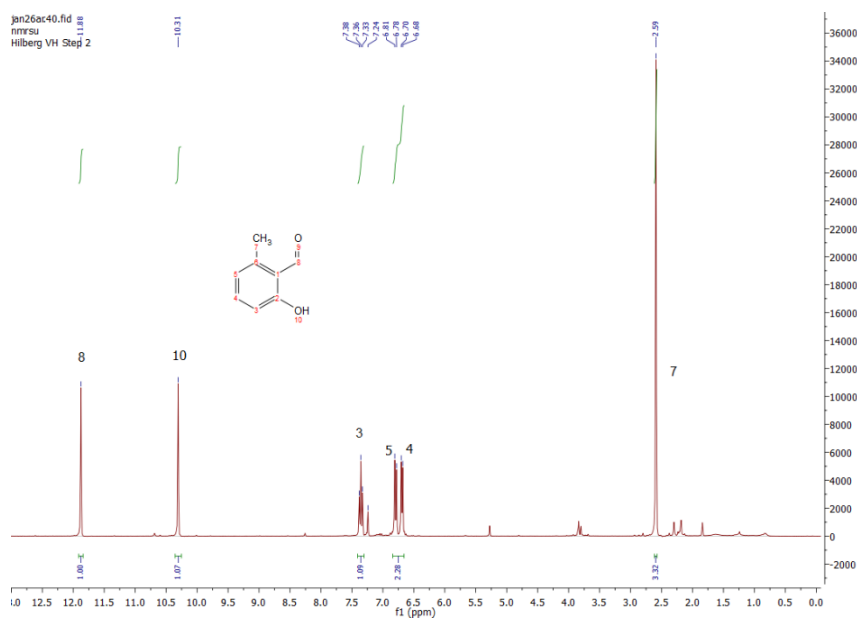


Figure 66: ^1H -NMR spectrum of 2-hydroxy-6-methylbenzaldehyde.¹¹¹

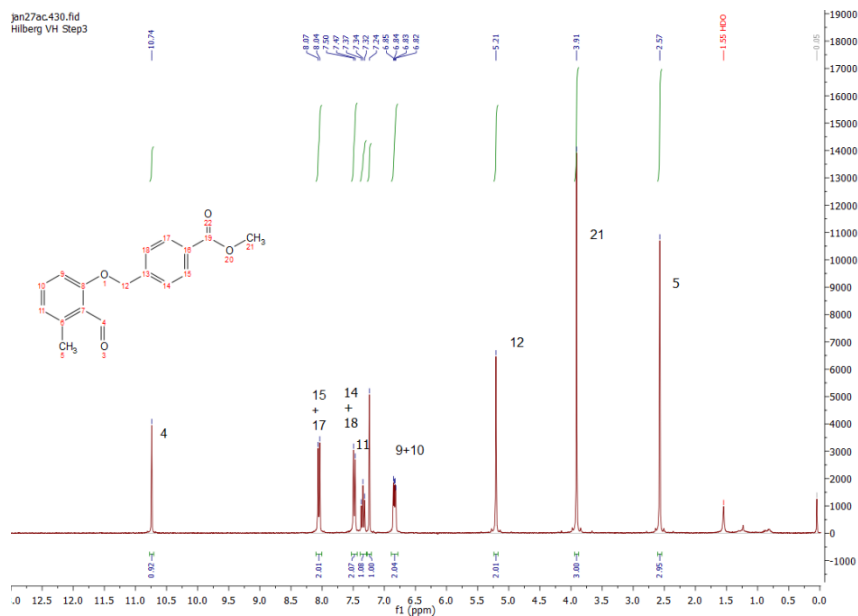


Figure 67: ¹H-NMR spectrum of Methyl 4-((2-formyl-3-methylphenoxy)methyl)benzoate.¹¹¹

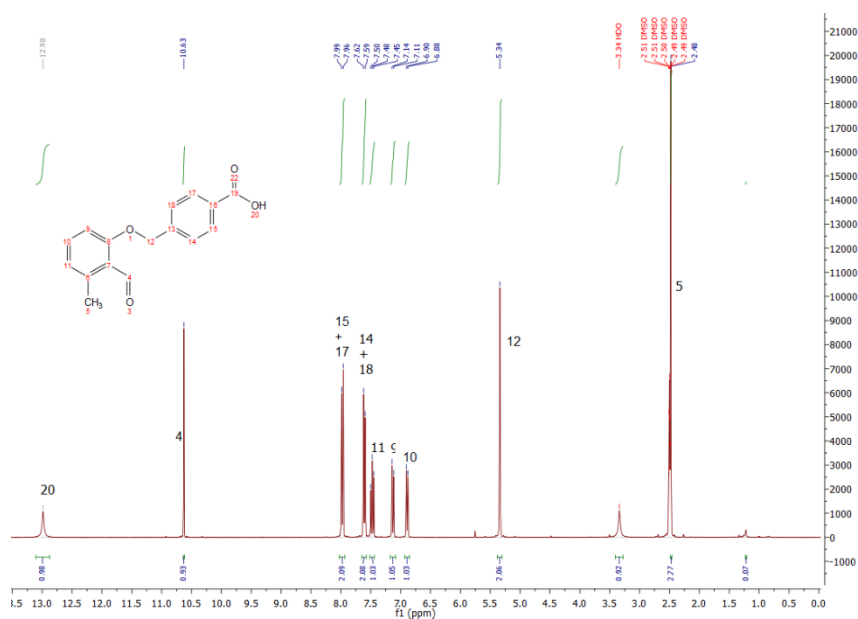


Figure 68: ¹H-NMR spectrum of 4-((2-formyl-3-methylphenoxy)methyl)benzoic acid.¹¹¹

8.1.2. UV/Vis spectrum

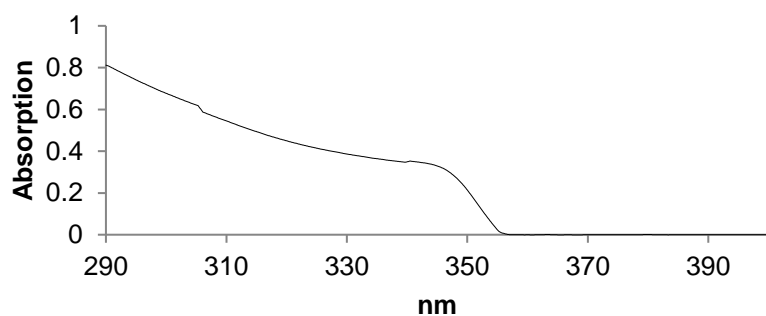


Figure 69: UV-Vis diagram of photoenol **2** in DCM.¹¹¹

8.2. Peptide analysis

8.2.1. Peptide 4

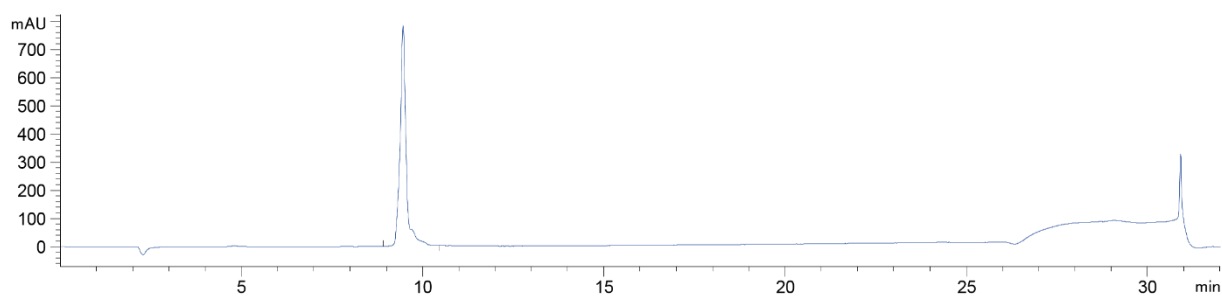


Figure 70: HPLC diagram at 220nm of peptide **4**, $t_R = 9.45$ min, Gradient: 10-60% B.

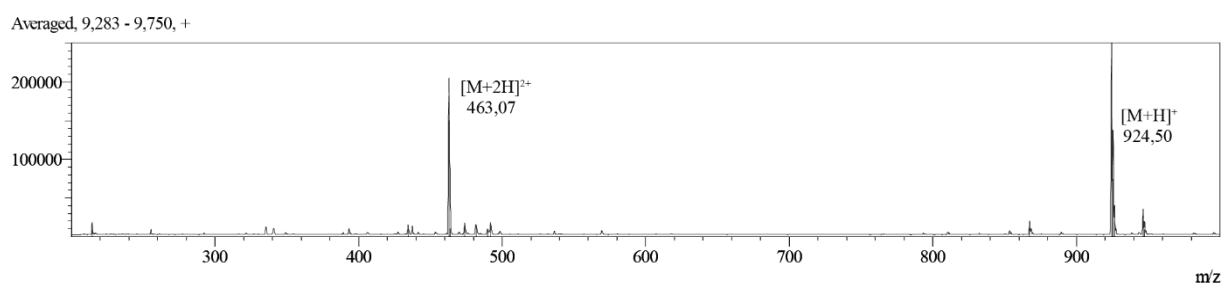


Figure 71: ESI-MS spectrum of peptide **4**, Gradient: 10-100% B.

8.2.2. Peptide 4.1

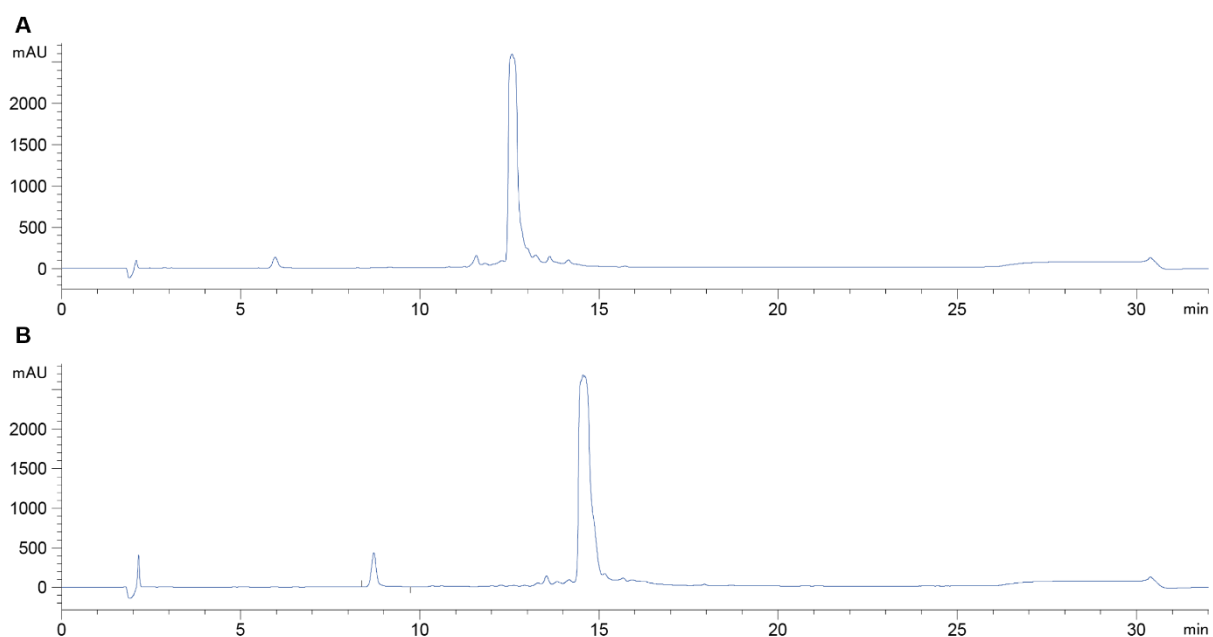


Figure 72: HPLC diagram at 280nm of the two isomers (A and B) of peptide 4.1. t_R = 12.57 min and 14.55 min, Gradient: 10-60% B. Fractions were combined.¹¹¹

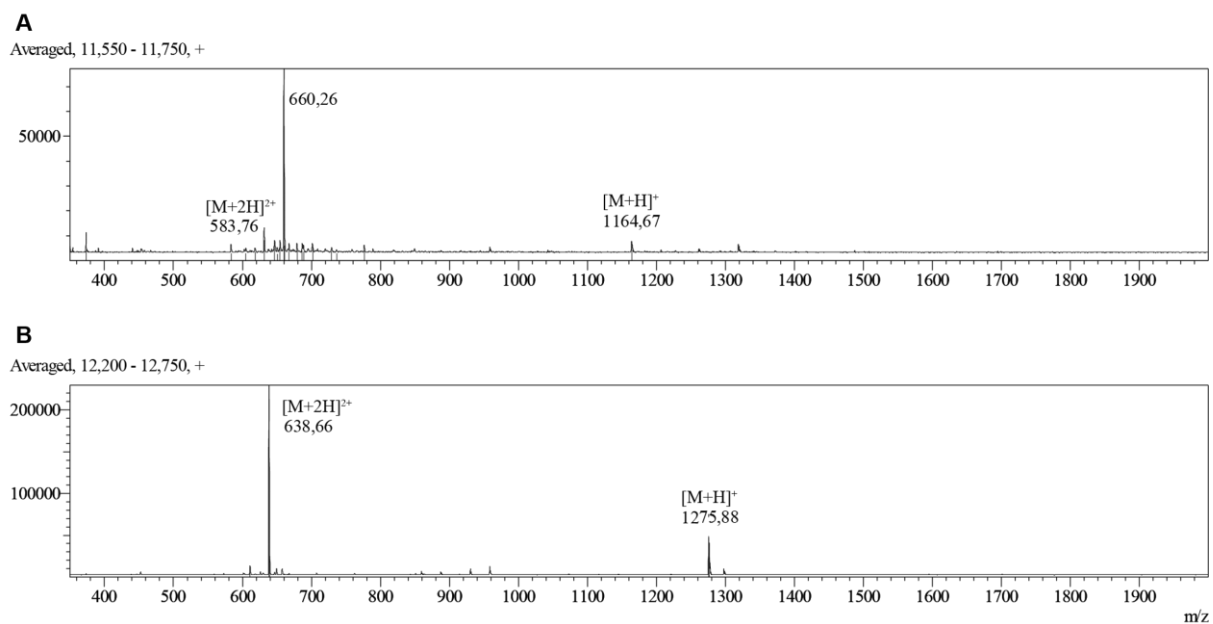


Figure 73: ESI-MS spectra of peptide 4.1, depicting the masses of the main species (A and B), Gradient: 30-100% B.

8.2.3. Peptide 14

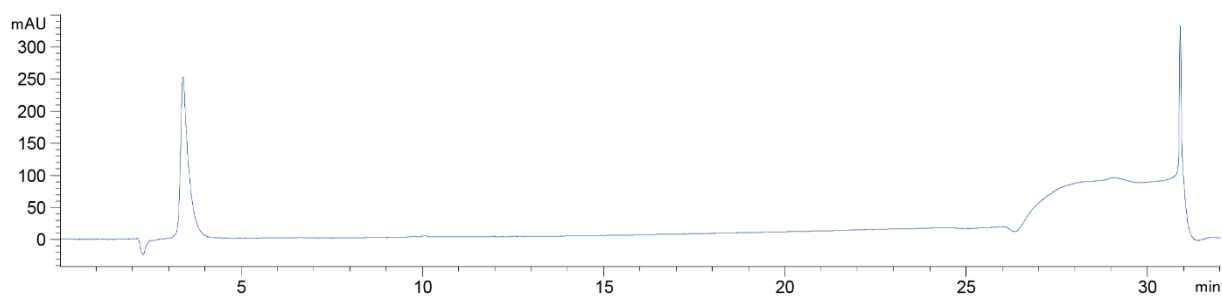


Figure 74: HPLC diagram at 220nm of peptide **14**, $t_R = 3.38$ min, Gradient: 10-60% B.

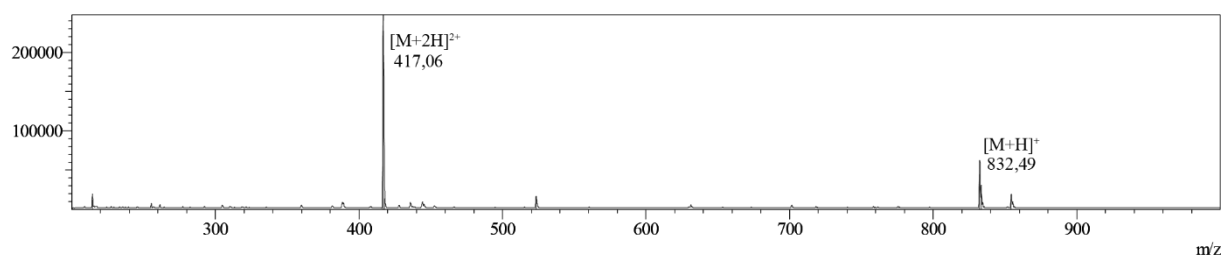


Figure 75: ESI-MS spectrum of peptide **14**, Gradient: 10-60% B.

8.3. Data of TNBS assays

8.3.1. Part I

Table 10: Single results of TNBS assay of papers 5

	1	2	3	4	5	Average loading	Standard deviation
Result [$\mu\text{mol/g}$]	7.2	7.8	8.0	7.9	8.3	7.8	0.44
Result [nmol/g]	80.9	88.2	89.4	88.2	92.7	87.9	5.0

8.3.2. Part II

Table 11: Initial comparison and comparison against fibers.

Paper	Average loading [$\mu\text{mol/g}$]	Standard deviation [$\mu\text{mol/g}$]
5	16.0	1.3
15	15.3	0.3
19	13.5	1.0
22	15.3	0.3

Table 12: Testing of different TEMPO oxidations with strategy 3.

Paper	Average loading [$\mu\text{mol/g}$]	Standard deviation [$\mu\text{mol/g}$]
19 (Batch 1)	13.9	0.2
19 (Batch 2)	14.5	0.2

Table 13: Single results of TNBS assay of papers from part II. Final comparison with BSA blocked papers.

Paper	Batch 1 [$\mu\text{mol/g}$]	Batch 2 [$\mu\text{mol/g}$]	Batch 3 [$\mu\text{mol/g}$]	Average loading [$\mu\text{mol/g}$]	Standard deviation [$\mu\text{mol/g}$]
5	7.54	12.5	8.47	9.52	2.66
15	12.1	12.4	12.4	12.33	0.16
19	10.4	11.2	11.5	11.00	0.58
22	11.2	11.3	10.9	11.16	0.23

8.4. SDS-PAGE of tGFP derivatives

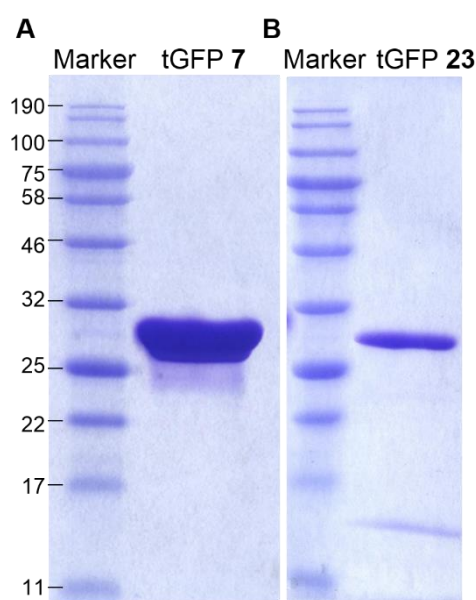


Figure 76: SDS-gel for mass verification of tGFP 7 and 23.

8.5. Data of tGFP quantification

Table 14: Values determined by comparing tGFP fluorescence intensities against a standard curve.

sample	1	2	3	4	5	6	7	8	9	average	standard deviation
protein load of 8 [μmol/g]	0.21	0.19	0.16	0.16	0.15	0.16	0.15	0.17	0.16	0.17	0.02
Adsorption control [μmol/g]	0.00	0.00	0.00	0.00	0.00	0.01	0.00	0.00	0.02	0.01	0.01

8.6. CLSM Part II

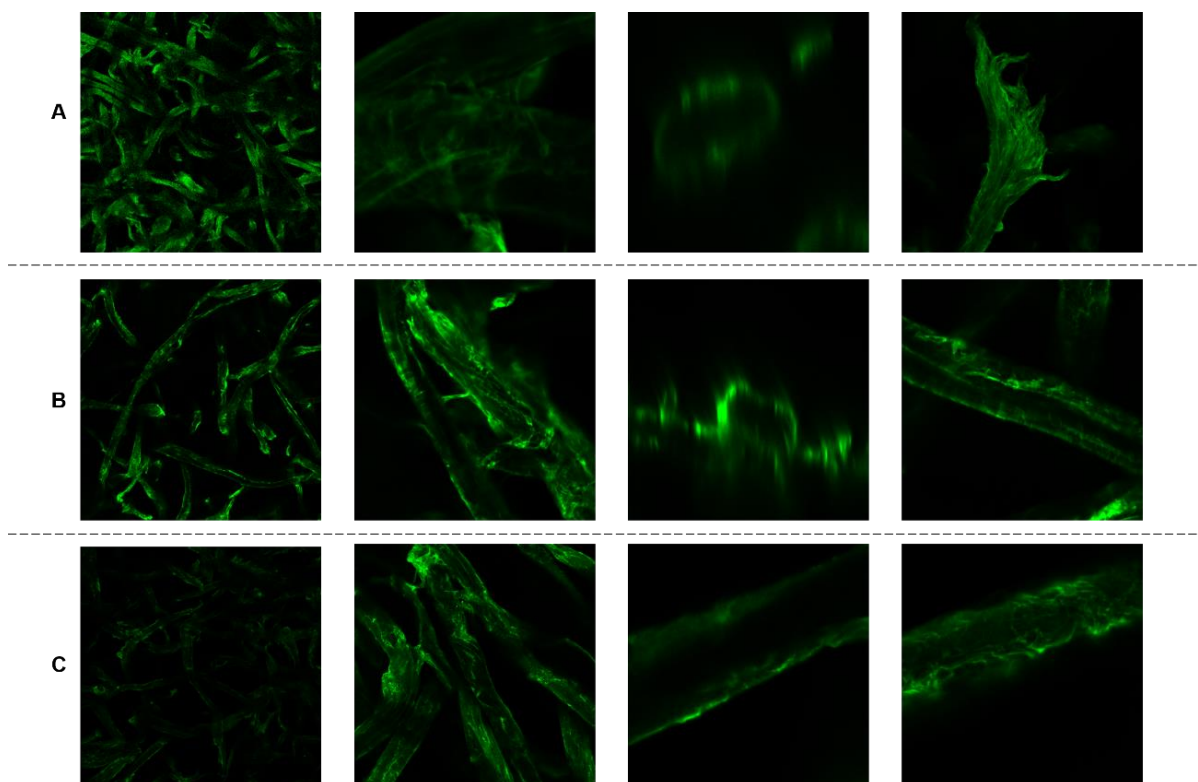


Figure 77: CLSM images of products 25 (A), 26 (B) and 27 (C). After Liebich et al.¹⁰¹

9. Register

9.1. List of figures

- Figure 1: An early bedside urinary test kit comprising several components including test papers showing the complex setup of early urine testing. ©Wellcome Collection. Attribution 4.0 International (CC BY 4.0)⁷ 1
- Figure 2: Shares of the individual paper grades in the total annual paper production in Germany in 2021. Total output is 21.0 million metric tons.²² 3
- Figure 3: Supramolecular structure of cellulose. Depiction of the morphological hierarchy of a cellulose fiber, divided in macrofibrils, microfibrils, and the cellulose polymer. After Hillscher et al.²³ 4
- Figure 4: Chemical structures of AGU (light blue)), cellobiose (dark blue), the non-reducing at the left side of the chains, and respectively the reducing end groups (red) of a cellulose polymer chain. After Hillscher et al.²³ 5
- Figure 5: Schematic depiction of the native cellulose supramolecular structure with intermolecular hydrogen bridges in blue and intramolecular ones in green. After Hillscher et al.²³ 5
- Figure 6: Schematic depiction of the different immobilization methods for biomolecules on surfaces. **A** non-site-specific, non-covalent immobilization e.g., by physical adsorption. **B** non-site-specific, covalent immobilization by covalent binding using intrinsic functional groups of the biomolecule. **C** site-specific, non-covalent immobilization e.g., by bioaffinity coupling. **D** site-specific, covalent binding by bio-orthogonal coupling. The dashed lines between the biomolecule and the surface in **A** and **C** visualize weak physical interactions, whereas the solid lines in **B** and **D** represent covalent bonds respectively. After Steen Redeker et al.³⁸ 7
- Figure 7: Exemplary functionalization of cellulose hydroxyls. 8
- Figure 8: TEMPO-mediated cellulose oxidation. After Saito et al.⁴⁶ 10
- Figure 9: Mechanism of the sortase A-mediated transpeptidation. After Antos et al.⁵⁷ 12
- Figure 10: Mechanism of transpeptidation catalyzed by microbial transglutaminase. After Deweid et al.⁸⁰ 13
- Figure 11: Overview of the first investigated light-controlled peptide immobilization approach. Ready cellulose paper was functionalized with a recognition sequence **4** resulting in peptide-paper hybrid **5**. tGFP **7**, microbial transglutaminase (mTG) **9** and ZZ-protein **11** were coupled by sortase A (**6**) ligation as model proteins with different biologic function. Structures for visualization from PDB for tGFP (GFP; PDB-ID: 1EMA)⁹⁷, mTG (PDB-ID: 1IU4)⁹⁸ and ZZ-protein (Z-domain; PDB-ID: 2spz)⁹⁹. Preliminary experiments are not depicted. Modified after Hilberg et al.¹⁰⁰ 18
- Figure 12: Overview of the tested immobilization strategies. Starting materials are cotton-based substrates **A** treated with NaOH to increase amorphous regions in the fibers and **B** fibers reacted with TEMPO, NaBr and NaClO to generate reactive aldehydes in AGUs.

Letters C to F depict the examined combinations of linkers and recognition sequences. C 6-aminohexanoic acid and the triglycine building block were coupled subsequently on type A starting material. D Cadaverine and the triglycine building block were coupled subsequently on type B starting material. E A synthetic recognition peptide bearing an aminooxy linker was reacted with type B material. F Material of type A was first modified with a photoreactive moiety that undergoes a chemical reaction with the maleimide-bearing synthetic recognition peptide. The final connection of functional proteins with peptide/paper hybrid materials is depicted in G for srtA ligation and in H for mTG ligation. J The functional protein to be coupled with the cellulosic support, here tGFP. Protein structure for visualization from PDB for tGFP (GFP; PDB-ID: 1EMA). ⁹⁷ Modified after Liebich et al. ¹⁰¹	19
Figure 13: The four tested strategies for peptide immobilization on cellulose paper are depicted. Strategy 1: Light-controlled approach resulting in 5. Strategy 2: Oxime ligation approach resulting in 15. Strategy 3: Reductive amination approach resulting in 19. Strategy 4: Esterification approach resulting in 22.	21
Figure 14: Synthesis of paper 5.	22
Figure 15: Four-step synthesis of 4-((2-formyl-3-methylphenoxy)methyl)benzoic acid 2 (photoenol 2) starting from 2, 3-dimethylanisole. After Pauloehrl et al. ¹⁰⁶	23
Figure 16: Carbodiimide-mediated attachment of the photoenol moiety 2 to hydroxyl groups on fibers 1 resulting in products 3.1/3.2.	23
Figure 17: A TAMRA-peptide 4.1 for the light-controlled approach. B Recognition peptide 4 for the photochemical approach.	24
Figure 18: A Reaction scheme for the proof-of-concept experiment with the fluorescently labeled peptide 4.1, which is coupled in a Diels-Alder reaction to material 3.1 under irradiation, resulting in product 5.1. B Experimental setup for the preliminary studies comprising a photoreactor and a UV B terrarium lamp. C Enlarged image of a photoreactor. D Sketch of the photo-pattern sandwich. Modified after Hilberg et al. ¹⁰⁰ . 25	25
Figure 19: Oxime ligation of peptide 14 with TEMPO-oxidized fibers 13 resulting in fibers 15.	26
Figure 20: Recognition peptide 14.....	26
Figure 21: Build-up of the peptidic sequence after strategy 3. Cadaverine 16 is coupled with 2-picoline borane complex by reductive amination to TEMPO-oxidized fibers 13. Subsequent coupling of Boc-GGG-OH 18 followed by Boc-deprotection results in fibers 19.	27
Figure 22: Build-up of the peptidic sequence under strategy 4. Fmoc-6-aminohexanoic acid 20 is coupled under HATU/DIPEA activation to fibers 1. Subsequent Fmoc-deprotection with 20% piperidine in DMF results in 21. Coupling of Boc-GGG-OH 18 followed by Boc-deprotection results in fibers 22.	28
Figure 23: Sortase A (6) -mediated ligation of tGFP-LPETGGH ₆ 7 with to GGG-modified cellulose X resulting in tGFP immobilized product Y is depicted. mTG (24)-mediated of tGFP-DIPIGQGMTGH ₆ 23 to GGG-modified cellulose X resulting in tGFP immobilized	

product Y is depicted. Protein structure for visualization from PDB for tGFP (GFP; PDB-ID: 1EMA). ⁹⁷	29
Figure 24: Carbodiimide-mediated attachment of the photoenol moiety 2 to hydroxyl groups on cotton linters 1 resulting in product 3.1/3.2	31
Figure 25: (A) Carbodiimide-mediated attachment of the photoenol moiety 2 to hydroxyl groups on cotton linters 1 resulting in product 3.1 . C 1s XPS spectra of paper 1 (B) and photoenol functionalized paper 3 (C). Modified after Hilberg et al. ¹⁰⁰	32
Figure 26: CLSM images visualizing the tautomers of a photoenol-functionalized cellulosic paper. Modified after Hilberg et al. ¹⁰⁰	32
Figure 27: Reaction scheme for proof-of-principle experiment under strategy 1. Reaction starting with paper 1 via the PE-paper 3.2 to result in an immobilized fluorescently labeled peptide on paper (5.2) via Diels-Alder coupling. Modified after Hilberg et al. ¹⁰⁰	33
Figure 28: A Light-controlled Diels-Alder product 5.1 of photoenol-functionalized paper with a fluorescently labeled model peptide 4.1 in the self-made photoreactor. B Control reaction for CLSM of a photoenol-functionalized paper in the absence of the model peptide. C Control reaction for CLSM of unmodified filter paper in the presence of the model peptide. Modified after Hilberg et al. ¹⁰⁰	34
Figure 29: CLSM Images Ex: 552 nm, Em: 570-640 nm. A Plain filter paper 1 . B PE paper in the absence of the model peptide 3.2 . C Plain filter paper previously in contact with the model peptide (1 + 4.1). D Product 5.1 .E Analysis of the CSLM images. Fluorescence intensities are depicted as a mean of the whole image for images A-C. For image D the mean of three spots in the visually brightest (5.1 , high fluorescence) and darkest regions (5.1 , low fluorescence) was built.....	35
Figure 30: Reaction scheme for the subsequent immobilizations of the recognition peptide 4 to PE functionalized paper 3.2 resulting in peptide-functionalized paper 5. , and tGFP-LPETGGH ₆ resulting in product 8	35
Figure 31: A - D PE (right) and a tGFP-functionalized paper (left) with a star-shaped-pattern. A White light photograph B Fluorescence image $\lambda_{\text{ex}} = 365 \text{ nm}$, $\lambda_{\text{em}} = 595 \text{ nm}$. C Fluorescence image for tGFP detection in product 8 $\lambda_{\text{ex}} = 480 \text{ nm}$, $\lambda_{\text{em}} = 535 \text{ nm}$. D Stacked mage of B and C. Modified after Hilberg et al. ¹⁰⁰	36
Figure 32: Nucleophilic aromatic substitution reaction underlying the TNBS quantification method.	36
Figure 33: A Sortase A-mediated modification resulting in product 8 . B White light and fluorescence images of the standard curve. C White light and fluorescence images of one sample set consisting of a paper disc immobilized with peptide 5 , the adsorption control sample (AC) and the desired product 8 . D Result after comparison of the fluorescence intensities of the samples against the standard curve (n = 9). Modified after Hilberg et al. ¹⁰⁰	38
Figure 34: A Sortase A-mediated modification resulting in product 10 . B Reaction of the hydroxamate assay with the substrates ZQG and hydroxylamine, which are converted by mTG catalysis. The product forms a colored complex with iron(III) which is detectable at	

525 nm. C Semi-quantitative result of the readout of the hydroxamate assay with the desired product 10 and the adsorption control (AC). Protein structure for visualization from PDB for mTG (PDB-ID: 1IU4) ⁹⁸ . Modified after Hilberg et al. ¹⁰⁰	40
Figure 35: A Sortase A-mediated modification of 5 resulting in product 12 . B Scheme for the sequential procedure for the paper-based ELISA including the steps of analyte incubation, secondary antibody incubation and color development. C Result and overview of the performed paper-based ELISA with the respective controls (n = 3). “+” and “-” indicate whether the substance was added to the sample or not. “Image of result” represents an exemplary assay outcome. Modified after Hilberg et al. ¹⁰⁰	42
Figure 36: Synthetic approach to paper 5	44
Figure 37: A - C (Fluorescence) images of PE coupled to cotton linters fibers and pressed to papers. A White light image. B Fluorescence image taken from the emission of the papers at 595 nm (Ex: 365 nm). C Image taken from the emission of the papers at 535 nm (Ex: 480 nm). D Image analysis of B . E Image analysis of C	45
Figure 38: Diels-Alder reaction of fibers functionalized with PE 2 and maleimide-bearing peptide 4 resulting in functionalized fibers 5	46
Figure 39: A - C (Fluorescence) images of PE and peptide 4 coupled to cotton linters fibers and pressed to papers. A White light image. B Fluorescence image taken from the emission of the papers at 595 nm (Ex: 365 nm). C Image taken from the emission of the papers at 535 nm (Ex: 480 nm). D Comparative image analysis of B . E Comparative image analysis of C	46
Figure 40: Reaction scheme for the immobilization of tGFP-LPETGGH ₆ 7 to peptide-functionalized paper 5 resulting in product 25	47
Figure 41: A - C (Fluorescence) images of PE and peptide 4 coupled to cotton linters fibers and pressed to papers with following GFP ligation. A White light image. B Fluorescence image taken from the emission of the papers at 595 nm (Ex: 365 nm). C Image taken from the emission of the papers at 535 nm (Ex: 480 nm). D Comparative image analysis of B . E Comparative image analysis of C	48
Figure 42: Oxime ligation of peptide 14 with TEMPO-oxidized fibers 13 resulting in fibers 15	49
Figure 43: A Photographs, B white light images and C fluorescence images of the sortase A ligation products of the oxime ligation under three reaction conditions with different amounts of peptide. D Results of the fluorescence intensity analysis of images under C	50
Figure 44: Kinetic assessments of the sortase A ligation resulting in product 26 based on the underlying functionalization with or without the catalyst aniline (A) and of the autofluorescence of the underlying peptide modified papers 15 at the respective emission wavelength (B).	51
Figure 45: Introduction of the peptidic sequence under strategy 3. Cadaverine 16 is coupled with 2-picoline borane complex by reductive amination to TEMPO-oxidized fibers 13 resulting in amine-functionalized cotton linters fibers 17 . Subsequent coupling of 18	

followed by Boc deprotection results in fibers 19 . Subsequent coupling of Fmoc-G-OH followed by Fmoc deprotection results in fibers 19.x .	52
Figure 46: A Photograph of sortase A ligation products 17 (1), 19.x , and 19 including blank. B White light and C Fluorescence image of the same samples. D Results of the fluorescence intensity analysis of image C .	53
Figure 47: Introduction of the peptidic sequence under strategy 4. Fmoc-6-aminohexanoic acid 20 is coupled under HATU/DIPEA activation to fibers 1 . Subsequent Fmoc-deprotection with 20% piperidine in DMF results in product 21 . Coupling of 18 followed by Boc deprotection results in fibers 22 .	53
Figure 48: A TNBS assay of paper samples formed of the respectively functionalized fibers. n = 3, error bars depict the standard deviation. B White light image and C fluorescence image of the sortase A ligation including an adsorption control and blank. D Results of the fluorescence intensity analysis of image C .	54
Figure 49: Masses of cotton linters fibers before and after papermaking. eq.: Equivalents Fmoc-6-aminohexanoic acid used in the initial coupling reaction related to AGU. n = 9, error bars depict the standard deviation.	55
Figure 50: Coomassie blue stained SDS-PAGE after the overnight incubation at 37 °C of tGFP 23 with mTG 24 . For analysis a pre-stained protein ladder was used.	56
Figure 51: Essential steps of small-scale paper manufacturing: A Weighing of dry fibers. B Preparation of a fiber slurry. C Removing the paper along with the plunger. D Pressed paper.	57
Figure 52: Indirect TNBS assay for functionalized fibers 5 (strategy 1), 15 (strategy 2), 19 (strategy 3) and 22 (strategy 4). Error bars depict the standard deviation. n = 9. Modified after Liebich et al. ¹⁰¹	58
Figure 53: Fluorescence images of sortase A-mediated ligation (A) and mTG-mediated ligation (C) on peptidic papers 5 , 15 , 19 and 22 with the respective tGFP variant, including adsorption control (AC) and a blank for each approach. Blank corrected results from fluorescence analysis of the images for srtA ligation (B) and mTG ligation (D).	59
Figure 54: Fluorescence images of sortase A-mediated ligation (A) and mTG-mediated ligation (C) on peptidic fibers and papers 5 , 15 , 19 and 22 with the respective tGFP variant, including adsorption control (AC) and a blank for each approach. Blank corrected results from fluorescence analysis of the images for srtA ligation (B) and mTG ligation (D) from a single determination.	61
Figure 55: A Fluorescence image of sortase ligation products 27 on TEMPO-oxidized fibers with different aldehyde and carboxyl content, adsorption control (AC) and blank 19 . B Analysis of mean fluorescent intensities of two independent experiments. Standard deviations are depicted with error bars.	63
Figure 56: Exemplary fluorescence images of sortase A-mediated ligation (A) and mTG-mediated ligation (C) on BSA-blocked peptidic papers 5 , 15 , 19 and 22 of the same batch for both enzymatic ligations. Performed with the respective tGFP variant, including adsorption control (AC) and a blank for each approach. Blank corrected results from	

fluorescence analysis of the images for srtA ligation (B) and mTG ligation (D) from a triple determination. Each result was normalized to the sample with the strongest fluorescence at 535 nm. Average values were built upon normalized figures (n = 3). Modified after Liebich et al. ¹⁰¹	64
Figure 57: Analysis of two fluorescence images consecutively taken after 2 and additional 16 hours of sortase A ligation leading to products 25 (A), 26 (B), 27 (C) and 28 (D) including adsorption controls (AC) and blanks. Blanks were used for initial normalization of the image's fluorescence intensities separately for each strategy. Single determination.	65
Figure 58: Exemplary CLSM images of product 28 . A Global view of overlapping cotton linters fibers. B and C showing pronounced immobilization along fibrillar structures. D The lumen of the cotton linters fibers is not filled by tGFP. After Liebich et al. ¹⁰¹	66
Figure 59: CLSM: False color images of product 28 . Immobilized tGFP was co-localized with A mKOκ-CBM28 to identify amorphous cellulose, B mKOκ-CBM1Cel7a to identify crystalline cellulose, C and both CBM fusion proteins to identify additional binding sites in cotton linters fibers.	67
Figure 60: Graphical summary of work performed in this thesis. Potential applications described in the upper part I are not limited to the suggestions made.....	70
Figure 61: Structure of peptide 4 . MW = 923.42 g·mol ⁻¹	86
Figure 62: Structure of peptide 4.1 . MW = 1165.5 g·mol ⁻¹	87
Figure 63: Structure of peptide 14 . MW = 831.9 g·mol ⁻¹	88
Figure 64: Standard curve for tGFP quantification.....	93
Figure 65: ¹ H-NMR spectrum of 2-methoxy-6-methylbenzaldehyde. ¹¹¹	102
Figure 66: ¹ H-NMR spectrum of 2-hydroxy-6-methylbenzaldehyde. ¹¹¹	102
Figure 67: ¹ H-NMR spectrum of Methyl 4-((2-formyl-3-methylphenoxy)methyl)benzoate. ¹¹¹	103
Figure 68: ¹ H-NMR spectrum of 4-((2-formyl-3-methylphenoxy)methyl)benzoic acid. ¹¹¹	103
Figure 69: UV-Vis diagram of photoenol 2 in DCM. ¹¹¹	104
Figure 70: HPLC diagram at 220nm of peptide 4 , t _R = 9.45 min, Gradient: 10-60% B.....	104
Figure 71: ESI-MS spectrum of peptide 4 , Gradient: 10-100% B.....	104
Figure 72: HPLC diagram at 280nm of the two isomers (A and B) of peptide 4.1 . t _R = 12.57 min and 14.55 min, Gradient: 10-60% B. Fractions were combined. ¹¹¹	105
Figure 73: ESI-MS spectra of peptide 4.1 , depicting the masses of the main species (A and B), Gradient: 30-100% B.....	105
Figure 74: HPLC diagram at 220nm of peptide 14 , t _R = 3.38 min, Gradient: 10-60% B.....	106
Figure 75: ESI-MS spectrum of peptide 14 , Gradient: 10-60% B.....	106

Figure 76: SDS-gel for mass verification of tGFP 7 and 23.....	107
Figure 77: CLSM images of products 25 (A), 26 (B) and 27 (C). After Liebich et al. ¹⁰¹	108

9.2. List of tables

Table 1: Immobilization strategies used within the two parts of the work.	71
Table 2: Specifications of TEMPO-oxidized fibers.	78
Table 3: Composition of 15% separation and stacking gel. Volume for 5 gels.	84
Table 4: Backbone amino acids and building blocks used.	86
Table 5: Utilized concentrations of tGFP 7 calculated into loading on paper.	93
Table 6: Required Materials for paper-based ELISA	94
Table 7: Overview of the reactants input for esterification of paper with PE 2	95
Table 8: Overview of the peptide 14 input for oxime ligation.	96
Table 9: Overview of the reaction mixture input for esterification of paper 1 with compound 21.	98
Table 10: Single results of TNBS assay of papers 5	106
Table 11: Initial comparison and comparison against fibers.	106
Table 12: Testing of different TEMPO oxidations with strategy 3.....	107
Table 13: Single results of TNBS assay of papers from part II. Final comparison with BSA blocked papers.	107
Table 14: Values determined by comparing tGFP fluorescence intensities against a standard curve.....	108

9.3. List of abbreviations and symbols

μ PAD	Microfluidic paper-based analytical device
ACN	Acetonitrile, methyl cyanide
AGU	Anhydroglucose unit
Ahx	6-Aminohexanoic acid
ASSURED	Affordable, sensitive, specific, user friendly, rapid and robust, equipment free, deliverable
Boc	<i>tert</i> -butyloxycarbonyl protecting group
BSA	Bovine serum albumin
c	Concentration
CBM	Carbohydrate binding module
CLSM	Confocal laser scanning microscopy
CMC	Carboxymethyl cellulose
CNC	crystalline nanocellulose
DAD	diode array detector
DCM	dichloro methane
Dde	2-Acetyldimedone
DIPEA	<i>N,N</i> -Diisopropylethylamine
DMAP	<i>N,N</i> -Dimethylpyridin-4-amine
DMF	<i>N,N</i> -Dimethylformamide
DMSO	(Methanesulfinyl)methane, Dimethyl sulfoxide
dYT	double yeast tryptone
ϵ	Molar extinction coefficient
EDC	1-Ethyl-3-(3-dimethylaminopropyl)carbodiimide
ELISA	Enzyme-linked immunosorbent assay
ESI	Electrospray ionization
EtOAc	Ethyl acetate
Fmoc	fluorenylmethoxycarbonyl protecting group
HATU	Hexafluorophosphate Azabenzotriazole Tetramethyl Uronium
HBTU	Hexafluorophosphate Benzotriazole Tetramethyl Uronium
hIgG	Human immunoglobulin G
HPLC	High Performance Liquid Chromatography
HRP	Horseradish peroxidase
IgG	Immunoglobulin G
IMAC	Immobilized metal ion affinity chromatography

LC	Liquid chromatography
MBA	4-maleimidobutyric acid
mKOκ	mKusabira-Orange-kappa
MS	Mass spectrometry
mTG	microbial Transglutaminase
MW	Molecular weight
NaBr	Sodium bromide
NaClO	Sodium hypochlorite
NaOH	Sodium hydroxide
NHS	N-hydroxysuccinimide
NMR	Nuclear Magnetic Resonance
NTA	Nitrilotriacetic acid
PAGE	Polyacrylamid gel electrophoresis
PBS	Phosphate buffered saline
PBS-T	Phosphate buffered saline containing Tween
PDB-ID	RCSB Protein Data Bank - Identification number
PE	Photoenol
POCT	point-of-care testing
ROI	Region of interest
RP-HPLC	Reversed Phase HPLC
SDS	Sodium dodecyl sulfate
SPPS	Solid phase peptide synthesis
srtA	Sortase A
TAMRA	5-/6-Carboxytetramethylrhodamine
TBS	Tris buffered saline
TEMPO	2,2,6,6-Tetramethylpiperidinyloxy
TES	Triethylsilane
TFA	Trifluoroacetic acid
tGFP	Turbo Green Fluorescent Protein, <i>turbo</i> GFP
THF	Tetrahydrofuran
TNBS	Trinitrobenzene sulfonic acid
t _R	Retention time
Tris	Tris(hydroxymethyl)aminomethane
TWEEN	Polysorbate
UV	Ultraviolet

VIS	Visible
XPS	X-ray photoelectron spectroscopy
λ	Wavelength

10. References

- (1) Then, W. L.; Garnier, G. Paper diagnostics in biomedicine. *Reviews in Analytical Chemistry* **2013**, 32.
- (2) Böhm, A.; Biesalski, M. Paper-based microfluidic devices: A complex low-cost material in high-tech applications. *MRS Bulletin* **2017**, 42, 356–364.
- (3) Hristov, D. R.; Rodriguez-Quijada, C.; Gomez-Marquez, J.; Hamad-Schifferli, K. Designing Paper-Based Immunoassays for Biomedical Applications. *Sensors* **2019**, 19, 554.
- (4) Oliver, G. On Bedside Urinary Tests: Detection of Sugar in the Urine by Means of Test Papers. *The Lancet* **1883**, 121, 858–860.
- (5) Johnson, G. Clinical Lecture on the Various Modes of Testing for Sugar in the Urine. *British medical journal* **1884**, 1, 1–4.
- (6) Turner, N. The invention of the dipstick: Test papers to dipsticks in 72 years. *Journal of Renal Nursing* **2014**, 6, 99.
- (7) Wellcome Collection. The evolution of urine analysis : an historical sketch of the clinical examination of urine lecture memoranda, South African Medical Congress, Johannesburg, 1912. Attribution 4.0 International (CC BY 4.0). <https://wellcomecollection.org/works/s2hhypj3> (accessed December 10, 2022).
- (8) O’Farrell, B. Evolution in Lateral Flow–Based Immunoassay Systems. In *Lateral flow immunoassay*; Wong, R., Tse, H., Wong, R. C., Tse, H. Y., Eds.; Humana Press: New York, 2009; pp 1–33.
- (9) Martinez, A. W.; Phillips, S. T.; Butte, M. J.; Whitesides, G. M. Patterned paper as a platform for inexpensive, low-volume, portable bioassays. *Angewandte Chemie International Edition* **2007**, 46, 1318–1320.
- (10) Kosack, C. S.; Page, A.-L.; Klatser, P. R. A guide to aid the selection of diagnostic tests. *Bulletin of the World Health Organization* **2017**, 95, 639–645.
- (11) Martinez, A. W.; Phillips, S. T.; Whitesides, G. M.; Carrilho, E. Diagnostics for the developing world: microfluidic paper-based analytical devices. *Analytical Chemistry* **2010**, 82, 3–10.
- (12) Yager, P.; Domingo, G. J.; Gerdes, J. Point-of-Care Diagnostics for Global Health. *Annual Review of Biomedical Engineering* **2008**, 10, 107–144.
- (13) Doyle, B. Biosynthesis and Biodegradation of Cellulose. *Biochemical Education* **1992**, 20, 123.
- (14) Wendenburg, S.; Nachbar, M.-L.; Biesalski, M. Tailoring the Retention of Charged Model Compounds in Polymer Functionalized Paper-Based Microfluidic Devices. *Macromolecular Chemistry and Physics* **2017**, 218, 1600408.
- (15) Credou, J.; Berthelot, T. Cellulose: from biocompatible to bioactive material. *Journal of Materials Chemistry B* **2014**, 2, 4767–4788.
- (16) Holik, H. *Handbook of paper and board*; Wiley-VCH: Weinheim, 2013.
- (17) Blechschmidt, J. Begriffe und Papiersorten. In *Taschenbuch der Papiertechnik*, 3. Auflage; Naujock, H.-J., Blechschmidt, J., Eds.; Hanser eLibrary; Hanser: München, 2021; pp 13–36.
- (18) Naujock, H.-J.; Blechschmidt, J., Eds. *Taschenbuch der Papiertechnik*, 3. Auflage; Hanser eLibrary; Hanser: München, 2021.
- (19) DIN 6730:2017-09, *Papier, Pappe und Faserstoff* - Begriffe; Beuth Verlag GmbH: Berlin.
- (20) Bos, J. H.; Staberock, M.; Bos, J. H. *Das Papierbuch: Handbuch der Papierherstellung*, 2., korr. Aufl.; ECA Pulp & Paper b.v: Houten, 2006.

-
- (21) DIE PAPIERINDUSTRIE e. V. Statistiken zum Leistungsbericht PAPIER 2021: Papierkompass 2020. <https://www.papierindustrie.de/papierindustrie/statistik> (accessed February 3, 2022).
- (22) DIE PAPIERINDUSTRIE e. V. Statistiken zum Leistungsbericht PAPIER 2021: Statistische Kurzinformation - Zellstoff- und Papierindustrie in Deutschland - November 2021. <https://www.papierindustrie.de/papierindustrie/statistik> (accessed February 3, 2022).
- (23) Hillscher, L. M.; Liebich, V. J.; Avrutina, O.; Biesalski, M.; Kolmar, H. Functional paper-based materials for diagnostics. *Chemtexts* **2021**, 7, 14.
- (24) Klemm, D.; Heublein, B.; Fink, H.-P.; Bohn, A. Cellulose: fascinating biopolymer and sustainable raw material. *Angewandte Chemie International Edition* **2005**, 44, 3358–3393.
- (25) Cannon, R. E.; Anderson, S. M. Biogenesis of bacterial cellulose. *Critical Reviews in Microbiology* **1991**, 17, 435–447.
- (26) Sczostak, A. Cotton Linters: An Alternative Cellulosic Raw Material. *Macromolecular Symposia* **2010**, 294, 151.
- (27) Hsieh, Y. L. Chemical structure and properties of cotton. In *Cotton: Science and technology*; Gordon, S., Hsieh, Y.-L., Eds.; Woodhead Publishing series in textiles 59; CRC Press; Woodhead Publ: Boca Raton, Fla., Cambridge, 2007; pp 3–34.
- (28) Whewell, C. S.; Edwards, C. H.; Ingham, J. REVIEWS. *Journal of the Textile Institute Proceedings* **1955**, 46, P236-P237.
- (29) Blechschmidt, J. *Taschenbuch der Papiertechnik*; Hanser Verlag: München, 2010.
- (30) Rojas, O. J., Ed. *Cellulose Chemistry and Properties: Fibers, Nanocelluloses and Advanced Materials*; Advances in Polymer Science 271; Springer International Publishing: Cham, 2016.
- (31) Berg, J. M.; Stryer, L.; Tymoczko, J. L. *Stryer Biochemie*, 7. Aufl. 2013; Springer Berlin Heidelberg: Berlin, Heidelberg, 2013.
- (32) Klemm, D.; Philipp, B.; Heinze, T.; Heinze, U.; Wagenknecht, W. *Comprehensive cellulose chemistry*; Wiley-VCH: Weinheim, New York, Chichester, Brisbane, Singapore, Toronto, 1998.
- (33) Hearle, J. W. S. A fringed fibril theory of structure in crystalline polymers. *Journal of Polymer Science* **1958**, 28, 432–435.
- (34) Bansa, H.; Brannahl, G.; Köttelwesch, C.; Wächter, O., Eds. *Papierchemie: einige unentbehrliche Grundbegriffe: Dauerhaftigkeit von Papier: Vorträge des 4. Internationalen Graphischen Restauratorentages 31 : 1*; Zeitschrift für Bibliothekswesen und Bibliographie Sonderhefte 31; Klostermann: Frankfurt am Main, 1980.
- (35) Roy, D.; Semsarilar, M.; Guthrie, J. T.; Perrier, S. Cellulose modification by polymer grafting: a review. *Chemical Society reviews* **2009**, 38, 2046–2064.
- (36) Rusmini, F.; Zhong, Z.; Feijen, J. Protein immobilization strategies for protein biochips. *Biomacromolecules* **2007**, 8, 1775–1789.
- (37) Arola, S.; Tammelin, T.; Setälä, H.; Tullila, A.; Linder, M. B. Immobilization-stabilization of proteins on nanofibrillated cellulose derivatives and their bioactive film formation. *Biomacromolecules* **2012**, 13, 594–603.
- (38) Steen Redeker, E.; Ta, D. T.; Cortens, D.; Billen, B.; Guedens, W.; Adriaenssens, P. Protein engineering for directed immobilization. *Bioconjugate chemistry* **2013**, 24, 1761–1777.
- (39) Koczula, K. M.; Gallotta, A. Lateral flow assays. *Essays in biochemistry* **2016**, 60, 111–120.
- (40) Elter, A.; Bock, T.; Spiehl, D.; Russo, G.; Hinz, S. C.; Bitsch, S.; Baum, E.; Langhans, M.; Meckel, T.; Dörsam, E.; *et al.* Carbohydrate binding module-fused antibodies improve the performance of cellulose-based lateral flow immunoassays. *Scientific reports* **2021**, 11, 7880.

-
- (41) Brady, D.; Jordaan, J. Advances in enzyme immobilisation. *Biotechnology letters* **2009**, *31*, 1639–1650.
- (42) Camarero, J. A. Recent developments in the site-specific immobilization of proteins onto solid supports. *Biopolymers* **2008**, *90*, 450–458.
- (43) Beneov, E.; Krlov, B. Affinity Interactions as a Tool for Protein Immobilization. In *Affinity Chromatography*; Magdeldin, S., Ed.; IntechOpen: Erscheinungsort nicht ermittelbar, 2012.
- (44) Diekmann, S.; Siegmund, G.; Roecker, A.; Klemm, D. O. Regioselective Nitrilotriacetic Acid–Cellulose–Nickel-Complexes for Immobilisation of His6-Tag Proteins. *Cellulose* **2003**, *10*, 53–63.
- (45) Böhm, A.; Trosien, S.; Avrutina, O.; Kolmar, H.; Biesalski, M. Covalent Attachment of Enzymes to Paper Fibers for Paper-Based Analytical Devices. *Frontiers in chemistry* **2018**, *6*, 214.
- (46) Saito, T.; Okita, Y.; Nge, T. T.; Sugiyama, J.; Isogai, A. TEMPO-mediated oxidation of native cellulose: Microscopic analysis of fibrous fractions in the oxidized products. *Carbohydrate polymers* **2006**, *65*, 435–440.
- (47) Saito, T.; Isogai, A. Introduction of aldehyde groups on surfaces of native cellulose fibers by TEMPO-mediated oxidation. *Colloids and Surfaces A: Physicochemical and Engineering Aspects* **2006**, *289*, 219–225.
- (48) Nooy, A. E. de; Besemer, A. C.; van Bekkum, H. Selective oxidation of primary alcohols mediated by nitroxyl radical in aqueous solution. Kinetics and mechanism. *Tetrahedron* **1995**, *51*, 8023–8032.
- (49) Uth, C.; Zielonka, S.; Hörner, S.; Rasche, N.; Plog, A.; Orelma, H.; Avrutina, O.; Zhang, K.; Kolmar, H. A chemoenzymatic approach to protein immobilization onto crystalline cellulose nanoscaffolds. *Angewandte Chemie International Edition* **2014**, *53*, 12618–12623.
- (50) Sulaiman, S.; Mokhtar, M. N.; Naim, M. N.; Baharuddin, A. S.; Sulaiman, A. A review: potential usage of cellulose nanofibers (CNF) for enzyme immobilization via covalent interactions. *Applied biochemistry and biotechnology* **2015**, *175*, 1817–1842.
- (51) Hussack, G.; Luo, Y.; Veldhuis, L.; Hall, J. C.; Tanha, J.; Mackenzie, R. Multivalent anchoring and oriented display of single-domain antibodies on cellulose. *Sensors* **2009**, *9*, 5351–5367.
- (52) Li, M.; Yue, Y.; Zhang, Z.-J.; Wang, Z.-Y.; Tan, T.-W.; Fan, L.-H. Site-Specific and High-Loading Immobilization of Proteins by Using Cohesin-Dockerin and CBM-Cellulose Interactions. *Bioconjugate chemistry* **2016**, *27*, 1579–1583.
- (53) Kolb, H. C.; Finn, M. G.; Sharpless, K. B. Click Chemistry: Diverse Chemical Function from a Few Good Reactions. *Angewandte Chemie International Edition* **2001**, *40*, 2004–2021.
- (54) Deb, T.; Tu, J.; Franzini, R. M. Mechanisms and Substituent Effects of Metal-Free Bioorthogonal Reactions. *Chemical reviews* **2021**, *121*, 6850–6914.
- (55) Devaraj, N. K. The Future of Bioorthogonal Chemistry. *ACS Central Science* **2018**, *4*, 952–959.
- (56) Karaki, N.; Aljawish, A.; Humeau, C.; Muniglia, L.; Jasniewski, J. Enzymatic modification of polysaccharides: Mechanisms, properties, and potential applications: A review. *Enzyme and microbial technology* **2016**, *90*, 1–18.
- (57) Antos, J. M.; Truttmann, M. C.; Ploegh, H. L. Recent advances in sortase-catalyzed ligation methodology. *Current Opinion in Structural Biology* **2016**, *38*, 111–118.
- (58) Ton-That, H.; Liu, G.; Mazmanian, S. K.; Faull, K. F.; Schneewind, O. Purification and characterization of sortase, the transpeptidase that cleaves surface proteins of *Staphylococcus*

aureus at the LPXTG motif. *Proceedings of the National Academy of Sciences of the United States of America* **1999**, *96*, 12424–12429.

(59) Mazmanian, S. K.; Liu, G.; Ton-That, H.; Schneewind, O. Staphylococcus aureus sortase, an enzyme that anchors surface proteins to the cell wall. *Science (New York, N.Y.)* **1999**, *285*, 760–763.

(60) Ilangovan, U.; Ton-That, H.; Iwahara, J.; Schneewind, O.; Clubb, R. T. Structure of sortase, the transpeptidase that anchors proteins to the cell wall of Staphylococcus aureus. *Proceedings of the National Academy of Sciences of the United States of America* **2001**, *98*, 6056–6061.

(61) Suree, N.; Liew, C. K.; Villareal, V. A.; Thieu, W.; Fadeev, E. A.; Clemens, J. J.; Jung, M. E.; Clubb, R. T. The Structure of the Staphylococcus aureus Sortase-Substrate Complex Reveals How the Universally Conserved LPXTG Sorting Signal Is Recognized*. *Journal of Biological Chemistry* **2009**, *284*, 24465–24477.

(62) Popp, M. W.; Antos, J. M.; Grotenbreg, G. M.; Spooner, E.; Ploegh, H. L. Sortagging: a versatile method for protein labeling. *Nature chemical biology* **2007**, *3*, 707–708.

(63) Heck, T.; Pham, P.-H.; Yerlikaya, A.; Thöny-Meyer, L.; Richter, M. Sortase A catalyzed reaction pathways: a comparative study with six SrtA variants. *Catalysis Science and Technology* **2014**, *4*, 2946–2956.

(64) Pritz, S.; Wolf, Y.; Kraetke, O.; Klose, J.; Bienert, M.; Beyermann, M. Synthesis of biologically active peptide nucleic acid-peptide conjugates by sortase-mediated ligation. *The Journal of organic chemistry* **2007**, *72*, 3909–3912.

(65) Ton-That, H.; Mazmanian, S. K.; Faull, K. F.; Schneewind, O. Anchoring of Surface Proteins to the Cell Wall of Staphylococcus aureus: Sortase Catalyzed In Vitro Transpeptidation Reaction Using LPXTG Peptide and NH₂-GLY₃ Substrates. *Journal of Biological Chemistry* **2000**, *275*, 9876–9881.

(66) Huang, X.; Aulabaugh, A.; Ding, W.; Kapoor, B.; Alksne, L.; Tabei, K.; Ellestad, G. Kinetic Mechanism of Staphylococcus aureus Sortase SrtA. *Biochemistry* **2003**, *42*, 11307–11315.

(67) Frankel, B. A.; Kruger, R. G.; Robinson, D. E.; Kelleher, N. L.; McCafferty, D. G. Staphylococcus aureus sortase transpeptidase SrtA: insight into the kinetic mechanism and evidence for a reverse protonation catalytic mechanism. *Biochemistry* **2005**, *44*, 11188–11200.

(68) Chen, I.; Dorr, B. M.; Liu, D. R. A general strategy for the evolution of bond-forming enzymes using yeast display. *Proceedings of the National Academy of Sciences of the United States of America* **2011**, *108*, 11399–11404.

(69) Hirakawa, H.; Ishikawa, S.; Nagamune, T. Design of Ca²⁺-independent Staphylococcus aureus sortase A mutants. *Biotechnology and bioengineering* **2012**, *109*, 2955–2961.

(70) Valldorf, B.; Fittler, H.; Deweid, L.; Ebenig, A.; Dickgiesser, S.; Sellmann, C.; Becker, J.; Zielonka, S.; Empting, M.; Avrutina, O.; et al. An Apoptosis-Inducing Peptidic Heptad That Efficiently Clusters Death Receptor 5. *Angewandte Chemie International Edition* **2016**, *55*, 5085–5089.

(71) Antos, J. M.; Popp, M. W.-L.; Ernst, R.; Chew, G.-L.; Spooner, E.; Ploegh, H. L. A straight path to circular proteins. *Journal of Biological Chemistry* **2009**, *284*, 16028–16036.

(72) Dickgiesser, S.; Rasche, N.; Nasu, D.; Middel, S.; Hörner, S.; Avrutina, O.; Diederichsen, U.; Kolmar, H. Self-Assembled Hybrid Aptamer-Fc Conjugates for Targeted Delivery: A Modular Chemoenzymatic Approach. *ACS chemical biology* **2015**, *10*, 2158–2165.

- (73) Ando, H.; Adachi, M.; Umeda, K.; Matsuura, A.; Nonaka, M.; Uchio, R.; Tanaka, H.; Motoki, M. Purification and Characteristics of a Novel Transglutaminase Derived from Microorganisms. *Agricultural and Biological Chemistry* **1989**, *53*, 2613–2617.
- (74) Griffin, M.; Casadio, R.; Bergamini, C. M. Transglutaminases: Nature's biological glues. *Biochem J* **2002**, *368*, 377–396.
- (75) Greenberg, C. S.; Birckbichler, P. J.; Rice, R. H. Transglutaminases: multifunctional cross-linking enzymes that stabilize tissues. *FASEB journal : official publication of the Federation of American Societies for Experimental Biology* **1991**, *5*, 3071–3077.
- (76) Kashiwagi, T.; Yokoyama, K.; Ishikawa, K.; Ono, K.; Ejima, D.; Matsui, H.; Suzuki, E. Crystal Structure of Microbial Transglutaminase from *Streptovorticillium mobaraense* *. *Journal of Biological Chemistry* **2002**, *277*, 44252–44260.
- (77) Pasternack, R.; Dorsch, S.; Otterbach, J. T.; Robenek, I. R.; Wolf, S.; Fuchsbaauer, H. L. Bacterial pro-transglutaminase from *Streptovorticillium mobaraense*--purification, characterisation and sequence of the zymogen. *European journal of biochemistry* **1998**, *257*, 570–576.
- (78) Zotzel, J.; Keller, P.; Fuchsbaauer, H.-L. Transglutaminase from *Streptomyces mobaraensis* is activated by an endogenous metalloprotease. *European journal of biochemistry* **2003**, *270*, 3214–3222.
- (79) Zotzel, J.; Pasternack, R.; Pelzer, C.; Ziegert, D.; Mainusch, M.; Fuchsbaauer, H.-L. Activated transglutaminase from *Streptomyces mobaraensis* is processed by a tripeptidyl aminopeptidase in the final step. *European journal of biochemistry* **2003**, *270*, 4149–4155.
- (80) Deweid, L.; Avrutina, O.; Kolmar, H. Microbial transglutaminase for biotechnological and biomedical engineering. *Biological Chemistry* **2019**, *400*, 257–274.
- (81) Juettner, N. E.; Schmelz, S.; Kraemer, A.; Knapp, S.; Becker, B.; Kolmar, H.; Scrima, A.; Fuchsbaauer, H.-L. Structure of a glutamine donor mimicking inhibitory peptide shaped by the catalytic cleft of microbial transglutaminase. *The FEBS journal* **2018**, *285*, 4684–4694.
- (82) Ohtsuka, T.; Ota, M.; Nio, N.; Motoki, M. Comparison of substrate specificities of transglutaminases using synthetic peptides as acyl donors. *Bioscience, biotechnology, and biochemistry* **2000**, *64*, 2608–2613.
- (83) Sugimura, Y.; Yokoyama, K.; Nio, N.; Maki, M.; Hitomi, K. Identification of preferred substrate sequences of microbial transglutaminase from *Streptomyces mobaraensis* using a phage-displayed peptide library. *Archives of biochemistry and biophysics* **2008**, *477*, 379–383.
- (84) Siegmund, V.; Schmelz, S.; Dickgiesser, S.; Beck, J.; Ebenig, A.; Fittler, H.; Frauendorf, H.; Piater, B.; Betz, U. A. K.; Avrutina, O.; *et al.* Locked by Design: A Conformationally Constrained Transglutaminase Tag Enables Efficient Site-Specific Conjugation. *Angewandte Chemie International Edition* **2015**, *54*, 13420–13424.
- (85) Fontana, A.; Spolaore, B.; Mero, A.; Veronese, F. M. Site-specific modification and PEGylation of pharmaceutical proteins mediated by transglutaminase. *Advanced Drug Delivery Reviews* **2008**, *60*, 13–28.
- (86) Ebenig, A.; Juettner, N. E.; Deweid, L.; Avrutina, O.; Fuchsbaauer, H.-L.; Kolmar, H. Efficient Site-Specific Antibody-Drug Conjugation by Engineering a Nature-Derived Recognition Tag for Microbial Transglutaminase. *Chembiochem: a European journal of chemical biology* **2019**, *20*, 2411–2419.
- (87) Fiebig, D.; Schmelz, S.; Zindel, S.; Ehret, V.; Beck, J.; Ebenig, A.; Ehret, M.; Fröls, S.; Pfeifer, F.; Kolmar, H.; *et al.* Structure of the Dispa Autolysis-inducing Protein from *Streptomyces mobaraensis* and Glutamine Cross-linking Sites for Transglutaminase. *The Journal of biological chemistry* **2016**, *291*, 20417–20426.

- (88) Takazawa, T.; Kamiya, N.; Ueda, H.; Nagamune, T. Enzymatic labeling of a single chain variable fragment of an antibody with alkaline phosphatase by microbial transglutaminase. *Biotechnology and bioengineering* **2004**, *86*, 399–404.
- (89) Ota, M.; Sawa, A.; Nio, N.; Ariyoshi, Y. Enzymatic ligation for synthesis of single-chain analogue of monellin by transglutaminase*. *Biopolymers* **1999**, *50*, 193–200.
- (90) Malešević, M.; Migge, A.; Hertel, T. C.; Pietzsch, M. A fluorescence-based array screen for transglutaminase substrates. *Chembiochem : a European journal of chemical biology* **2015**, *16*, 1169–1174.
- (91) Rachel, N. M.; Pelletier, J. N. Biotechnological applications of transglutaminases. *Biomolecules* **2013**, *3*, 870–888.
- (92) Strop, P. Versatility of microbial transglutaminase. *Bioconjugate chemistry* **2014**, *25*, 855–862.
- (93) Tanaka, Y.; Doi, S.; Kamiya, N.; Kawata, N.; Kamiya, S.; Nakama, K.; Goto, M. A chemically modified glass surface that facilitates transglutaminase-mediated protein immobilization. *Biotechnology letters* **2008**, *30*, 1025–1029.
- (94) Tischer, T.; Claus, T. K.; Bruns, M.; Trouillet, V.; Linkert, K.; Rodriguez-Emmenegger, C.; Goldmann, A. S.; Perrier, S.; Börner, H. G.; Barner-Kowollik, C. Spatially controlled photochemical peptide and polymer conjugation on biosurfaces. *Biomacromolecules* **2013**, *14*, 4340–4350.
- (95) Shagin, D. A.; Barsova, E. V.; Yanushevich, Y. G.; Fradkov, A. F.; Lukyanov, K. A.; Labas, Y. A.; Semenova, T. N.; Ugalde, J. A.; Meyers, A.; Nunez, J. M.; *et al.* GFP-like proteins as ubiquitous metazoan superfamily: evolution of functional features and structural complexity. *Molecular biology and evolution* **2004**, *21*, 841–850.
- (96) Ruhaak, L. R.; Steenvoorden, E.; Koeleman, C. A. M.; Deelder, A. M.; Wuhler, M. 2-picoline-borane: a non-toxic reducing agent for oligosaccharide labeling by reductive amination. *PROTEOMICS* **2010**, *10*, 2330–2336.
- (97) Ormo, M.; Remington, S. J. *Green Fluorescent Protein from Aequorea Victoria*, 1996.
- (98) Kashiwagi, T.; Yokoyama, K.; Ishikawa, K.; Ono, K.; Ejima, D.; Matsui, H.; Suzuki, E. *Crystal Structure Analysis of the Microbial Transglutaminase*, 2002.
- (99) Montelione, G. T.; Tashiro, M.; Tejero, R.; Lyons, B. A. *Staphylococcal Protein A, Z-Domain*, NMR, 10 STRUCTURES, 1998.
- (100) Hilberg, V.; Avrutina, O.; Ebenig, A.; Yanakieva, D.; Meckel, T.; Biesalski, M.; Kolmar, H. Light-Controlled Chemoenzymatic Immobilization of Proteins towards Engineering of Bioactive Papers. *Chemistry - A European Journal* **2019**, *25*, 1746–1751.
- (101) Liebich, V. J.; Avrutina, O.; Habermann, J.; Hillscher, L. M.; Langhans, M.; Meckel, T.; Biesalski, M.; Kolmar, H. Toward Fabrication of Bioactive Papers: Covalent Immobilization of Peptides and Proteins. *Biomacromolecules* **2021**, *22*, 2954–2962.
- (102) Nicolaou, K. C.; Snyder, S. A.; Montagnon, T.; Vassilikogiannakis, G. The Diels-Alder Reaction in Total Synthesis. *Angewandte Chemie International Edition* **2002**, *41*, 1668–1698.
- (103) Segura, J. L.; Martín, N. o-Quinodimethanes: Efficient Intermediates in Organic Synthesis. *Chemical reviews* **1999**, *99*, 3199–3246.
- (104) Hildebrandt, K.; Elies, K.; D'hooge, D. R.; Blinco, J. P.; Barner-Kowollik, C. A Light-Activated Reaction Manifold. *Journal of the American Chemical Society* **2016**, *138*, 7048–7054.
- (105) Oehlenschlaeger, K. K.; Mueller, J. O.; Heine, N. B.; Glassner, M.; Guimard, N. K.; Delaittre, G.; Schmidt, F. G.; Barner-Kowollik, C. Light-induced modular ligation of conventional RAFT polymers. *Angewandte Chemie International Edition* **2013**, *52*, 762–766.

- (106) Pauloehrl, T.; Delaittre, G.; Winkler, V.; Welle, A.; Bruns, M.; Börner, H. G.; Greiner, A. M.; Bastmeyer, M.; Barner-Kowollik, C. Adding spatial control to click chemistry: phototriggered Diels-Alder surface (bio)functionalization at ambient temperature. *Angewandte Chemie International Edition* **2012**, *51*, 1071–1074.
- (107) Jullian, M.; Hernandez, A.; Maurras, A.; Puget, K.; Amblard, M.; Martinez, J.; Subra, G. N-terminus FITC labeling of peptides on solid support: the truth behind the spacer. *Tetrahedron Letters* **2009**, *50*, 260–263.
- (108) Nilsson, B.; Moks, T.; Jansson, B.; Abrahmsén, L.; Elmblad, A.; Holmgren, E.; Henrichson, C.; Jones, T. A.; Uhlén, M. A synthetic IgG-binding domain based on staphylococcal protein A. *Protein engineering* **1987**, *1*, 107–113.
- (109) Dorr, B. M.; Ham, H. O.; An, C.; Chaikof, E. L.; Liu, D. R. Reprogramming the specificity of sortase enzymes. *Proceedings of the National Academy of Sciences of the United States of America* **2014**, *111*, 13343–13348.
- (110) Tanaka, T.; Kamiya, N.; Nagamune, T. N-terminal glycine-specific protein conjugation catalyzed by microbial transglutaminase. *FEBS letters* **2005**, *579*, 2092–2096.
- (111) Hilberg, V. *Ortsgerichtete Biofunktionalisierung von papierbasierten Materialien*. Masterthesis, 2017.
- (112) Beyer, M.; Felgenhauer, T.; Ralf Bischoff, F.; Breitling, F.; Stadler, V. A novel glass slide-based peptide array support with high functionality resisting non-specific protein adsorption. *Biomaterials* **2006**, *27*, 3505–3514.
- (113) Schindelin, J.; Arganda-Carreras, I.; Frise, E.; Kaynig, V.; Longair, M.; Pietzsch, T.; Preibisch, S.; Rueden, C.; Saalfeld, S.; Schmid, B.; *et al.* Fiji: an open-source platform for biological-image analysis. *Nature methods* **2012**, *9*, 676–682.
- (114) Kindermann, M.; George, N.; Johnsson, N.; Johnsson, K. Covalent and selective immobilization of fusion proteins. *Journal of the American Chemical Society* **2003**, *125*, 7810–7811.
- (115) Plant, A. L.; Locascio-Brown, L.; Haller, W.; Durst, R. A. Immobilization of binding proteins on nonporous supports. Comparison of protein loading, activity, and stability. *Applied biochemistry and biotechnology* **1991**, *30*, 83–98.
- (116) Shriver-Lake, L. C.; Donner, B.; Edelstein, R.; Breslin, K.; Bhatia, S. K.; Ligler, F. S. Antibody immobilization using heterobifunctional crosslinkers. *Biosensors and Bioelectronics* **1997**, *12*, 1101–1106.
- (117) Taylor, R. H.; Fournier, S. M.; Simons, B. L.; Kaplan, H.; Hefford, M. A. Covalent protein immobilization on glass surfaces: application to alkaline phosphatase. *Journal of biotechnology* **2005**, *118*, 265–269.
- (118) Viswanathan, R.; Labadie, G. R.; Poulter, C. D. Regioselective covalent immobilization of catalytically active glutathione S-transferase on glass slides. *Bioconjugate chemistry* **2013**, *24*, 571–577.
- (119) Miller, E. A.; Baniya, S.; Osorio, D.; Al Maalouf, Y. J.; Sikes, H. D. Paper-based diagnostics in the antigen-depletion regime: High-density immobilization of rcSso7d-cellulose-binding domain fusion proteins for efficient target capture. *Biosensors & bioelectronics* **2018**, *102*, 456–463.
- (120) Dai, G.; Hu, J.; Zhao, X.; Wang, P. A colorimetric paper sensor for lactate assay using a cellulose-Binding recombinant enzyme. *Sensors and Actuators B: Chemical* **2017**, *238*, 138–144.

-
- (121) Folk, J. E.; Cole, P. W. Mechanism of action of guinea pig liver transglutaminase. I. Purification and properties of the enzyme: identification of a functional cysteine essential for activity. *Journal of Biological Chemistry* **1966**, *241*, 5518–5525.
- (122) Kieliszek, M.; Misiewicz, A. Microbial transglutaminase and its application in the food industry. A review. *Folia microbiologica* **2014**, *59*, 241–250.
- (123) Ohtsuka, T.; Sawa, A.; Kawabata, R.; Nio, N.; Motoki, M. Substrate specificities of microbial transglutaminase for primary amines. *Journal of agricultural and food chemistry* **2000**, *48*, 6230–6233.
- (124) Tagami, U.; Shimba, N.; Nakamura, M.; Yokoyama, K.; Suzuki, E.; Hirokawa, T. Substrate specificity of microbial transglutaminase as revealed by three-dimensional docking simulation and mutagenesis. *Protein engineering, design & selection : PEDS* **2009**, *22*, 747–752.
- (125) Rickert, M.; Strop, P.; Lui, V.; Melton-Witt, J.; Farias, S. E.; Foletti, D.; Shelton, D.; Pons, J.; Rajpal, A. Production of soluble and active microbial transglutaminase in *Escherichia coli* for site-specific antibody drug conjugation. *Protein science: a publication of the Protein Society* **2016**, *25*, 442–455.
- (126) Nakamura, Y.; Shibasaki, S.; Ueda, M.; Tanaka, A.; Fukuda, H.; Kondo, A. Development of novel whole-cell immunoadsorbents by yeast surface display of the IgG-binding domain. *Applied microbiology and biotechnology* **2001**, *57*, 500–505.
- (127) Chen, C.; Huang, Q.-L.; Jiang, S.-H.; Pan, X.; Hua, Z.-C. Immobilized protein ZZ, an affinity tool for immunoglobulin isolation and immunological experimentation. *Biotechnology and applied biochemistry* **2006**, *45*, 87–92.
- (128) Cheng, C.-M.; Martinez, A. W.; Gong, J.; Mace, C. R.; Phillips, S. T.; Carrilho, E.; Mirica, K. A.; Whitesides, G. M. Paper-based ELISA. *Angewandte Chemie International Edition* **2010**, *49*, 4771–4774.
- (129) Gryczynski, Z.; Gryczynski, I. *Practical Fluorescence Spectroscopy*; A Chapman & Hall Book CRC Press imprint of Taylor & Francis: Boca Raton, FL, London, New York, 2020.
- (130) Agten, S. M.; Suylen, D. P. L.; Hackeng, T. M. Oxime Catalysis by Freezing. *Bioconjugate Chem.* **2016**, *27*, 42–46.
- (131) Knauer, S.; Koch, N.; Uth, C.; Meusinger, R.; Avrutina, O.; Kolmar, H. Sustainable Peptide Synthesis Enabled by a Transient Protecting Group. *Angewandte Chemie International Edition* **2020**, *59*, 12984–12990.
- (132) Guigo, N.; Mazeau, K.; Putaux, J.-L.; Heux, L. Surface modification of cellulose microfibrils by periodate oxidation and subsequent reductive amination with benzylamine: a topochemical study. *Cellulose* **2014**, *21*, 4119–4133.
- (133) Azzam, F.; Galliot, M.; Putaux, J.-L.; Heux, L.; Jean, B. Surface peeling of cellulose nanocrystals resulting from periodate oxidation and reductive amination with water-soluble polymers. *Cellulose* **2015**, *22*, 3701–3714.
- (134) Sirviö, J. A.; Visanko, M.; Laitinen, O.; Ämmälä, A.; Liimatainen, H. Amino-modified cellulose nanocrystals with adjustable hydrophobicity from combined regioselective oxidation and reductive amination. *Carbohydrate polymers* **2016**, *136*, 581–587.
- (135) Boraston, A. B.; Ghaffari, M.; Warren, R. A. J.; Kilburn, D. G. Identification and glucan-binding properties of a new carbohydrate-binding module family. *Biochemical Journal* **2002**, *361*, 35–40.
- (136) Tsutsui, H.; Karasawa, S.; Okamura, Y.; Miyawaki, A. Improving membrane voltage measurements using FRET with new fluorescent proteins. *Nature methods* **2008**, *5*, 683–685.
- (137) Lehtiö, J.; Sugiyama, J.; Gustavsson, M.; Fransson, L.; Linder, M.; Teeri, T. T. The binding specificity and affinity determinants of family 1 and family 3 cellulose binding
-

modules. *Proceedings of the National Academy of Sciences of the United States of America* **2003**, *100*, 484–489.

(138) Salis, A.; Boström, M.; Medda, L.; Cugia, F.; Barse, B.; Parsons, D. F.; Ninham, B. W.; Monduzzi, M. Measurements and theoretical interpretation of points of zero charge/potential of BSA protein. *Langmuir* **2011**, *27*, 11597–11604.

(139) Böhm, A.; Carstens, F.; Trieb, C.; Schabel, S.; Biesalski, M. Engineering microfluidic papers: effect of fiber source and paper sheet properties on capillary-driven fluid flow. *Microfluid Nanofluid* **2014**, *16*, 789–799.

(140) Bump, S.; Böhm, A.; Babel, L.; Wendenburg, S.; Carstens, F.; Schabel, S.; Biesalski, M.; Meckel, T. Spatial, spectral, radiometric, and temporal analysis of polymer-modified paper substrates using fluorescence microscopy. *Cellulose* **2015**, *22*, 73–88.

(141) Auernhammer, J.; Langhans, M.; Schäfer, J.-L.; Keil, T.; Meckel, T.; Biesalski, M.; Stark, R. W. Nanomechanical subsurface characterisation of cellulosic fibres. *SN Applied Sciences* **2022**, *4*.

(142) Deweid, L.; Neureiter, L.; Englert, S.; Schneider, H.; Deweid, J.; Yanakieva, D.; Sturm, J.; Bitsch, S.; Christmann, A.; Avrutina, O.; *et al.* Directed Evolution of a Bond-Forming Enzyme: Ultrahigh-Throughput Screening of Microbial Transglutaminase Using Yeast Surface Display. *Chemistry – A European Journal* **2018**, *24*, 15195–15200.

(143) Gasteiger, E.; Hoogland, C.; Gattiker, A.; Duvaud, S.; Wilkins, M. R.; Appel, R. D.; Bairoch, A. Protein Identification and Analysis Tools on the ExPASy Server. In *The proteomics protocols handbook*; Walker, J. M., Ed.; Humana Press: Totowa, NJ, 2005; pp 571–607.

Erklärungen

§8 Abs. 1 lit. c der Promotionsordnung der TU Darmstadt

Ich versichere hiermit, dass die elektronische Version meiner Dissertation mit der schriftlichen Version übereinstimmt und für die Durchführung des Promotionsverfahrens vorliegt.

§8 Abs. 1 lit. d der Promotionsordnung der TU Darmstadt

Ich versichere hiermit, dass zu einem vorherigen Zeitpunkt noch keine Promotion versucht wurde und zu keinem früheren Zeitpunkt an einer in- oder ausländischen Hochschule eingereicht wurde.

§9 Abs. 1 der Promotionsordnung der TU Darmstadt

Ich versichere hiermit, dass die vorliegende Dissertation selbstständig und nur unter Verwendung der angegebenen Quellen verfasst wurde.

§9 Abs. 2 der Promotionsordnung der TU Darmstadt

Die Arbeit hat bisher noch nicht zu Prüfungszwecken gedient.

Darmstadt, den

(Name und Unterschrift)